CENTER FOR TRANSPORTATION INFRASTRUCTURE AND SAFETY

Lightweight Concrete Modification Factor for Shear Friction

by

Lesley H. Sneed
and
Dane M. Shaw

A National University Transportation Center at Missouri University of Science and Technology

Disclaimer

The contents of this report reflect the views of the author(s), who are responsible for the facts and the accuracy of information presented herein. This document is disseminated under the sponsorship of the Department of Transportation, University Transportation Centers Program and the Center for Transportation Infrastructure and Safety NUTC program at the Missouri University of Science and Technology, in the interest of information exchange. The U.S. Government and Center for Transportation Infrastructure and Safety assumes no liability for the contents or use thereof.

Technical Report Documentation Page

1. Report No.	2. Government Accession No.	3. Recipient's Catalog No.
NUTC R276 / R317		

4. Title and Subtitle	5. Report Date
Lightweight Concrete Modification Factor for Shear Friction	October 2013
	6. Performing Organization Code

7. Author/s	8. Performing Organization Report No.
Lesley Sneed	Project #00034650 / 00040840

9. Performing Organization Name and Address	10. Work Unit No. (TRAIS)
Center for Transportation Infrastructure and Safety/NUTC program Missouri University of Science and Technology 220 Engineering Research Lab Rolla, MO 65409	11. Contract or Grant No. DTRT06-G-0014

12. Sponsoring Organization Name and Address	13. Type of Report and Period Covered
U.S. Department of Transportation Research and Innovative Technology Administration 1200 New Jersey Avenue, SE Washington, DC 20590	Final
	14. Sponsoring Agency Code

15. Supplementary Notes

16. Abstract

This report describes the results of a study initiated to examine the influence of concrete unit weight on the direct shear transfer across an interface of concretes cast at different times. This type of interface is common with structural precast concrete connections, such as corbels, for which shear friction design provisions are commonly used. Increasing use of lightweight aggregate concretes prompted this investigation to determine the appropriateness of current shear friction design provisions with respect to all-lightweight and sand-lightweight concrete. The experimental investigation included thirty-six push-off test specimens, each of which was constructed with a cold-joint at the interface shear plane. Test variables included unit weight of concrete (108, 120, and 145 pcf), target compressive strength of concrete (5000 and 8000 psi), and interface condition (smooth or roughened). A constant amount of reinforcing steel was provided across the shear plane. Results suggest that concrete unit weight did not play a significant role in the interface shear strength for the cold-joint specimens in this study. Results were also compared with shear friction design provisions in both the ACI 318 code and the PCI Design Handbook. Shear strengths computed using the coefficient of friction approach was conservative for the sand-lightweight and all-lightweight cold-joint specimens in this study. The value of the effective coefficient of friction *e* computed using the PCI Design Handbook approach was found to be conservative for both roughened and smooth non-monolithic interfaces for each concrete type. Finally, the use of the lightweight concrete modification factor in the calculation for the effective coefficient of friction □*e* was found to be conservative for the sand-lightweight and all-lightweight cold-joint specimens in this study. This study is sponsored by the Precast/Prestressed Concrete Institute Daniel P. Jenny Fellowship Program and the National University Transportation Center at the Missouri University of Science and Technology in Rolla, Missouri.

17. Key Words	18. Distribution Statement
Bridge superstructures, lightweight concrete	No restrictions. This document is available to the public through the National Technical Information Service, Springfield, Virginia 22161.

19. Security Classification (of this report)	20. Security Classification (of this page)	21. No. Of Pages	22. Price
unclassified	unclassified	132	

Form DOT F 1700.7 (8-72)

ABSTRACT

This report describes the results of a study initiated to examine the influence of concrete unit weight on the direct shear transfer across an interface of concretes cast at different times. This type of interface is common with structural precast concrete connections, such as corbels, for which shear friction design provisions are commonly used. Increasing use of lightweight aggregate concretes prompted this investigation to determine the appropriateness of current shear friction design provisions with respect to all-lightweight and sand-lightweight concrete. The experimental investigation included thirty-six push-off test specimens, each of which was constructed with a cold-joint at the interface shear plane. Test variables included unit weight of concrete (108, 120, and 145 pcf), target compressive strength of concrete (5000 and 8000 psi), and interface condition (smooth or roughened). A constant amount of reinforcing steel was provided across the shear plane. Results suggest that concrete unit weight did not play a significant role in the interface shear strength for the cold-joint specimens in this study. Results were also compared with shear friction design provisions in both the ACI 318 code and the PCI Design Handbook. Shear strengths computed using the coefficient of friction μ approach were conservative for the sand-lightweight and all-lightweight cold-joint specimens in this study. The value of the effective coefficient of friction μ_e computed using the PCI Design Handbook approach was found to be conservative for both roughened and smooth non-monolithic interfaces for each concrete type. Finally, the use of the lightweight concrete modification factor λ in the calculation for the effective coefficient of friction μ_e was found to be conservative for the sand-lightweight and all-lightweight cold-joint specimens in this study. This study is sponsored by the Precast/Prestressed Concrete Institute Daniel P. Jenny Fellowship Program and the National University Transportation Center at the Missouri University of Science and Technology in Rolla, Missouri.

TABLE OF CONTENTS

LIST OF FIGURES

LIST OF TABLES

NOMENCLATURE

Symbol	Description
A_{cr}	area of concrete shear interface, in^2
A_{vf}	area of shear reinforcement across shear plane, in^2
f'_c	28-day concrete compressive strength, lb/in^2
f_{ct}	tensile strength of concrete, measured by splitting tensile strength, lb/in^2
f_s	stress in reinforcement, lb/in^2
f_y	yield stress of reinforcement, lb/in^2
P_c	active clamping force, lb
V	shear force, lb
V_n	nominal shear strength, lb
v_n	nominal shear stress, lb/in^2
V_u	ultimate shear strength, lb
v_u	ultimate shear stress, lb/in^2
α	angle relative to interface
λ	modification factor reflecting the reduced mechanical properties of lightweight concrete, relative to normalweight concrete of the same compressive strength.
μ	coefficient of friction
μ_e	effective coefficient of friction
μ_k	coefficient of kinetic friction
μ_s	coefficient of static friction
ρ	shear friction reinforcement ratio, A_v/A_c
σ	normal stress, lb/in^2
τ	shear stress, lb/in^2
ϕ	capacity reduction factor
ACI	American Concrete Institute
ASCE	American Society of Civil Engineers
ASTM	American Society for Testing and Materials
DC-LVDT	direct current - linear voltage displacement transducer
PCI	Precast/Prestressed Concrete Institute

1. INTRODUCTION

1.1. PROBLEM STATEMENT

Lightweight aggregate concretes are being used increasingly in precast concrete construction to reduce member weight and shipping costs. Precast concrete elements commonly incorporate connections that are designed based on the shear friction concept to transfer forces across an interface, such as the column corbel shown in Figure 1.1. Previous studies discussed in Section 2 have shown that interface surface preparation, reinforcement ratio, concrete strength, and concrete type in terms of unit weight (normalweight, sand-lightweight, or all-lightweight) have significant impacts on the shear transfer strength. The shear friction design provisions presented in the PCI Design Handbook 7th Edition (2011) and the ACI 318 code (2011) are largely empirical and are based on physical test data, yet little data exist on specimens constructed with lightweight aggregate concretes, especially for non-monolithic construction of the interface.

Shear friction design provisions in both the ACI 318 code (2011) and the PCI Design Handbook 7th Edition (2011) include a modification factor λ that is intended to account for influence of concrete unit weight on the resulting interface friction. In particular, the modification factor λ is intended to account for reduced values of the mechanical properties of lightweight aggregate concretes relative to normalweight concrete of the same compressive strength. The modification factor λ is incorporated into the coefficient of friction μ in the PCI Design Handbook and the ACI 318 code and into the effective coefficient of friction μ_e in the PCI Design Handbook.

To account for the influence of interface surface preparation, current shear friction design provisions presented in the PCI Design Handbook 7th Edition (2011) and the ACI 318 code (2011) define four interface conditions (cases) summarized in Table 1.1. For each case, specific values and limits on the coefficient of friction and maximum shear capacity are given. Cases 2 and 3 refer to a non-monolithic, or "cold-joint," interface. Cold-joint conditions can be the result of precast plant practices where a projecting element is cast in advance and then inserted into the fresh concrete when the supporting element is cast or in the opposite sequence. For example, Figure 1.2 shows precast column corbels that have been cast in advance of the supporting precast column element. The far left and far right figures represent two corbels cast at two different facilities. The resulting interface roughness contributes to two distinctly different shear interface conditions shown in terms of surface roughness. The PCI Design Handbook also notes that the use of self-consolidating concrete (SCC) can lead to conditions in which projecting elements are cast against supporting elements after the concrete has partially hardened. The result may be a cold-joint condition with a relatively smooth interface on the SCC concrete face on which fresh concrete is placed.

This study examines the shear transfer of lightweight aggregate concretes across a cold-joint with a roughened or smooth interface (Cases 2 and 3 in Table 1.1). Results are compared to normalweight concrete of the same concrete strength and interface condition. This work is needed to fill in a gap in the literature with respect to the direct shear transfer strength of lightweight aggregate concretes across a non-monolithic interface. The topic of this research was identified by the Precast/Prestressed Concrete Institute (PCI) as a key research need for the precast concrete industry.

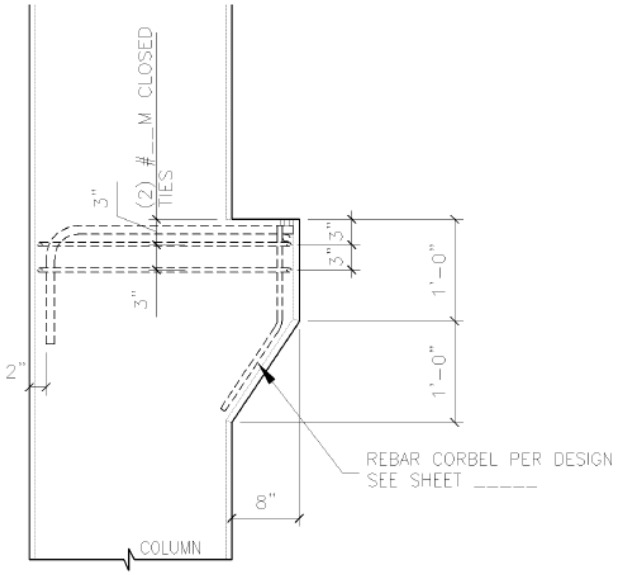

Figure 1.1. Typical precast corbel design (Metromont Inc.)

Table 1.1. Shear Interface Conditions[1]

Case	Interface Condition
1	Concrete to concrete, cast monolithically
2	Concrete to hardened concrete, with roughened surface
3	Concrete placed against hardened concrete not intentionally roughened
4	Concrete to steel

[1] Outlined in PCI Design Handbook 7th Edition (2011)

Figure 1.2. Precast button corbel - Facility #1 (left), precast button corbel in place (center), and precast button corbel - Facility #2 (right)

1.2. GOAL AND OBJECTIVES

The overall goal of this research project was to determine the influence of lightweight aggregate on the direct shear transfer across a plane of concretes cast at different times. Specific objectives were to:

a) Determine and account for precast plant practices and procedures typically used to prepare the partially hardened concrete surface;
b) Evaluate the shear friction performance of specimens containing lightweight aggregate concretes with respect to normalweight concrete control specimens;
c) Evaluate current and previous shear friction design provisions in the PCI Design Handbook and the ACI 318 code for applicability to lightweight aggregate concrete sections cast using non-monolithic construction; and
d) Determine appropriate coefficients of friction for concretes with lightweight aggregates for the case of plastic concrete placed against hardened concrete.

1.3. SCOPE

To achieve the goal and objectives outlined in Section 1.2, the scope of this project included:

a) Evaluation of precast plant practices to determine procedures and surface preparation techniques commonly used to construct projecting elements such as ledges and corbels;
b) Design, construction, and testing of a matrix of test specimens in which the parameters varied included target concrete unit weight (108 pcf, 120 pcf, and 145 pcf); specified concrete compressive strength (5000 psi and 8000 psi), and interface surface preparation (troweled smooth and roughened to 0.25 in. amplitude);
c) Analysis of the influence of concrete type (unit weight) on the interface friction including the effects of each of the parameters mentioned above; and
d) Development of recommendations for an appropriate modification factor λ for lightweight aggregate concretes for shear friction.

1.4. SUMMARY OF CONTENT

The problem statement, scope, and objectives of this study are presented in the introductory Section 1. Section 2 summarizes the background investigation conducted for this study. The content in Section 2 includes a literature review, which is comprised of a review of the current and previous design provisions, previous research performed on the topic of shear friction, and the results of a precast facility survey used in defining the shear interface conditions examined in this program. Section 3 is a summary of the experimental work performed, including test specimen design, dimensions, material properties, and test results. Analysis of the test results is discussed in detail in Section 4 including a comparison of the test results from this study to results from previous literature presented in Section 2. Finally, Section 5 contains the summary of key findings of this study, conclusions, and recommendations for shear friction design provisions for lightweight aggregate concretes.

2. BACKGROUND INVESTIGATION

2.1. INTRODUCTION

The design of reinforced concrete connections has been studied since the mid-20th century. In concrete elements such as corbels and ledger beams, discrete cracks may develop at an interface, and the transfer of forces must bridge that crack. There are several mechanisms to transfer these forces at these locations, one of which is friction of the interface. The transfer of shear at the interface via friction is discussed in detail in Section 2.2. Shear friction studies that were reviewed for this project are summarized in Section 2.3. Current and previous design provisions for design using shear friction principles are presented in Section 2.4. Finally, findings from a precast facility survey are presented in Section 2.5.

2.2. INTERFACE SHEAR FRICTION

2.2.1. Shear Friction. Shear friction theory was introduced in the mid-1960s and continues to be a topic of investigation today. The shear-friction hypothesis is a simplification of the transfer of forces from one surface to another via friction. The shear, which causes slippage of one surface relative to the other, is resisted by friction that results from a clamping force that is normal to the interface as shown in Figure 2.1 (Birkeland and Birkeland 1966, ACI Committee 445 1999). Although this simplification allows for transfer of forces across an existing crack plane, it is imperative that the mechanism that governs the failure of elements designed with this approach be understood.

The shear friction approach is a valuable design tool where discontinuities are present in reinforced concrete. In these "disturbed regions", the typical shear-flexure theory does not strictly apply, although it is still critical to account for the transfer of forces. For elements such as corbels and ledger beams there exists little or no redundancy, and, thus, their design is critical to the structural integrity of the overall system. Several studies have investigated the transfer of forces in these types of elements for normalweight concrete applications; however, very few studies have investigated lightweight aggregate concretes. Although lightweight aggregate concretes have been used in civil engineering constuction for many years, it has only been in the last twenty years that they have been accepted as a valuable and viable structural option. As such, their use has spread to elements that are designed using shear friction theory. Due to the lack of knowledge of lightweight aggregate concretes, shear friction design provisions in the ACI 318 code (2011) and the PCI Design Handbook (2004, 2011) have incorporated a modification factor, λ, which is intended to account for reduced values of the mechanical properties of lightweight concrete relative to normalweight concrete of the same compressive strength. While the current design provisions have been shown in general to be conservative, this approach may result in inefficient designs.

For elements subjected to direct shear transfer, sustained or repeated (cyclic) loading has been shown to exhibit little effect on the shear transfer behavior (Walraven et al. 1987). Therefore direct shear transfer is usually investigated under monotonic loading. In order to monitor the transfer of forces across the interface, the slip of the two faces relative to one another and the

dilation of the crack that develops along the shear plane must be measured. In addition to these measurements, it is beneficial to monitor strain levels in any reinforcing steel crossing the plane. In doing so, it is possible to determine the clamping force normal to the shear plane, as well as cohesion of the two surfaces of the interface.

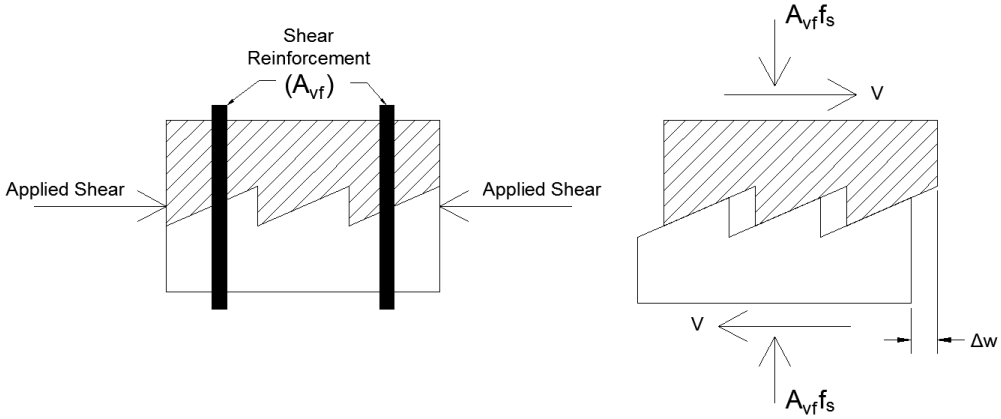

Figure 2.1. Shear friction hypothesis adapted from Birkeland and Birkeland (Birkeland and Birkeland 1966)

2.2.2. Shear Friction Mechanism. Interface shear transfer is a function of the shear interface condition. While concrete is generally strong in direct shear, cracks may form at any location under various loading conditions. The current ACI 318 code provisions assume that such a crack will form along the shear plane and that reinforcement is provided across the crack location (ACI Committee 318 2011). Accordingly, for the case of monolithic concrete, the shear plane may be either initially uncracked or cracked (also referred to as precracked). On the other hand, a non-monolithic (or cold-joint) condition may exist as a result of concrete placement practices where the concrete on either side of the shear plane was placed at different times.

In addition to interface condition, several factors have been shown to influence the ultimate shear transfer strength across an interface. These factors include aggregate interlock, the presence of shear reinforcement and any resulting dowel action, the interface surface preparation, the type of aggregate used, and any constraints applied normal to the shear plane (Hsu, Mau, and Chen 1987). Other researchers including Mattock, Raths, and Walraven have determined that cohesion of the interface plays a significant role in the shear friction mechanism. An example of the evaluation of the cohesion component is shown in Section 2.4.5.

It should be noted that for concrete elements cast monolithically, the shear friction model is not applicable until a crack develops along the interface and the two surfaces "engage" one another. In order to engage the two surfaces, the concrete from one surface must interact with that of the other surface. The aggregate present along the shear plane will cause roughness that will in turn cause separation of the two faces. This interaction mechanism is only possible if the separation of the two faces is restrained either internally or with some external system. If this restraint is provided, friction between the two surfaces is introduced, and the shear is transferred via shear friction. This interaction is important for two reasons with respect to elements without a crack along the shear plane. First, a relatively high force is required to induce the crack and engage the

two surfaces. After the crack develops, the aggregate will interlock, and friction is introduced. As a result, the peak load applied (V_u) may be significantly higher than the residual capacity (V_{ur}). Second, after the crack is induced, further reduction in load will occur as the slip increases due to the shearing of aggregate along the shear plane resulting in a smoother interface. The presence or absence of a crack at the shear friction interface represents a challenge when determining the appropriate coefficient of friction for use in the shear friction model.

2.2.2.1. Coefficient of friction. While the traditional coefficient of friction is not applicable for concrete elements cast monolithically, the shear friction design provisions are based on the assumption that a crack will form along the shear plane and that friction will develop. Equation 2.1 can be derived from classical mechanics where F is the peak applied shear force, μ is coefficient of friction, and N is the normal clamping force. This relationship is shown in Figure 2.2 (note that μ can also be referred to the static coefficient of friction μ_s as indicated in Figure 2.2.).

$$F_f = \mu N \tag{2.1}$$

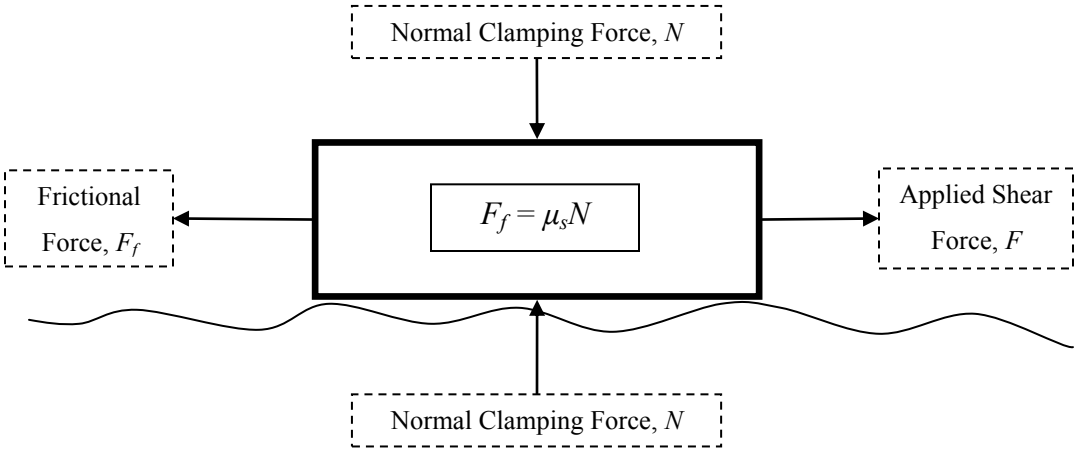

Figure 2.2. Simplified shear friction mechanism

The coefficient of friction μ is equal to the ratio of the shear stress τ to the normal stress σ acting across the shear interface. Manipulation of these parameters leads to the calculation shown in Equation 2.2, where A_{cv} is the area of the shear interface, $A_{vf}f_s$ is the passive clamping force provided by the reinforcing steel, V is the shear applied to the interface, and P_c is the active clamping force (external), if present.

$$\mu = \frac{\tau}{\sigma} = \frac{V \big/ A_{cv}}{(A_{vf} f_s + P_c) \big/ A_{cv}} = \frac{V}{A_{sf} f_s + P_c} \tag{2.2}$$

2.2.2.2. Effective coefficient of friction. Design provisions for shear friction in the PCI Design Handbook 7th Edition (2011) refer to an "effective coefficient of friction" term μ_e. This term was introduced to include the cohesion between surfaces and to better predict the shear transfer capacity based on available test data. The use of the effective coefficient of friction is discussed in further detail in Section 2.3.1.1.

2.3. SHEAR FRICTION DESIGN PROVISIONS

For design purposes, if there is no external clamping force, Equation 2.2 be rearranged in the form of Equation 2.3 in terms of the area of shear reinforcement required across the shear plane, noting that the design shear force is limited to $V=V_n=V_u/\phi$, and the stress in the reinforcement f_s is limited to the yield stress f_y.

$$A_{vf} = \frac{V_u}{\phi f_y \mu} \tag{2.3}$$

Equation 2.3 can be rearranged in the form of Equation 2.4 in terms of the coefficient of friction μ. Equation 2.4 is also the form that will be used to estimate the coefficient of friction for each test specimen in the experimental program (Section 4.4).

$$\mu = \frac{V_u}{\phi f_y A_{vf}} \tag{2.4}$$

The shear friction design provisions presented in both the 6th and 7th Editions of the PCI Design Handbook (2004, 2011) and the ACI 318 code (2011) are in the form of Equation 2.3, however, there are several key differences. The sections that follow summarize shear friction design provisions from recent versions of the PCI Design Handbook and the current ACI 318 code and highlight the differences.

2.3.1. PCI Design Handbook. Shear friction design provisions in the 6th and 7th Editions of the PCI Design Handbook are presented in this section. Definition of the crack interface conditions (cases) are the same in both editions, although limitations on the effective coefficient of friction μ_e and the maximum nominal shear strength differ.

2.3.1.1. PCI Design Handbook 6th Edition. The calculation of the area of shear friction reinforcement A_{vf} required by the 6th Edition of the PCI Design Handbook is shown in Equation 2.5, where; V_u is the applied factored shear force (limited by the values in Table 2.1) f_y is the yield stress of reinforcement ($f_y \leq$ 60ksi), ϕ is the strength reduction factor equal to 0.75, and μ_e is the effective coefficient of friction calculated using Equation 2.6. It is important to note that μ_e in Equation 2.6 is a function of the lightweight modification factor term squared (λ^2), since λ is also included in the term μ (see Table 2.1).

$$A_{vf} = \frac{V_u}{\phi f_y \mu_e} \tag{2.5}$$

$$\mu_e = \frac{1000 \lambda A_{cr} \mu}{V_u} \tag{2.6}$$

Equations 2.5 and 2.6 are applicable for all four crack interface conditions, or cases, presented in Table 2.1. Here it is also important to understand to derivation of Equation 2.6. While it is dimensionally ambiguous, the basis of this equation was developed by Charles Raths in 1977. Equation 2.7 represents the original equation proposed by Raths.

$$\mu_e = \frac{1400}{v_u} = \frac{37.42}{\sqrt{\rho_v f_y}} \quad (\mu=1.4) \tag{2.7}$$

Modifying this equation and extending it to include variables that account for the effect of concrete density and the coefficient of friction, Equation 2.8 is presented. Recognizing the C_s term as the effect of concrete density λ and v_u as shear stress, it can be seen that Equation 2.8 is the same as Equation 2.6.

$$\mu_e = \frac{1000 C_s^2 \mu}{v_u} = \frac{1000 \lambda A_{cr} \mu}{V_u} \tag{2.8}$$

Table 2.1. Shear Friction Coefficients for PCI Design Handbook 6th Edition (2004)

Case	Crack Interface Condition	μ	Max μ_e	Max $V_n=V_u\phi$
1	Concrete to concrete, cast monolithically	1.4λ	3.4	$0.30\lambda^2 f'_c A_{cr} \leq 1000\lambda^2 A_{cr}$
2	Concrete to hardened concrete, with roughened surface	1.0λ	2.9	$0.25\lambda^2 f'_c A_{cr} \leq 1000\lambda^2 A_{cr}$
3	Concrete placed against hardened concrete not intentionally roughened	0.6λ	2.2	$0.20\lambda^2 f'_c A_{cr} \leq 800\lambda^2 A_{cr}$
4	Concrete to steel	0.7λ	2.4	$0.20\lambda^2 f'_c A_{cr} \leq 800\lambda^2 A_{cr}$

2.3.1.2. PCI Design Handbook 7th Edition. Significant revisions were made to the shear friction design provisions in the 7th Edition of the PCI Design Handbook (2011) relative to the 6th Edition (2004) discussed in Section 2.3.1.1. First, Equation 2.9 was introduced, where the area of shear reinforcement A_{vf} can be determined as a function of the coefficient of friction μ instead of using the effective coefficient of friction μ_e. It should be noted that previous editions of the PCI

Design Handbook included the coefficient of friction μ only in the calculation of the effective coefficient of friction μ_e (see Section 2.3.1.1 Equation 2.6). Second, the use of Equation 2.10 (which is the same equation as Equation 2.5 in Section 2.3.1.1) and the effective coefficient μ_e was limited to crack interface conditions of Cases 1 and 2 in Table 2.2 and to sections where load reversal does not occur. Table 2.2 summarizes the shear friction coefficients and their limitations based on the PCI Design Handbook 7th Edition. Third, it is important to note that in using Equation 2.11, the maximum value of V_u/ϕ (shown in Table 2.2) no longer includes the λ^2 reduction factor.

$$A_{vf} = \frac{V_u}{\phi f_y \mu} \tag{2.9}$$

$$A_{vf} = \frac{V_u}{\phi f_y \mu_e} \tag{2.10}$$

$$\mu_e = \frac{\phi 1000 \lambda A_{cr} \mu}{V_u} \tag{2.11}$$

Table 2.2. Shear Friction Coefficients for PCI Design Handbook 7th Edition (2011)

Case	Crack Interface Condition	μ	Max μ_e	Max Vu/ϕ
1	Concrete to concrete, cast monolithically	1.4λ	3.4	$0.30\lambda f'_c A_{cr} \leq 1000\lambda A_{cr}$
2	Concrete to hardened concrete, with roughened surface	1.0λ	2.9	$0.25\lambda f'_c A_{cr} \leq 1000\lambda A_{cr}$
3	Concrete placed against hardened concrete not intentionally roughened	0.6λ	Not applicable	$0.20\lambda f'_c A_{cr} \leq 800\lambda A_{cr}$
4	Concrete to steel	0.7λ	Not applicable	$0.20\lambda f'_c A_{cr} \leq 800\lambda A_{cr}$

2.3.1.3. ACI 318 Code. The design provisions for shear friction presented in the ACI 318 code (2011) are based on the coefficient of friction μ and do not include the effective coefficient of friction μ_e. The current ACI 318 code (2011) shear friction design provisions are presented in Equations 2.12 and 2.13. Equation 2.12 presents the basic provision for reinforcement normal to the crack interface and is applicable for all four interface conditions defined in Table 1.1. In Equation 2.12, the nominal shear strength is expressed as a function of the reinforcement crossing the shear plane A_{vf}, the yield stress of the shear reinforcement f_y (where $f_y \leq 60$ksi), and the coefficient friction μ. Equation 2.12 is similar to Equation 2.9 in Section 2.3.1.2 from the PCI Design Handbook 7th Edition (2011), where $V_u = \phi V_n$. In addition to the basic provision of Equation 2.12, the ACI 318 code also presents Equation 2.13 for elements

in which the shear reinforcement is oriented at an angle α to the interface. This parameter was not investigated in this study, but the equation is presented here for completeness.

$$V_n = \mu A_{vf} f_y \tag{2.12}$$

$$V_n = A_{vf} f_y (\mu \sin\alpha + \cos\alpha) \tag{2.13}$$

For normalweight concrete that is either placed monolithically or against hardened concrete that has been roughened to an amplitude of 0.25 in., the maximum value of V_n in Equation 2.12 and Equation 2.13 is the smallest of $0.2f'_cA_c$, $(480 + 0.08f'_c)A_c$, and $1600A_c$. For all other cases, the maximum value of V_n in Equation 2.12 and Equation 2.13 is the smallest of $0.2f'_cA_c$ and $800A_c$.

2.4. PREVIOUS STUDIES

This section describes previous studies on shear transfer, and in particular shear friction, that have led to shear friction design provisions and requirements for reinforced concrete structures. These studies also served as the basis for designing the experiments discussed in Section 3.

2.4.1. Hanson, 1960. The study performed by Hanson in 1960 included the investigation of precast bridge elements with respect to composite action between precast girders and cast-in-place deck slabs. A total of 62 pushoff specimens and 10 precast T-shaped girders were tested to investigate the horizontal shear mechanism. Test variables off this study included the effects of adhesive bond, roughness, keys, and stirrups. The pushoff specimens in this study had variable shear areas ranging from 48 in^2 to 192 in^2. Concrete compressive strengths ranged from approximately 3000 psi to 6000 psi. Reinforcing steel used was Grade 50. Key findings of this investigation included:

1. Concrete strength was found to influence the initial peak values for all specimens tested. However, concrete strength was not isolated systematically in this study.
2. The depth of the roughness at the interface was found to not affect the shear-carrying capacity of the section.
3. Pushoff tests were shown to be valuable in determining the strength of horizontal shear connection for composite action.
4. Further investigation was recommended to address the effects of concrete strength, stirrup size, stirrup percentage, and repeated loading.

2.4.2. Birkeland and Birkeland, 1966. Birkeland and Birkeland's 1966 paper discussed the application of shear friction to precast concrete construction. The authors noted that for elements such as corbels, bearing shoes, and ledger beams, there are situations where conventional shear-flexure and principal tension analyses are not applicable. Therefore, the shear friction model was developed as a simple physical model to explain the transfer of forces and predict the lower-bound strength of the connection. Application of the shear friction design tool to heavily loaded sections was discussed. In the Birkeland and Birkeland report, the role of interface preparation was explained due to the nature of the shear friction hypothesis. Also, this

paper discussed the normal clamping force that is required in order to engage the friction aspect of this model as shown in Figure 2.1.

The definition of shear friction developed in this reference is the basis for the current design provisions in Section 2.3 of this report. Analysis of studies performed by Anderson (1960) and Hanson (1960) resulted in the recommendation for limitations due to the bounds of the research performed to date. These recommendations included a maximum reinforcing bar size of No. 6, yield stress of interface reinforcement less than or equal to 60 ksi, a maximum reinforcement ratio of 1.5%, a minimum concrete compressive strength of 4000 psi, and a limiting shear stress of 800 psi. Additionally, the interface reinforcement should be fully anchored. Finally, for elements cast non-monolithically, the authors indicated the interface should be cleaned of laitance and any external loads accounted for.

2.4.3. Mast, 1968. The report presented by Mast in 1968 focused on the auxiliary reinforcement in precast concrete connections. Elements of consideration were bearing shoes, anchoring bars, and confining hoops. Mast discussed the inability to verify the presence, or absence, of fabrication defects in precast connections. As a result, designers typically assume a cracked condition for design of these elements. Where cracks in connections are present, the shear friction hypothesis can be applied. As discussed in prior research, the rough surface provided at the interface causes the elements to separate, or "dialate," as shown in Figure 2.3, and engage the auxiliary reinforcement. Mast also explained that the shear friction hypothesis must account for any tension normal to the shear plane as it will have a significant influence on the resulting frictional force and, in turn, the ultimate shear transfer capacity.

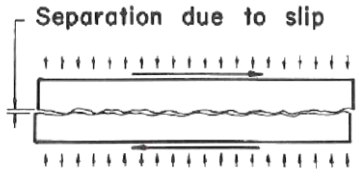

Figure 2.3. Separation due to shear along a crack (Mast 1968)

2.4.4. Hofbeck, Ibrahim, and Mattock, 1969. Hofbeck, Ibrahim, and Mattock's study (1969) tested the effects of a pre-existing crack, reinforcement variations, influence of concrete strength, and dowel action present along the shear plane of precast concrete elements. A total of 38 shear push-off specimens were tested in the study. The average concrete compressive strength was 4,500 psi, and reinforcement was provided normal to a 50 in^2 shear plane. The concrete was cast monolithically, and the maximum aggregate size used was 7/8 in. The external clamping force was varied from 0 psi to 1,500 psi, and the yield stress of reinforcement ranged from 50 ksi to 66 ksi. Two shear plane conditions were compared, initially cracked and initially uncracked. In addition to shear plane condition, a series of the initially uncracked specimens had rubber sleeves provided around the shear reinforcement in order to investigate the contribution of dowel action to the shear friction model.

The testing procedure used was similar to that in other studies (Hoff 1993, Mattock 2001, Kahn and Mitchell 2002). Pre-cracking was performed on some of the specimens to quantify the strength of the connection in locations where cracks developed due to aspects such as shrinkage or service level loads. Pre-cracking was completed by applying a line load to the shear interface until a crack formed.

A concentric loading was provided with roller release to allow lateral translation. Measurements including applied load and relative slip of elements were reported. A key conclusion of this study was that dowel action of reinforcing bars crossing the shear plane provides minimal contribution to ultimate shear in initially uncracked sections but is substantial for specimens with pre-existing cracks. Another important conclusion was that with the presence of the pre-existing crack, a reduction in ultimate shear transfer strength and increase in slip at all levels of load was experienced.

2.4.5. Mattock and Hawkins, 1972. The study completed by Mattock and Hawkins in 1972 investigated the shear transfer strength of monolithic reinforced concrete. The variables investigated included the concrete strength, shear plane characteristics, and direct stress applied normal to the shear interface. In this study, three variations of the push-off specimen were used shown in Figure 2.4. The first specimen was a standard push-off specimen that was similar to prior research. The second specimen was a pull-off type specimen. The third specimen was a modified push-off used to evaluate the effect of shear reinforcement oriented at various angles relative to the shear plane. Mattock and Hawkins investigated both pre-cracked and initially uncracked shear plane conditions.

Investigation of the modified pushoff specimen was performed to test the effect of compressive stress transverse to the shear plane. Concrete compressive strengths for these specimens ranged from 3,500 psi to 6,500 psi. The results of these specimens were plotted against the standard pushoff specimens after being normalized for concrete strength. A key finding of this investigation was that combining the normal stress and the stress in the reinforcement yielded the net clamping stress.

Another key conclusion of this study was that a pre-existing crack along the shear plane will reduce the ultimate shear transfer and increase slip for all levels of load. It was also found that, for uncracked elements, direct tension stresses parallel to the shear plane reduce the resulting shear transfer strength. Due to this, the authors explained that the shear transfer strength is developed by truss action and the formation of a compression strut upon propagation of the first diagonal tension crack (Figure 2.5). Finally, elements containing large amounts of shear reinforcement and a pre-existing crack will have a resulting failure similar to that of the uncracked element. This behavior was attributed to the shear surfaces locking against one another resembling a monolithic uncracked element.

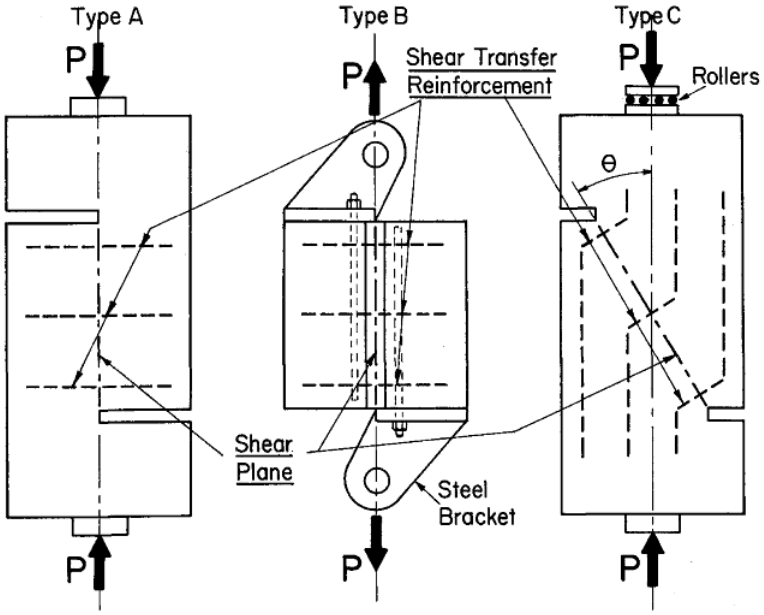

Figure 2.4. Shear transfer test specimens by Mattock and Hawkins (1972): push-off, pull-off, and modified push-off from left to right

Based on the results of this study, Mattock and Hawkins proposed a modified shear friction equation shown in Equation 2.14 in which the lead term of 200 represents the cohesion of the interface due to interface interaction and a term referred to as asperity shear.

$$v_u = 200 + 0.8(\rho_v f_y + \sigma_{nc}) \tag{2.14}$$

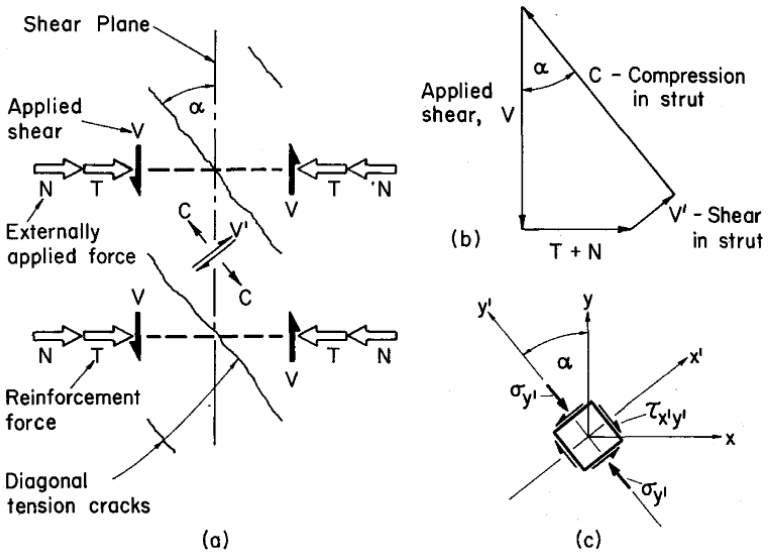

Figure 2.5. Shear transfer in initially uncracked concrete (Mattock and Hawkins 1972)

2.4.6. Paulay, Park, and Phillips, 1974. The study by Paulay, Park, and Phillips in 1974 investigated the shear resistance mechanisms along horizontal construction joints. The principal mechanisms included bond of the surfaces, dowel action of the interface reinforcement, and interface shear along roughened surfaces. The study included thirty push-off type specimens constructed with horizontal construction joints, shown in Figure 2.6, and six that were cast monolithically. Several surface preparations were investigated: trowelled, rough (chemical retarder), rough scraped, rough washed, rough chiseled, and keyed. Concrete compressive strengths ranged from 2900 psi to 4350 psi. A key finding of this study was that an adequately reinforced construction joint that has been cleaned and roughened will develop interface shear strength equal to or greater than that of the remaining structure. However, should a loss of bond be experienced, the ultimate shear strength will be reduced, and the slip of the joint will be significantly increased at moderate load levels. Another conclusion of the study was that for cyclic loading, strength capacities were not affected and should be maintained for a large number of load cycles. Finally, the contribution of dowel action to the ultimate shear strength was determined to be approximately fifteen percent.

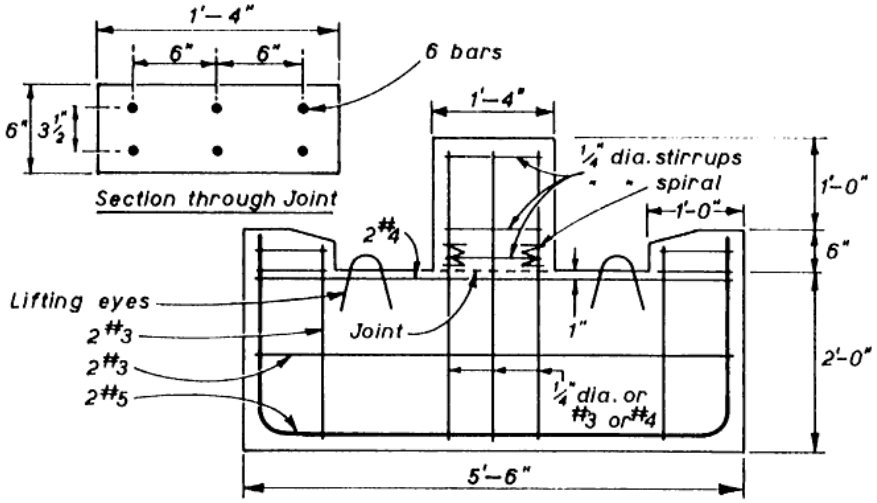

Figure 2.6. Test specimen used by Pauley et al. (1974)

2.4.7. Mattock, Johal, and Chow, 1975. The study completed in 1975 by Mattock, Johal, and Chow investigated shear friction specimens with moment or tension acting across the shear plane. The specimens used in this program included a corbel push-off specimen and a push-off specimen with direct tension applied normal to the shear plane, shown in Figure 2.7. The test variables included eccentricity of the applied loading, distribution of reinforcing steel across the shear plane, and the level of tension normal to the shear plane. A key finding of this research was that for elements subject to combined moment and shear, the ultimate shear transfer capacity is not reduced as long as the applied moment does not exceed the ultimate flexural strength of the section. However, if moment and shear are to be transferred across a crack, the transfer reinforcement should be located in the flexural tension zone.

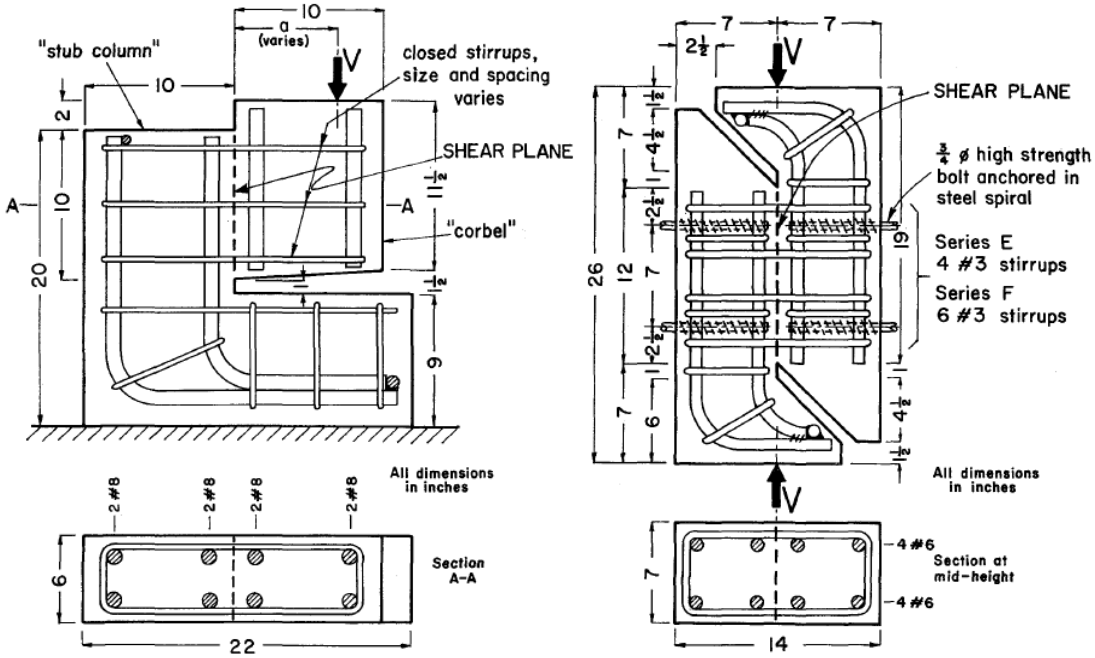

Figure 2.7. Corbel type push-off specimen, left, and compression with applied tension push-off specimen, right, by Mattock et al. (1975)

2.4.8. Mattock, Li, and Wang, 1976. The experimental study completed in 1976 by Mattock, Li, and Wang investigated the influence of aggregate type on the shear transfer strength and behavior. Four types of aggregates were investigated, including natural gravels and sand, rounded lightweight aggregate, crushed angular lightweight aggregate, and sand-lightweight aggregate. Dry concrete densities ranged from 92 to 148 lbs/ft^3. Other test variables included concrete strength and the presence of an existing crack along the shear plane before the application of the shear load. The concrete was cast monolithically, and concrete compressive strength ranged from 2000 psi to 6000 psi. A total of ten series of specimens were included. Specimens used in this study were the push-off specimens. Results of this study indicated that the shear transfer strength of lightweight aggregate concrete is less than that of sand and gravel concrete of the same compressive strength. In addition, it was found that the shear transfer strength was not significantly affected by the type of lightweight aggregate. Finally, this study recommended the use of the lightweight modification factor, λ, in the calculation of the shear transfer strength to reflect the reduced shear strength of lightweight aggregate concretes relative to normalweight concrete with the same compressive strength. The authors recommended that the coefficient of friction μ should be multiplied by 0.75 for all-lightweight concretes not less than 92 lb/ft^2 and should be multiplied by 0.85 for sand-lightweight concretes not less than 105 lb/ft^2.

Additionally comparison of the applied shear force-slip relations for specimens of the same concrete type (normalweight, sand-lightweight, or all-lightweight) and same interface condition indicates that the deformation behavior was more brittle for specimens with higher compressive strengths.

2.4.9. Shaihk, 1978. The study by Shaihk in 1978 analyzed previous research and proposed revisions to the PCI Manual on Design of Connections in Precast Prestressed Concrete (1973). Specimens containing normalweight and lightweight aggregate concretes were considered, as well as those with different interface conditions.

The general linear equation proposed by Birkeland (1968) was modified by Raths (1977) using the effective coefficient of friction recognizing the parabolic relationship observed between the shear stress and net clamping stress. Calculation of the proposed cross-sectional reinforcement area, A_{vf}, is presented in Equation 2.15, and the effective coefficient of friction μ_e is presented in Equation 2.16.

$$A_{vf} = \frac{V_u}{\phi f_y \mu_e} \tag{2.15}$$

$$\mu_e = \frac{1000 C_s^2 \mu}{v_u} \tag{2.16}$$

In Equation 2.16, C_s is the strength reduction coefficient for lightweight aggregate concrete (equivalent to λ), and the coefficient of friction μ ranges from 0.4 for cold-joint smooth interfaces up to 1.4 for monolithic concrete. This modified equation was evaluated with respect to equations proposed by Birkeland (1968), Mattock (1974) and Raths (1977). The conclusion of this study was that the proposed equations were conservative and acceptable for the design of prestressed concrete.

2.4.10. Hsu, Mau, and Chen, 1987. The study by Hsu, Mau, and Chen in 1987 presented the theory of shear transfer in initially cracked concrete. The approach taken in this study was that of the truss model. Specimens used to evaluate the acceptance of the model were those tested in previous Mattock studies. Specimens used for comparison were push-off specimens with the shear interface initially uncracked. Hsu et al. applied the softened truss model to the direct shear transfer and found that it successfully predicted the ultimate shear transfer strength.

2.4.11. Hoff, 1993. Hoff's study published in 1993 evaluated material properties and mechanical testing of high-strength lightweight aggregate concrete for use in Arctic applications. To evaluate the effects on shear capacity, push-off specimens similar to other studies (Mattock 1976, Hofbeck et al. 1969, and Kahn and Mitchell 2002) were tested. Each specimen had a shear area of 84 in^2. Parameters investigated included reinforcement normal to the shear plane and aggregate type. The loading configuration was similar to that presented in previous research. Loading was applied concentrically to the crack plane, and a lateral release was provided. Measurements recorded included slip of the crack plane, dilation of the crack plane, and applied shear. Maximum load was defined where high levels of slip were experienced with little to no increase in applied shear. A key finding of this study was that for critical areas, where sand-

lightweight concretes are used, it may be prudent to use a reduced reduction factor to estimate the shear transfer strength. However, with the introduction of high-strength mixtures, existing code provisions were determined to be adequate. In addition, the aggregate type (crushed vs. pelletized) was found to play a significant role in the post-cracking behavior.

2.4.12. Mattock, 2001. The study completed in 2001 by Mattock examined the provisions in the ACI 318 code (1999) used to design the shear reinforcement required to cross an existing or potential crack in a given connection. Specific consideration was made for high-strength concrete and the limitations set forth by the code on the shear strength V_n. An important distinction was made regarding the interface condition and the presence of a crack at the location of applied load prior to the application of the shear force. This investigation included specimens with initially cracked non-monolithic interfaces that were either roughened or smooth. The pre-cracked interface was intended to represent the lower bound shear transfer condition, which would result in a conservative estimation for the code changes proposed.

2.4.13. Kahn and Mitchell, 2002. The study by Kahn and Mitchell (2002) focused on expanding the applicability of shear friction model presented in the ACI 318 code (1999) to high-strength concrete. A total of 50 shear friction push-off specimens with a shear plane of 60 in^2, shown in Figure 2.8, were tested. Parameters varied were the reinforcement provided normal to the shear plane, concrete compressive strength, and shear interface condition. The reinforcement ratio varied from 0.37 to 1.47%, and the target concrete compressive strength varied from 4000 psi to 14,000 psi. Three shear interface conditions were tested including cold-joint, initially uncracked, and pre-cracked conditions with two replicates of each. The load was applied concentric to the shear plane. The load was increased monotonically until failure, and testing ceased at a slip of 0.25 in. Data reported included slip of the shear plane and applied load until failure. Results were reported in terms of the ultimate shear stress, residual shear stress, and clamping force provided by reinforcement normal to the shear plane. The initial cracks along the shear plane were observed to occur at 50 to 75% of the ultimate capacity. Ultimate capacity was defined as the load corresponding to a slip of 0.2 in. A key conclusion of Kahn and Mitchell's study was that for concrete strengths from 6800 psi to 17,900 psi, the current ACI 318 code (1999) shear friction design provisions provided conservative estimates for the interface shear strength of high-strength concretes. The authors also recommended that the upper limit on the shear stress of 800 psi be removed. With the inclusion of high-strength concrete data, the upper limit was proposed to be 20% of the 28-day compressive strength. Finally the observed behavior of the cold joint and initially uncracked specimens was reported to be nearly the same.

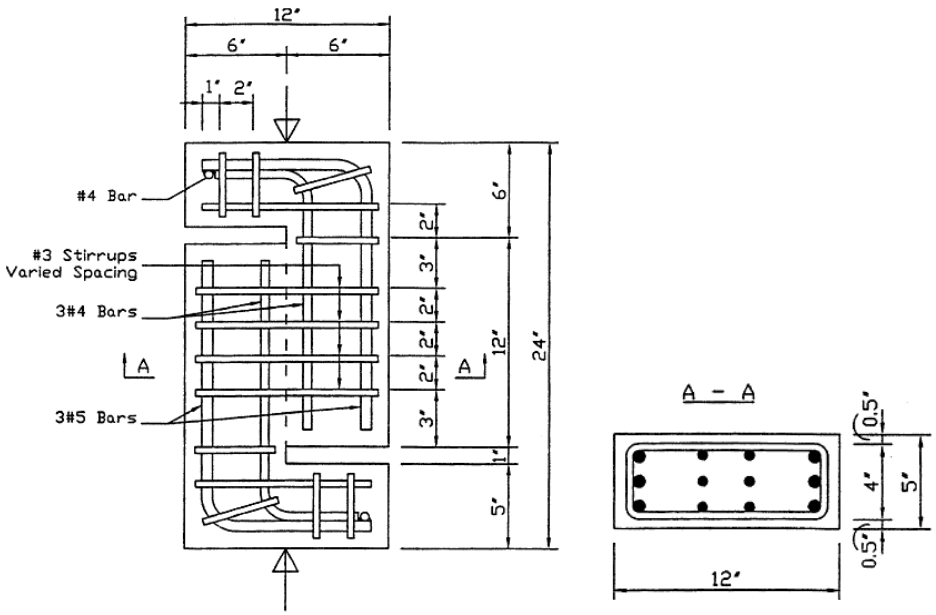

Figure 2.8. Typical design of push-off specimens by Kahn and Mitchell (2002)

2.4.14. Tanner, 2008. The paper by Tanner published in 2008 compared the shear friction design provisions based on the effective coefficient of friction approach in the 4th, 5th, and 6th Editions of the PCI Design Handbook (1992, 1999, 2004, respectively). Tanner pointed out several inconsistencies between the provisions in the 4th, 5th, and 6th Editions of the PCI Design Handbook and the original equations used in their development. He noted that changes to the 6th Edition of the PCI Design Handbook (2004) in which μ_e was revised to be based on the factored shear demand (V_u) instead of shear strength (V_n) were inconsistent with the original test data. He also noted that changes to the load factor and phi factors that were reflected in the 6th Edition further exacerbate the issue. Finally, he noted that there is some confusion regarding the use of the lightweight modification factor λ and whether or not it should be squared (refer to discussion in Section 2.3.1).

2.4.15. Harries, Zeno, and Shahrooz, 2012. The study by Harries, Zeno, and Shahrooz in 2012 included a comprehensive review of previous experimental investigations. This study indicated that current design rationales presented by the ACI 318 code (2011) and the AASHTO specifications (2007) do not sufficiently capture actual behavior of elements subject to direct shear transfer. As a result, incorrect limit states are applied. The experimental work presented in this study indicated that a large number of parameters affect the shear friction performance. This paper presented behavior of specimens (shown in Figure 2.9) from zero load through initial cracking, peak loading, and post cracking. The findings of this study indicated that the current models for shear friction are too simplistic and potentially misleading. In addition, it was found that the use of high-strength reinforcing steel prevents crack widths from reaching levels that would allow for yielding of steel crossing the crack interface.

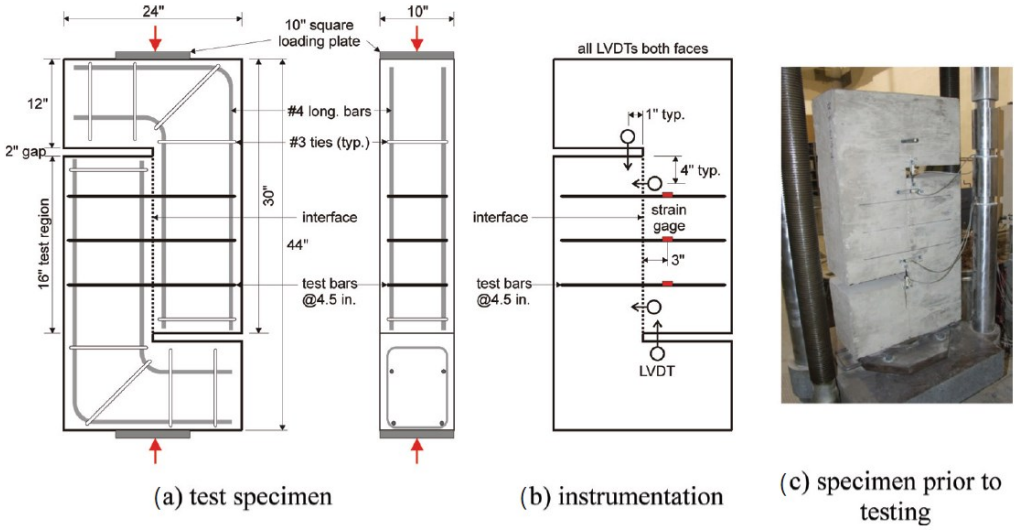

Figure 2.9. Test specimen and instrumentation arrangement by Harries et al (2012)

2.5. PRECAST PRODUCER SURVEY

To achieve the objectives outlined in Section 1.2, an on-site precast producer survey was conducted. The goal of this survey was to observe fabrication procedures currently in use by the precast industry in the preparation of cold-joint surfaces, as well as discuss lightweight aggregate concrete mixture design techniques. Two PCI producer members provided support for travel to their respective precast plant facilities and allowed documentation for this project.

In the construction of certain precast concrete elements, it can be beneficial to cast certain components in advance to reduce the amount of formwork required and minimize challenges associated with concrete placement. One such element that is commonly cast in advance is a "button corbel." These elements are corbel protrusions that may be included in column or wall elements to support other elements, similar to ledger beams. By casting button corbels in advance, the supporting elements such as columns are able to be cast horizontally, and the corbel can be tied into the main reinforcement of the column. As the concrete in the column element is cast, the corbel is embedded into the concrete matrix on the finished surface. As a result, a simplified set of formwork is able to complete the column element, which does not need to accommodate the protruding corbel. An example of button corbels is shown in Figure 2.10. In the design of these elements, shear friction could be a valuable tool for an engineer. However, due to a lack of test data on direct shear transfer of lightweight aggregate concrete mixtures across a cold-joint interface, these elements are typically designed considering load transfer due to bearing of the lower edge of the corbel. The precast button corbel is embedded in fresh concrete surface at a specified depth allowing a bearing surface at the base of the corbel to be achieved.

To investigate the applicability of the shear friction transfer in these elements, it is critical to replicate the casting procedures and preparations. Many different types of concrete are used in the precast industry, and many different levels of surface roughness are possible. Figure 2.10

shows two examples of the range of surface preparations possible for an element of this type. In the top-left of the figure, the finished surface is nearly form smooth. In contrast, the bottom middle figure shows a similar corbel element that is cast with a much less workable concrete mixture and that is left "as cast" with no finishing procedure. The resulting roughened surface has an amplitude in excess of 0.25 in. specified by the ACI 318 code (2011) and the PCI Design Handbook 7th Edition (2011). It is important to note that these corbels are from two different precast facilities and represent the extreme cases of the interface conditions considered in this study. As a result, this study focused on Case 2 and 3 interface conditions presented in Tables 2.1 and 2.2.

Figure 2.10. Precast facility #1 button corbel (top-left), final placement of corbel (top-right), and precast facility #2 button corbel (bottom)

3. EXPERIMENTAL PROGRAM

3.1. INTRODUCTION

This section summarizes the experimental program including materials used, test specimen design, test specimen fabrication, test setup, and test results. Test results are presented in terms of relations between applied shear force, slip, dilation, and interface steel strain as well as peak and post-peak shear forces. Discussion of the test results and analysis of the data are presented in Section 4.

3.2. SPECIMEN DESIGN

The experimental program included 36 push-off specimens used to investigate the direct shear transfer across an interface of concrete cast at different times. The test variables included concrete unit weight, compressive strength of concrete, and shear interface surface preparation. Three concrete unit weights were used in conjunction with two target compressive strengths and two surface preparations as shown in Table 3.1. Specimen designation notation is shown in Figure 3.1. All specimens had a cold-joint provided along the shear plane of the specimen. The shear plane area was 49.5 in^2. Shear reinforcement consisting of three No. 3 closed tie stirrups was provided normal to the shear plane for all specimens in this study. The resulting reinforcement ratio was approximately 1.33%, which is similar to that used in design of shear elements and results in an upper-bound solution to this investigation.

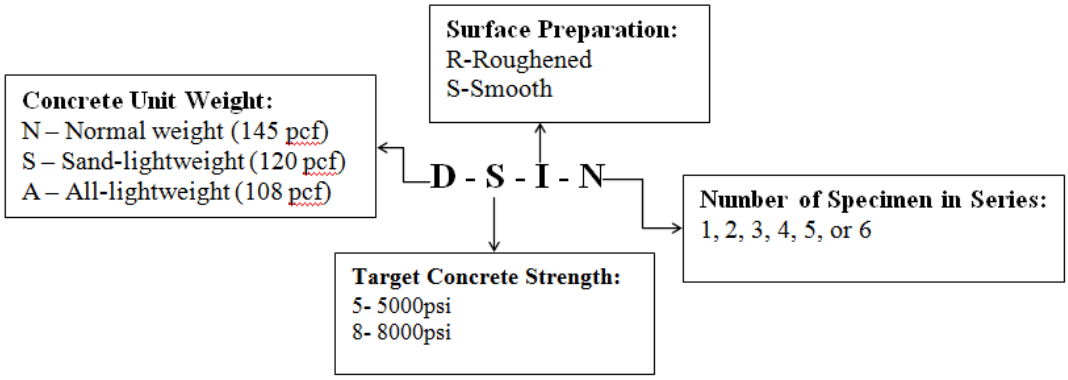

Figure 3.1. Specimen designation notation

Table 3.1. Test Specimen Matrix

Target Compressive Strength	Target Concrete Unit weight	Interface Condition	Specimen ID[1]
5000 psi	145 lb/ft^3	Roughened	N-5-R-4
			N-5-R-5
			N-5-R-6
		Smooth	N-5-S-4
			N-5-S-5
			N-5-S-6
	120 lb/ft^3	Roughened	S-5-R-1
			S-5-R-2
			S-5-R-3
		Smooth	S-5-S-1
			S-5-S-2
			S-5-S-3
	108 lb/ft^3	Roughened	A-5-R-1
			A-5-R-2
			A-5-R-3
		Smooth	A-5-S-1
			A-5-S-2
			A-5-S-3
8000 psi	145 lb/ft^3	Roughened	N-8-R-1
			N-8-R-2
			N-8-R-3
		Smooth	N-8-S-1
			N-8-S-2
			N-8-S-3
	120 lb/ft^3	Roughened	S-8-R-1
			S-8-R-2
			S-8-R-3
		Smooth	S-8-S-1
			S-8-S-2
			S-8-S-3
	108 lb/ft^3	Roughened	A-8-R-1
			A-8-R-2
			A-8-R-3
		Smooth	A-8-S-1
			A-8-S-2
			A-8-S-3

[1] Specimen designation is shown in Figure 3.1

3.3. MATERIALS

The materials used in this study included three types of concrete, namely normalweight concrete, sand-lightweight concrete, and all-lightweight concrete, and reinforcing steel bars. Aggregates

used in the production of the concrete mixtures are summarized in Section 3.3.1, the resulting concrete mixtures are summarized in Section 3.3.2, and reinforcing steel bars are summarized in Section 3.3.3.

3.3.1. Aggregates. This section describes the aggregates used in this program including normalweight and lightweight aggregates.

3.3.1.1. Normalweight aggregates. The normalweight aggregates used in this study included coarse and fine aggregates. The coarse aggregates used were crushed dolomite from the Jefferson City formation, and fine aggregates were natural river sand. Aggregates met standards set by ASTM C33. The coarse aggregate gradation used was selected to consist of 100% passing the 1/2 in. sieve and less than 5% passing the #8 sieve. This gradation is referred to as a 1/2 in. clean washed material. The ASTM C33 designation is a sieve #8.

3.3.1.2. Lightweight aggregates. Lightweight expanded aggregates were used in the production of the sand-lightweight and all-lightweight concrete mixtures discussed in the subsequent sections. The lightweight aggregate used in both the sand-lightweight and all lightweight mixtures was supplied by Buildex Inc. and was an expanded shale product. Specific information regarding the preparation and material properties of the structural lightweight aggregates is presented in the following sections.

3.3.1.2.1. Lightweight aggregate saturation. Lightweight aggregates are inherently susceptible to high absorption values (relative to normalweight aggregates). This is a result of the production procedure used and the resulting high capillary void structure of the aggregates themselves. As a result, it is imperative that lightweight aggregates are saturated to saturated surface dry (SSD) condition prior to batching concrete. While achieving the SSD condition on a small scale is easily done, replicating this procedure for large-scale concrete production can be cumbersome. To achieve total saturation of the aggregates used in this program, a saturation tank was created using a large liquid storage tank pictured in Figure 3.2. The tank was initially filled with the required volume of lightweight aggregate, then water was added to completely cover the material. The tank was allowed to sit undisturbed for a period of 48 hours. After the minimum 48 hour period the tank was then drained using the built in valve assembly. The outflow of the tank was passed over a #200 sieve to ensure any materials inadvertently discharged were filtered from the outflow and returned to the saturation tank.

It is important to note that depending on the gradation of aggregates used, the absorption values can range from slightly less than 10% to over 30%. Also, depending on the type of base material used (shale, slate, or clay) these absorption values can vary as well. This study examines only shale-based materials with two specific ASTM structural gradations discussed in Section 3.3.1.2.2.

Figure 3.2. Aggregate saturation tank

3.3.1.2.2. Lightweight aggregate gradations. The sand-lightweight concrete mixtures in this study included lightweight coarse aggregate. The gradation chosen for coarse aggregate in the sand-lightweight concrete mixtures was an ASTM C330 blended gradation with 100% passing a 1/2 in. sieve and less than 10% passing the #8 sieve. The all-lightweight concrete mixtures in this study included a gradation similar to that used in the sand-lightweight concretes. The selected gradation was a gradation with 100% passing a 1/2 in. sieve and 100% retained on the pan. A complete sieve analysis of these gradations is presented in Table 3.2.

3.3.1.2.3. Lightweight aggregate properties. This section outlines the material properties of the lightweight aggregates used in this program. Table 3.3 presents the specific gravity, dry unit weight, absorption, and saturated density of the two selected lightweight aggregate gradations provided by the manufacturer. The values reported are average production values and were verified in the Concrete Materials Laboratory in the Butler-Carlton Building at Missouri S&T prior to inclusion in this study. An important ASTM C 127/128 deviation to note is the calculation of the percent absorption. Due to the instabilities observed during pumping of expanded aggregates, this standard is not to be used in the determination of the percent absorption at ambient pressures.

Table 3.2. Lightweight Aggregate Gradations

	Sieve Designation	Percent Retained		Percent Passing	
		Gradation	Specification (Note 1)	Gradation	Specification (Note 1)
3/8 in. x No. 8 Gradation	1/2 in.	0	0	100	100
	3/8 in.	1	0-20	99	80-100
	No. 4	82	60-95	18	5-40
	No. 8	99	80-100	1	0-20
	No. 16	99	90-100	1	0-10
3/8 in. x No. 0 Gradation	1/2 in.	0	0	100	100
	3/8 in.	0	0-10	100	90-100
	No. 4	13	10-35	87	65-90
	No. 8	49	35-65	51	35-65
	No. 16	67	-----	33	-----
	No. 30	79	-----	21	-----
	No. 50	86	75-90	14	10-25
	No. 100	93	85-95	7	5-15

1. ASTM C330 structural concrete aggregate gradation.

Table 3.3. Lightweight Aggregate Material Properties

ASTM Gradation	**Bulk Specific Gravity**[1]	**Density**[2] (lb/ft^2)	**Percent Absorption** (%)	**Saturated Density** (lb/ft^2)
3/8 in. x No. 8	1.3	44	20	54
3/8 in. x No. 0	1.45	54	10	65

[1] ASTM C127 / ASTM C128, Bulk Specific Gravity
[2] ASTM C29, Loose unit weight at 6% saturation

3.3.2. Concrete Mixtures. The concrete mixtures used in specimen construction were selected by trial batching a matrix of mixture designs to achieve the desired plastic and hardened concrete properties. Concrete mixtures contained portland cement, water, coarse aggregates, fine aggregates, and high range water reducers (where applicable). Normalweight aggregates used in the production of normalweight and sand-lightweight concretes met or exceeded ASTM C33 specification requirements. All lightweight aggregates used in the production of the sand-lightweight and all-lightweight concretes met or exceeded the requirements set forth by ASTM C330. The sand-lightweight and all-lightweight concrete mixtures were developed based on discussions with precast partners and application of ACI 211.2-98. All concrete mixtures were batched, mixed, and cast in the Concrete Materials Laboratory in Butler-Carlton Hall at Missouri S&T. Mixing was performed in a 6 cubic foot rotary drum mixer shown in Figure 3.3. Mixture proportions are provided in Table 3.4. Additional discussion on the normalweight, sand-lightweight, and all-lightweight mixture designs is provided in Sections 3.3.2.1, 3.3.2.2, and 3.3.2.3 respectively.

The plastic and hardened concrete properties of the selected concrete mixtures are summarized in Table 3.5 and Table 3.6 respectively. Fresh concrete unit weight was determined in accordance with ASTM C138. Air content of normalweight concrete mixtures was determined in accordance with ASTM C231 through the use of the Pressure Method. Air content of mixtures containing lightweight aggregates was determined in accordance with ASTM C173 through use of the Volumetric Method. Figure 3.4 shows photos of the pressure meter and volumetric meter. Slump was determined in accordance with ASTM C143. The concrete compressive strength was determined at 28 days (which also corresponded to the test date of the corresponding test specimens) from three 4 in. x 8 in. cylinders in accordance with ASTM C39. The cylinders were cast and cured in accordance to ASTM C31. Neoprene pads and steel retaining rings were used for compression testing of the cylinders to decrease the influence of surface imperfections created during casting. The compressive strength cylinders were loaded at approximately 500 lbs/sec in the 200-kip Tinius Olsen load frame in the Load Frame Laboratory in Butler-Carlton Hall at Missouri S&T. Split cylinder tests were performed on the day of testing the corresponding test specimens to measure the splitting tensile strength with three 4 in. x 8 in. cylinders at a loading rate of approximately 100 lbs/sec using the same 200-kip Tinius Olsen load frame. Modulus of elasticity was determined in accordance with ASTM C469 using the Tinius Olsen Load Frame and on-board data acquisition. The modulus of elasticity yoke is shown in Figure 3.4. Figure 3.5 shows a photo of the Tinius Olsen load frame used in all material property testing.

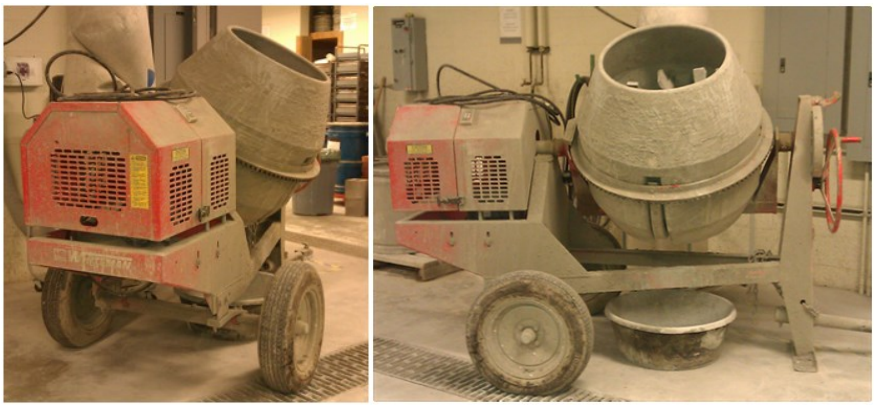

Figure 3.3. Rotary drum mixer

Figure 3.4. Pressure meter, volumetric meter, and modulus of elasticity yoke (from left to right)

Figure 3.5. Tinius Olsen load frame

3.3.2.1. Normalweight concrete. The two normalweight concrete mixture designs for this study included target compressive strengths of 5000 psi and 8000 psi. The target fresh concrete unit weight was 145 lbs/ft^3. The water-cement ratio of the 5000 psi mixture was 0.60, while the water-cement ratio of the 8000 psi mixture was reduced to 0.45 in order to achieve the higher compressive strength. The aggregate used in the production of the normalweight concretes met ASTM C33 Sieve Size 7 gradation requirement (0.5 in. clean). Additional discussion on the aggregates is presented in Section 3.3.1. Mixture proportions are given in Table 3.4. Both normalweight mixtures contained the same nominal size and percentage of coarse aggregates in order to minimize variance in aggregate interlock along the shear friction interface.

3.3.2.2. Sand-lightweight Concrete. The two sand-lightweight concrete mixtures used in this study included target compressive strengths of 5000 psi and 8000 psi. The typical approach for designing the sand-lightweight mixtures was used, which includes the use of lightweight coarse aggregate and normalweight fine aggregate to achieve unit weights from 115 to 120 lbs/ft^3. The target fresh concrete unit weight for the sand-lightweight mixtures was 118 to 120 lbs/ft^3. The lightweight aggregate used for the sand-lightweight mixtures was an expanded shale meeting ASTM C330. The normalweight fine aggregate was ASTM C33. Additional discussion on the aggregates is presented in Section 3.3.1.

In order to proportion the 8000 psi mixture, mixture optimization was performed by maintaining aggregate proportions and adjusting the water-cement ratio with the inclusion of high range water reducers. The high range water reducer used was BASF Glenium 7500 meeting ASTM C494. Cementitious materials were restricted to cement because introduction of replacements, such as silica fume, would result in additional test variables. Mixture proportions are summarized in Table 3.4.

3.3.2.3. All-lightweight Concrete. The two all-lightweight concrete mixtures used in this study included target compressive strengths of 5000 psi and 8000 psi. For typical all-lightweight concrete mixtures, both coarse and fine aggregates are replaced with lightweight aggregates. Although it is possible to achieve mixtures of lower unit weights, the mixtures employed in this study consisted of only portland cement, coarse aggregates, fine aggregates, water, and a high range water reducer. By using only these four materials, comparison can be made among the mixtures without introduction of variables such as chemical admixtures and supplementary cementious materials. The target fresh concrete unit weight for the all-lightweight mixtures was 105 lbs/ft^3. Additional discussion on the aggregates used is presented in Section 3.3.1. Mixture proportions are provided in Table 3.4.

Table 3.4. Concrete Mixture Proportions

Concrete Type and Target Compressive Strength	Mixture Design Quantities (lbs/yd^3) [1]					
	Coarse Aggregate	Fine Aggregate	Water	Cement[5]	HRWR[6] (oz/cwt)	w/c ratio
Normalweight - 5000 psi [2]	1728	1302	310	517	0	0.60
Normalweight - 8000 psi	1728	1146	305	678	2	0.45
Sand Lightweight - 5000 psi [3]	834	1523	281	518	0	0.54
Sand Lightweight - 8000 psi	876	1510	195	650	6	0.30
All-lightweight - 5000 psi [4]	1885		305	726	2	0.42
All-lightweight - 8000 psi	1892		264	800	4	0.33

[1] All weights are for 1 cubic yard of concrete unless indicated otherwise.
[2] Normalweight concrete coarse and fine aggregate were ASTM C33.
[3] Sand-lightweight coarse aggregate is ASTM C330 and fine aggregate were ASTM C33.
[4] All-lightweight concrete coarse and fine aggregates were ASTM C330.
[5] Cement was Type I/II
[6] High range water reducer was BASF Glenium 7500 and was ASTM C494.

Table 3.5. Plastic Concrete Properties

Concrete Type and Target Compressive Strength	Density (lb/ft^3)	Air (%)	Slump (in.)
Normalweight - 5000 psi [1]	147.0	2.5	4.5
Normalweight - 5000 psi [2]	145.0	1.5	5.0
Normalweight - 8000 psi	144.0	2.5	4.0
Sand Lightweight - 5000 psi	118.0	4.5	4.0
Sand Lightweight - 8000 psi	118.0	4.0	5.0
All-lightweight - 5000 psi	108.0	3.5	6.0
All-lightweight - 8000 psi	109.0	4.5	6.0

[1] Batch 1 - Specimens N-5-S-1,2,3 and N-5-R-1,2,3 removed from study.
[2] Batch 2 - Specimens N-5-S-4,5,6 and N-5-R-4,5,6 cast as replacements for Specimens N-5-S-1,2,3 and N-5-R-1,2,3.

Table 3.6. Hardened Concrete Properties

Concrete Type	Target Compressive Strength (psi)	28-Day Compressive Strength (psi)	Compressive Strength at Test Day (psi)	Splitting Tensile Strength (psi)	Modulus of Elasticity (psi)
Normalweight	5000 [1]	5500	5500	410	3900000
Normalweight	5000 [2]	4860	4860	420	3700000
Normalweight	8000	7550	7550	540	3800000
Sand Lightweight	5000	4600	4600	320	3650000
Sand Lightweight	8000	7200	7200	510	3750000
All-lightweight	5000	6080	6080	510	2900000
All-lightweight	8000	7840	7840	520	3300000

[1] Batch 1 - Specimens N-5-S-1,2,3 and N-5-R-1,2,3 removed from study.
[2] Batch 2 - Specimens N-5-S-4,5,6 and N-5-R-4,5,6 cast as replacements for Specimens N-5-S-1,2,3 and N-5-R-1,2,3.

3.3.3. Reinforcing Steel Bars. All reinforcing steel bars used in this experimental program were ASTM A615 Grade 60 provided by Ambassador Steel Corporation. Mill certifications were provided for quality assurance, and properties reported by the manufacturer were verified by conducting tensile tests of representative samples. Reinforcing bar testing was performed in accordance with ASTM A370. The average measured yield stress of the No. 3 and No. 5 bars was determined to be 66,230 psi and 66,470 psi, respectively. Elongation at fracture was determined to be 9.5% and 12% for the No. 3 and No. 5 bars, respectively. Stress-strain plots for the tensile tests are shown in Figure 3.6, in which values of stress were the applied force divided by the nominal cross sectional area of the bar. Values of strain were measured using uniaxial electrical resistance gages attached to the steel reinforcing bar. Strain gages were type EA-06-125UN-120/LE by Vishay Micro-measurements. The strain results were verified using an 8.0 in. extensometer attached to the reinforcing bar, which was removed upon yielding of the specimen. A summary of the measured results is provided in Table 3.7.

Table 3.7. Reinforcing Steel Bar Properties

Specimen ID[1]	Bar ID	Yield Stress (lb/in^2)	Peak Stress (lb/in^2)	Modulus of Elasticity (lb/in^2)	% Elongation at Break
60-5-1	No. 5	68,375	99,250	31,055,000	12.50
60-5-2	No. 5	66,680	99,325	27,110,000	11.75
60-5-3	No. 5	64,360	99,290	23,850,000	12.00
AVERAGE		**66,470**	**99,290**	**29,080,000**	**12.0**
60-3-1	No. 3	67,945	102,540	29,300,000	8.75
60-3-2	No. 3	66,390	101,295	28,520,000	8.75
60-3-3	No. 3	64,360	99,290	29,905,000	10.75
AVERAGE		**66,230**	**101,040**	**29,240,000**	**9.50**

[1] Specimen ID notation; first indicates reinforcement grade, second indicates bar size, and third |indicates specimen number.

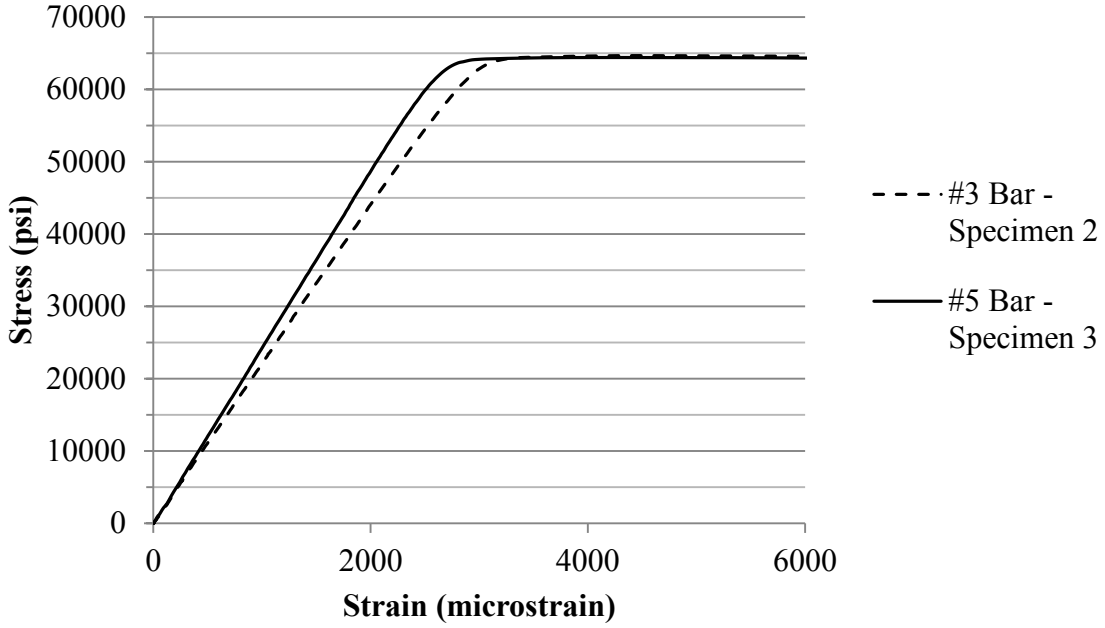

Figure 3.6. Typical stress vs. strain for reinforcing steel bar tensile coupon tests.

3.4. Specimen Fabrication.

Fabrication of specimens took place in the summer and fall of 2012. A total of 45 specimens were cast and tested for the completion of this program including 3 trial specimens and 6 specimens that were omitted and later reconstructed because of undesired failures discussed in Section 3.5.1.

3.4.1. Reinforcing Steel Bar Cage Preparation. Reinforcing steel bar cages were constructed in the High Bay Structural Engineering Research Laboratory at Missouri S&T. Reinforcing bars were ASTM A615 Grade 60 steel as indicated in Section 3.3.3. Each specimen included three No. 3 closed tie stirrups placed normal to the shear plane. As shown in Figure 3.7, these ties were secured to a reinforcing cage that extended into the flange of each side of the element. Reinforcing steel bars used in the elements parallel to the shear plane were No. 5. No. 3 closed ties were used to confine the No. 5 bars within the flange elements. Minimum cover of 0.5 in. was provided at the intended shear plane, and 0.75 in. was provided in the remainder of the specimen. The complete reinforcing steel cage detail is shown in Figure 3.7. Dimensions shown in the figure are measured to the nearest 0.25 in.

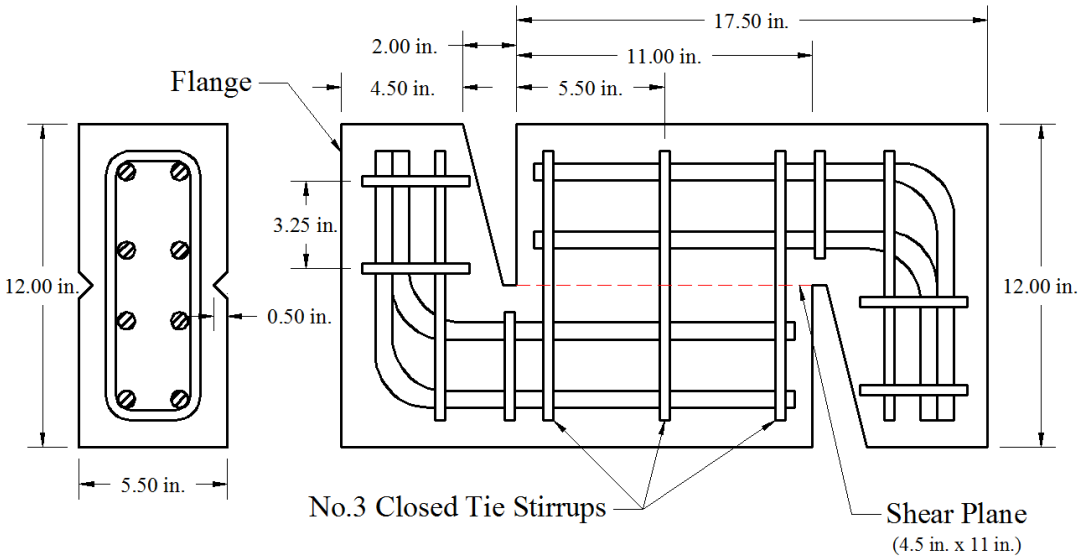

Figure 3.7. Reinforcing steel bar cage detail

3.4.2. Formwork and Assembly. All specimens were cast in two stages to achieve the non-monolithic (cold-joint) condition along the shear plane. Specialized formwork shown in Figure 3.8 was designed and constructed to allow for full exposure of the shear plane in order to complete the required surface preparations. Custom formwork was constructed using 0.75 in. thick grade B plywood, 2 in. by 6 in. lumber, and 0.25 in. thick steel plate for fabrication of inserts. Steel inserts were used to form negative cavities at the ends of the shear plane (see Figure 3.7). These cavities allowed for compression of the specimen and slip of the shear plane of up to 0.5 in. With the exception of the cold-joint, the specimen used in this study was modeled after earlier tests performed by Mattock and Hawkins (1972) in addition to others discussed in Section 2.4. The overall dimensions of the specimen were 12 in. by 24 in. by 5.5 in. The shear plane area was approximately 49.5 in.^{2}, which is consistent with previous research.

Figure 3.8. Test specimen formwork

3.4.3. Concrete Placement and Shear Interface Preparation. Casting of specimens for this program required the formation a cold-joint condition along the shear plane. To achieve the cold-joint, specimens were cast in two lifts, and the interface between the lifts was either

trowelled smooth or roughened to 0.25 in. amplitude as specified in both the ACI 318 code (2011) and the PCI Design Handbook 7th Edition (2011). Placement of the second lift was completed a minimum of eight hours after placement of the first lift. A specialized instrument shown in Figure 3.9 was fabricated to accomplish roughening of the shear plane. This instrument was made of a 0.1875 in. aluminum rod that was bent 90 degrees at the end. The instrument was used to score the surface of the shear interface in the direction perpendicular to the direction of loading (see Figure 3.9). The cross-section of the score was vee-shaped with scoring occurring at approximately 1 in. intervals. The roughening procedure was completed approximately three hours after casting to allow initial set of the concrete to occur. After roughening was completed the interface was cleaned with compressed air before measuring the surface roughness. Depth of the roughened surface amplitude was measured in 10 locations selected at random on the shear plane as shown in Figure 3.10. The average of these measurements, taken as shown in Figure 3.10, for each specimen is presented in Table 3.8. The average value of measured scoring line depth, that is, its measure of roughness, ranged between 0.245-0.254 in. for all specimens with a roughened interface.

Figure 3.9. Specialized roughening instrument and technique

Figure 3.10. Surface roughness measurement

Table 3.8. Average Measured Surface Roughness

Smooth Specimens		Roughened Specimens	
Specimen Series	**Average Surface Roughness (in.)**	**Specimen Series**	**Average Surface Roughness (in.)**
N-5-S	N/A (0.0)	N-5-R	0.245
S-5-S	N/A (0.0)	S-5-R	0.247
A-5-S	N/A (0.0)	A-5-R	0.254
N-8-S	N/A (0.0)	N-8-R	0.249
S-8-S	N/A (0.0)	S-8-R	0.250
A-8-S	N/A (0.0)	A-8-R	0.250

3.4.4. Curing. To reduce the introduction of environmental variables, all specimens in this program were cured in a 100 percent humidity and 70 degree Fahrenheit environment. Each specimen was initially covered with moist burlap and plastic for 24 hours after which time it was removed from the forms, marked, and placed in the moist-cure environment. The specimens were maintained in the moist cure environment for the full 28-days prior to testing. On the day of

testing, specimens were removed from the moist-cure environment. Casting and test dates are summarized in Table 3.9.

Table 3.9. Specimen Casting and Test Dates

Specimen Series	Concrete Placement Date	Test Date	Age at Test Date (days)
N-5-R-4,5,6[1]	12/18/2012	1/15/2013	28
N-5-S-4,5,6[1]	12/18/2012	1/15/2013	28
N-8-R	9/15/2012	10/12/2012	28
N-8-S	9/15/2012	10/12/2012	28
S-5-R	7/26/2012	8/22/2012	28
S-5-S	7/26/2012	8/22/2012	28
S-8-R	11/21/2012	12/18/2012	28
S-8-S	11/21/2012	12/18/2012	28
A-5-R	8/28/2012	9/24/2012	28
A-5-S	8/28/2012	9/24/2012	28
A-8-R	12/10/2012	1/7/2013	28
A-8-S	12/10/2012	1/7/2013	28

[1] Specimens N-5-R-4,5,6 and N-5-S-4,5,6 were constructed to replace specimens N-5-R-1,2,3 and N-5-S-1,2,3 due to failures discussed in Section 3.5.1

3.5. TEST SETUP

Previous studies on shear friction have utilized different specimen sizes, support conditions, loading conditions, and initial conditions of the shear plane interface as discussed in Section 2.4. Special considerations must be made for each condition with regards to testing procedure. Therefore, in developing the test setup for this study, several specimens were constructed to perform trial testing to confirm the support conditions and data acquisition. This section describes the test setup including the support conditions, loading protocol, types of measurements taken, and loading procedure. Included in this section is a discussion of changes made to the original test setup to mitigate issues that developed during testing.

3.5.1. Support Conditions. The first trial tests conducted included a hemispherical head allowing rotation at the top of the specimen and a roller setup at the base of the specimen as shown in Figure 3.11. The roller system was included to allow lateral translation of the specimen and to provide concentric application of load. To provide uniform bearing a set of neoprene pads with a durometer of 40 was provided at the locations of bearing. A similar setup was used in prior research performed by Hofbeck et al. (1969) and others. In addition to monitoring dilation and slip of the shear interface, the lateral translation of the roller system was monitored. The trial specimens tested included normalweight 5000 psi specimens with smooth and roughened interfaces. Testing of the smooth interface specimens resulted in failures as expected along the shear plane. Issues with this setup were uncovered when testing the specimens with roughened interfaces. These specimens achieved significantly higher loads than their smooth interface specimen counterparts, and failures occurred in the flanges of the specimens prior to shear plane failure. An example of this type of failure is shown in Figure 3.12. The problems were attributed

to specimen geometry (shear plane area) and high interfacial shear friction, which resulted in higher than expected shear forces required to cause the direct shear failure intended. Thus premature failure occurred outside of the shear interface, which prompted a modification to the support fixity.

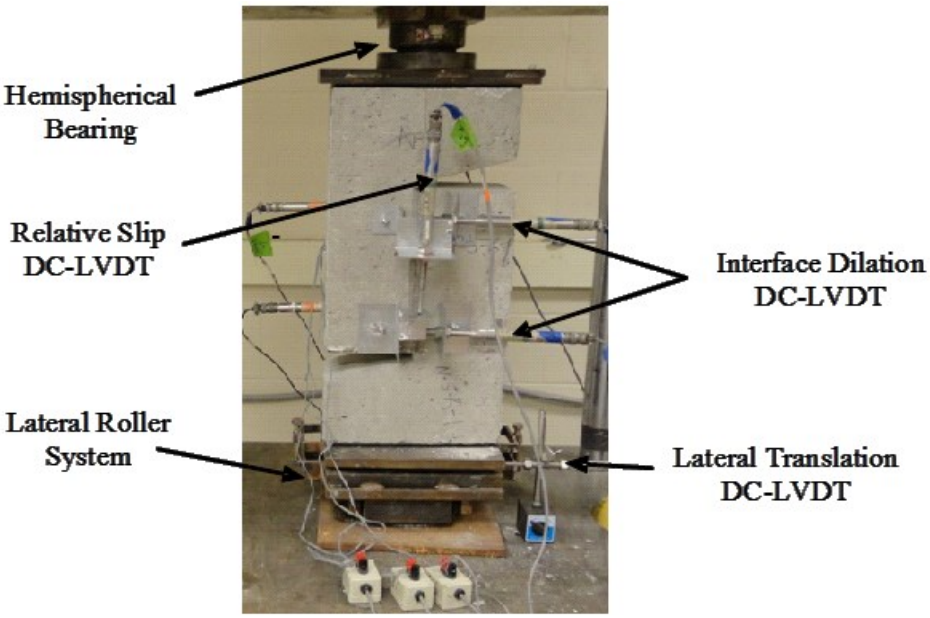

Figure 3.11. Initial specimen fixity conditions and instrumentation

Figure 3.12. Premature flange failure

Failures resulting from the pin-roller fixity condition were mitigated by removing the roller system. The removal of the roller system was justified due to minimal lateral translation measured prior to flexural cracking of the flange shown in Figure 3.12. It was observed during testing that the specimen began to translate laterally once the flexural cracks occurred, which

further exacerbated the eccentricity of loading. The result was unequal distribution of loading at both the top and bottom locations of bearing. By removing the lateral roller at the base of the specimen, uniform distribution of the load was maintained, and the eccentricity of the loading minimized. With subsequent trials the premature flange failure shown in Figure 3.12 was minimized but not entirely eliminated. To further improve the test setup, a primary prestressing system was implemented to provide confinement of the flange normal to the shear interface. This system is detailed in Section 3.5.3.1.

3.5.2. Loading Protocol. The testing frame used in the study was the 200-kip Tinius Olsen Load Frame located in the Missouri S&T Load Frame Laboratory. For this experimental program, all specimens were tested under displacement control at a rate of 0.015 in. per minute. Specimens were tested until one of the following conditions occurred: a target slip of 0.3 in. was reached, or a sudden and significant drop in applied load occurred. Previous researchers have investigated different initial conditions of the shear interface, including uncracked (monolithic casting), pre-cracked (monolithic casting), and cracked (non-monolithic casting). In the case of the pre-cracked interface condition, a force is applied as a line load parallel to the plane of the shear interface to develop a crack in the interface prior to loading of the specimen. Although this condition is commonly employed in aggregate interlock investigations, it is not consistent with the objective of this study. Thus, specimens investigated in this program were not pre-cracked. However, all specimens in this program had a construction joint at the shear interface.

3.5.3. Flange Prestressing/Confinement Systems. Failures exhibited by the trial specimens described in Section 3.5.1 prompted the development of prestressing systems to provide confinement of the flange elements of the specimen normal to the shear plane. A primary prestressing system, described in Section 3.5.3.1, was used in all tests, and a secondary system, described in Section 3.5.3.2, was used in the all-lightweight 8000 psi roughened specimens (Series A-8-R) as well as the normalweight 5000 psi roughened specimens (Series N-5-R). The inclusion of the secondary system for the normalweight 5000 psi roughened specimens was only precautionary. A complete record of the confinement system(s) used for each specimen is provided in Table 3.10. The confinement systems are described below.

3.5.3.1. Primary flange prestressing/confinement system. With the flange failures resulting in premature failures of the trial specimens, the primary prestressing system was developed as shown in Figure 3.13. The confinement system provided active confinement to the flanges of the specimen. Each all-thread rod was subjected to a torque of 50 lb-ft, which provided a clamping force of approximately 8,000 lbs or the equivalent precompression stress of 325 psi to the flange element. This procedure ensured the same level of prestressing was applied to all specimens. To ensure minimal effects to the shear plane, the strain in the reinforcing bars crossing the shear plane (discussed in Section 3.5.4) was monitored during the prestressing operation. The difference in strain before and after application of the prestressing systems was less than 50 microstrain. It should be noted that this value is within the noise of the data acquisition system for low level strain readings, and thus it was determined to be minimal.

3.5.3.2. Secondary flange prestressing/confinement system. When testing the last two sets of specimens, flange failures once again occurred influencing the peak load and post peak

behavior of the 8000 psi all-lightweight roughened interface specimens (Series A-8-R). After significant consideration, an additional prestressing system was included to provide confinement of the specimen flange in the direction perpendicular to the precompression provided by the primary system described in Section 3.5.3.1. The secondary system consisted of 0.5 in. thick steel plates that were clamped in place using 2 in. by 2 in. structural steel angle on the back face of the specimen and bolts mounted on the front face of the specimen. The secondary system was intended to be a passive system only to provide confinement of the flange in the event of a failure of the concrete cover. This system is shown in Figure 3.13.

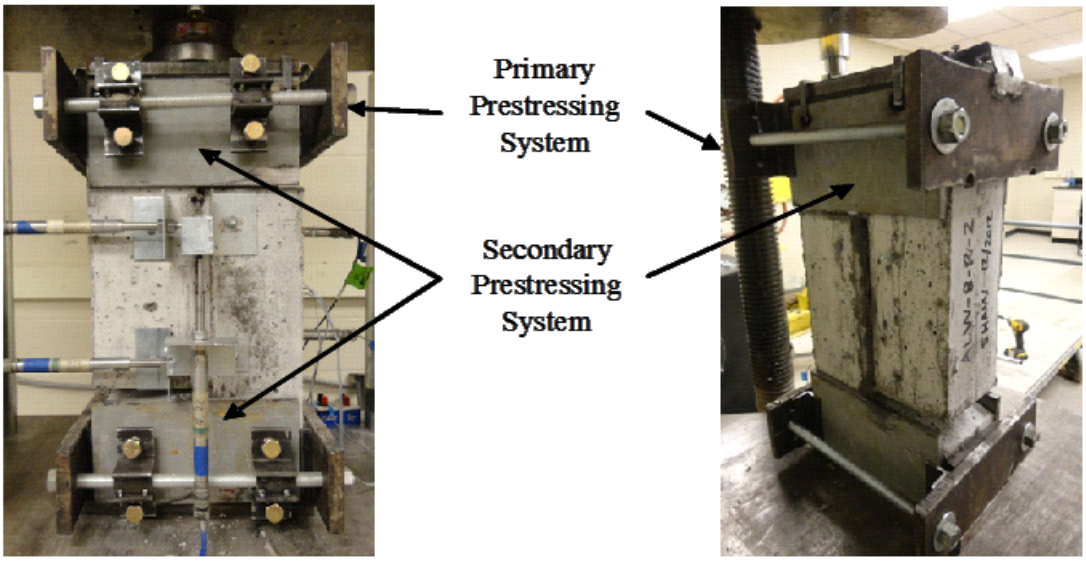

Figure 3.13. Primary and secondary flange confinement systems

Table 3.10. Prestressing System Application

Specimen ID	Failure Mode	Prestressing System	
		Primary	Secondary
N-5-S-1	Bearing/Flexure of Flange	Yes	No
N-5-S-2	Shear	Yes	No
N-5-S-3	Bearing/Flexure of Flange	Yes	No
N-5-S-4	Shear	Yes	No
N-5-S-5	Shear	Yes	No
N-5-S-6	Shear	Yes	No
N-5-R-1	Bearing/Flexure of Flange	Yes	No
N-5-R-2	Bearing/Flexure of Flange	Yes	No
N-5-R-3	Bearing/Flexure of Flange	Yes	No
N-5-R-4	Shear	Yes	Yes
N-5-R-5	Shear	Yes	Yes
N-5-R-6	Shear	Yes	Yes
S-5-S-1	Shear	Yes	No
S-5-S-2	Shear	Yes	No
S-5-S-3	Shear	Yes	No
S-5-R-1	Shear	Yes	No
S-5-R-2	Shear	Yes	No
S-5-R-3	Shear	Yes	No
A-5-S-1	Shear	Yes	No
A-5-S-2	Shear	Yes	No
A-5-S-3	Shear	Yes	No
A-5-R-1	Shear	Yes	No
A-5-R-2	Shear	Yes	No
A-5-R-3	Shear	Yes	No
N-8-S-1	Shear	Yes	No
N-8-S-2	Shear	Yes	No
N-8-S-3	Shear	Yes	No
N-8-R-1	Shear	Yes	No
N-8-R-2	Shear	Yes	No
N-8-R-3	Shear	Yes	No
S-8-S-1	Shear	Yes	No
S-8-S-2	Shear	Yes	No
S-8-S-3	Shear	Yes	No
S-8-R-1	Shear[1]	Yes	No
S-8-R-2	Shear[1]	Yes	No
S-8-R-3	Shear[1]	Yes	No
A-8-S-1	Shear	Yes	No
A-8-S-2	Shear	Yes	No
A-8-S-3	Shear	Yes	No
A-8-R-1	Shear[1]	Yes	No
A-8-R-2	Shear	Yes	Yes
A-8-R-3	Shear	Yes	Yes

[1] Bearing/Flexure of flange occurred after peak shear force was achieved.

3.5.4. Data Acquisition and Instrumentation. Originally there were twelve data channels that were subsequently reduced to eleven with the removal of the roller system as described in Section 3.5.1. Of the eleven channels, six were displacement measured with direct current-linear variable differential transducers (DC-LVDTs), three were strain measured with uniaxial strain gages, and the remaining two were load and global displacement reported from the on-board load cell of the Tinius Olsen load frame. Both the front and back faces of the specimens were instrumented as shown in Figure 3.14. Data were acquired at a rate of 1 sample per second. All channels were monitored during the loading procedure to ensure accuracy of the testing program and to document any anomalies observed during testing.

3.5.4.1. Direct Current-LVDTs. Direct current-linear variable differential transducers (DC-LVDTs) were used to monitor dilation, slip, and displacement. Specimens were instrumented with two DC-LVDTs located at the top and bottom of the shear plane, on the front face of the test specimen, to monitor dilation of the interface. A third DC-LVDT was used to measure slip of the interface throughout the loading procedure. This arrangement was mirrored on the back face of the specimen. All DC-LVDTs used in this program had a +/- 0.5 in. stroke. In order to facilitate mounting of the DC-LVDTs, a specialized attachment system was developed. Each set of specimen formwork had integral mounting bolts positioned to provide consistent mounting of DC-LVDTs. The integral mounting bolts are shown in Figure 3.15. One additional DC-LVDT was used to monitor the lateral translation of the roller support during trial testing only. This DC-LVDT is shown in Figure 3.14 although it was removed in later tests as discussed in Section 3.5.1.

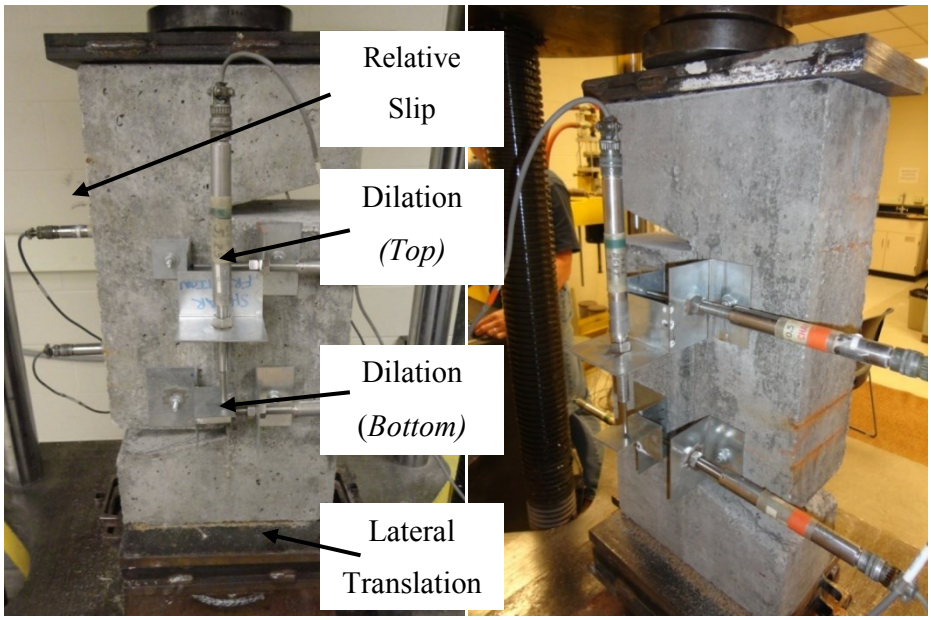

Figure 3.14. DC-LVDT instrumentation setup

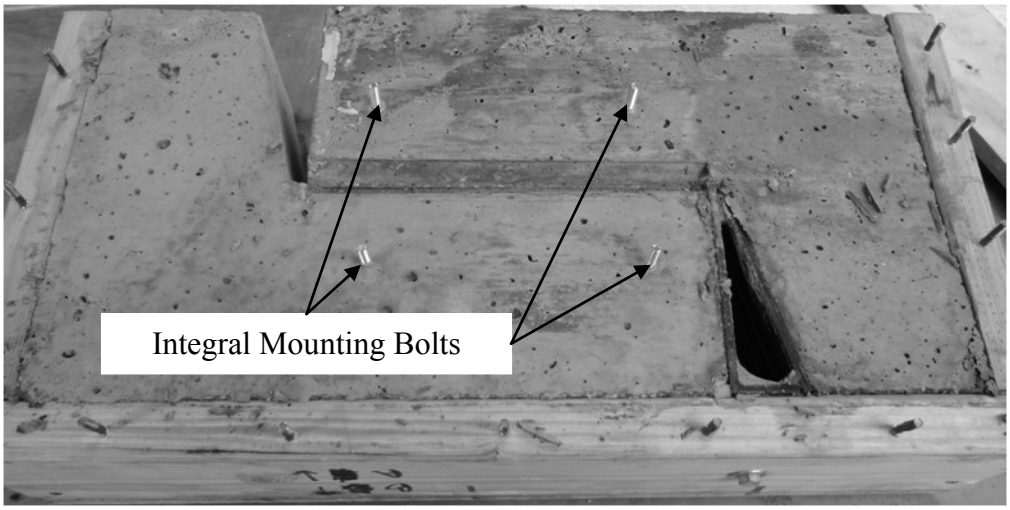

Figure 3.15. DC-LVDT integral mounting bolts

3.5.4.2. Strain gages. The same type of uniaxial electronic resistance strain gages (Vishay Micro-measurements EA-06-125UN-120/LE) were used on all of the reinforcing bars in this program, including reinforcing bar tensile testing discussed in Section 3.3.3. One strain gage was applied per the manufacturer's instructions to one leg of each of the stirrups crossing the shear interface. The strain gages were mounted to the exterior side face of the bars as shown in Figure 3.16. Care was taken to leave as much cross sectional area on the stirrup reinforcing bar while providing enough room for a smooth flat area for the strain gage to ensure adequate bond. After the strain gage was applied, a protective covering was placed over the strain gage (see Figure 3.16) to protect it from moisture or damage during placement of concrete. Special care was taken to ensure the gage was centered on the intended shear interface. Operation of all gages was verified after attachment and prior to concrete placement. However, gages in several specimens were damaged during interface preparation. All specimens had at least one functioning strain gage at the time of testing.

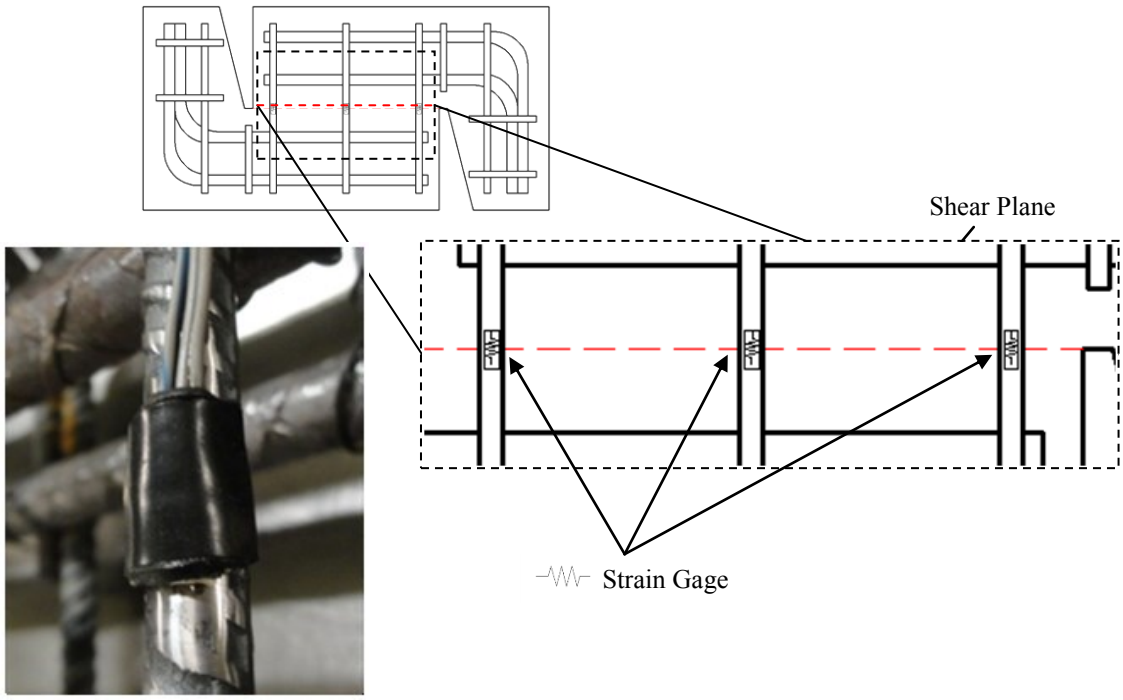

Figure 3.16. Strain gage protection and locations

3.6. TEST RESULTS

This section outlines the results obtained from the experimental program presented in this study. Critical values recorded for each specimen include peak (ultimate) applied load (shear force) V_u, slip at peak load, dilation at peak load, and residual load (shear force) V_{ur}. Residual load is defined as the load corresponding to a slip of 0.15 in. This slip value corresponds to maximum slip and before the effects of dowel action influence the load carrying capacity of the specimen, where the interface maintains the transfer of the applied load. Data presented for each series include the following relations: shear force-slip, shear force-dilation, stress-strain, slip-dilation, and shear force-dilation. Values of slip reported are the averages of the values measured on both faces of the specimen. Values of dilation reported are first averaged for the locations on each face and then averaged for both faces of the specimen. The strain values reported are the average of all functioning strain gages. A summary of testing results is provided in Table 3.11. In the table, shear stresses v_u and v_{ur} are defined as the corresponding shear force divided by the area of the shear plane (49.5 in^2). Discussion of the test results and analysis of the data reported within this section are presented in Section 4.

Table 3.11. Summary of Testing Results

Specimen ID	f'_c at test day (psi)	V_u (lbs)	v_u[1] (psi)	$v_{u,\,avg}$ (psi)	Slip at V_u (in)	Dilation at V_u (in)	V_{ur}[2] (lbs)	v_{ur}[1] (psi)	$v_{ur,\,avg}$ (psi)	$\left(\frac{v_u}{v_{ur}}\right)_{avg}$
N-5-R-4	4860	59060	1190	1115	0.013	0.007	39470	800	790	1.41
N-5-R-5	4860	53420	1080		0.010	0.006	40140	810		
N-5-R-6	4860	53440	1080		0.012	0.007	38360	770		
N-5-S-4	4860	32705	660	680	0.057	0.015	38150	770	683	1.06
N-5-S-5	4860	34680	700		0.022	0.008	31150	630		
N-5-S-6	4860	39155	790		0.031	0.007	32000	650		
S-5-R-1	4550	51430	1040	1117	0.010	0.007	30500	620	603	1.85
S-5-R-2	4550	50395	1020		0.014	0.008	29600	600		
S-5-R-3	4550	63905	1290		0.022	0.007	29300	590		
S-5-S-1	4550	38530	780	757	0.019	0.006	33200	670	610	1.24
S-5-S-2	4550	34110	690		0.016	0.003	27900	560		
S-5-S-3	4550	39795	800		0.021	0.007	29500	600		
A-5-R-1	6080	48440	980	1030	0.010	0.005	35000	710	800	1.29
A-5-R-2	6080	52800	1070		0.011	0.005	43000	870		
A-5-R-3	6080	51410	1040		0.013	0.004	40500	820		
A-5-S-1	6080	41470	840	813	0.021	0.006	38500	780	727	1.13
A-5-S-2	6080	40080	810		0.023	0.005	32000	650		
A-5-S-3	6080	39250	790		0.032	0.007	37000	750		
N-8-R-1	7550	74040	1500	1310	0.010	0.008	47500	960	873	1.50
N-8-R-2	7550	56090	1130		0.008	0.005	39050	790		
N-8-R-3	7550	64140	1300		0.007	0.005	43000	870		
N-8-S-1	7550	65570	1320	1173	0.010	0.006	49500	1000	937	1.25
N-8-S-2	7550	53305	1080		0.010	0.005	42950	870		
N-8-S-3	7550	55330	1120		0.001	0.006	46695	940		
S-8-R-1	7210	72045	1460	1390	0.007	0.006	43660	880	805	1.76
S-8-R-2	7210	67380	1360		0.010	0.006	36300	730		
S-8-R-3	7210	66725	1350		0.006	0.005	N/A	N/A		
S-8-S-1	7210	67025	1350	1237	0.007	0.006	44480	900	820	1.51
S-8-S-2	7210	57880	1170		0.005	0.003	36970	750		
S-8-S-3	7210	58865	1190		0.018	0.007	40340	810		
A-8-R-1	7845	61775	1250	1280	0.009	0.003	41330	830	853	1.51
A-8-R-2	7845	63935	1290		0.008	0.007	45800	930		
A-8-R-3	7845	64125	1300		0.009	0.006	39450	800		
A-8-S-1	7845	46090	930	983	0.011	0.004	37790	760	807	1.22
A-8-S-2	7845	48035	970		0.012	0.006	40185	810		
A-8-S-3	7845	51740	1050		0.012	0.004	42140	850		

[1] Shear stresses *vu* and *vur* are defined as the applied shear load divided by the area of the shear plane (49.5 in^2).

[2] Residual load, *Vur*, is defined as the load at 0.15 in. of slip as discussed in Section 3.6.

[3] Specimens N-5-R-1,2,3 and N-5-S-1,2,3 are not included in due to incomplete testing results.

3.6.1. Normalweight Concrete Specimens. This section presents information regarding the normalweight concrete specimens tested in this program.

3.6.1.1. 5000 psi specimens. Specimens presented in this section include Series N-5-S and N-5-R. Testing of specimens N-5-R-1,2,3 and N-5-S-1,2,3 occurred on 6/28/2012. Specimens N-5-R-4,5,6 and N-5-S-4,5,6 were tested on 1/15/2013. N-5-S-1,3 and N-5-R-1,2,3 are omitted from this discussion because they exhibited premature flange failures as discussed in Section 3.5.1. Specimen N-5-S-2 was also discarded since the companion specimens were omitted. Therefore, the results of specimens N-5-S-4,5,6 and N-5-R-4,5,6 are presented herein. For specimens presented, no unforeseen failures or inconsistent results were recorded. Figure 3.17 shows the applied shear versus slip relations. Figure 3.18 shows the applied shear versus interface dilation relations. Figure 3.19 shows the slip versus dilation relations. Figure 3.20 shows the applied shear versus steel strain relations. Figure 3.21 shows the slip versus interface steel relations.

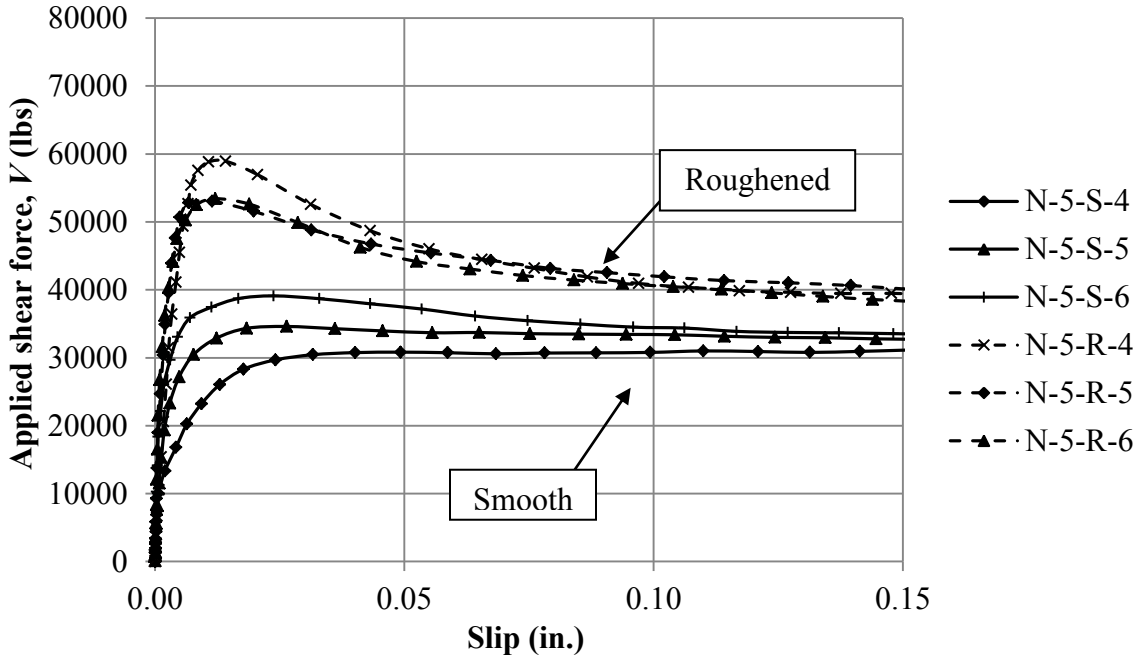

Figure 3.17. Applied shear force vs. slip relations for 5000 psi normalweight concrete specimens.

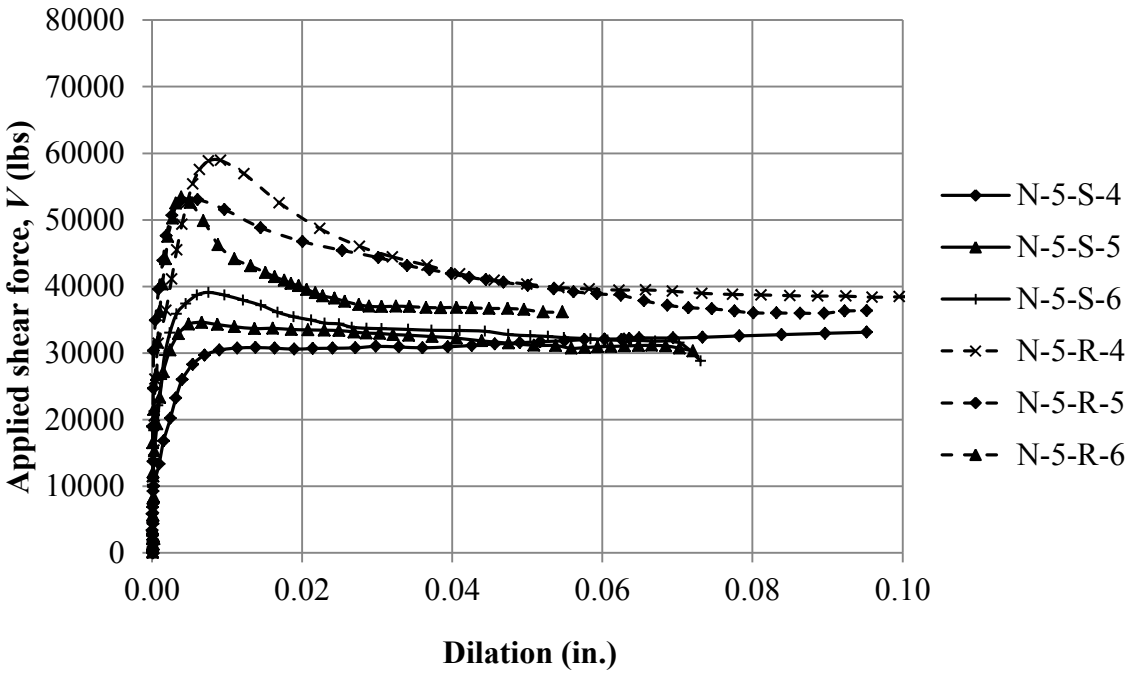

Figure 3.18. Applied shear force vs. interface dilation for 5000 psi normalweight concrete specimens.

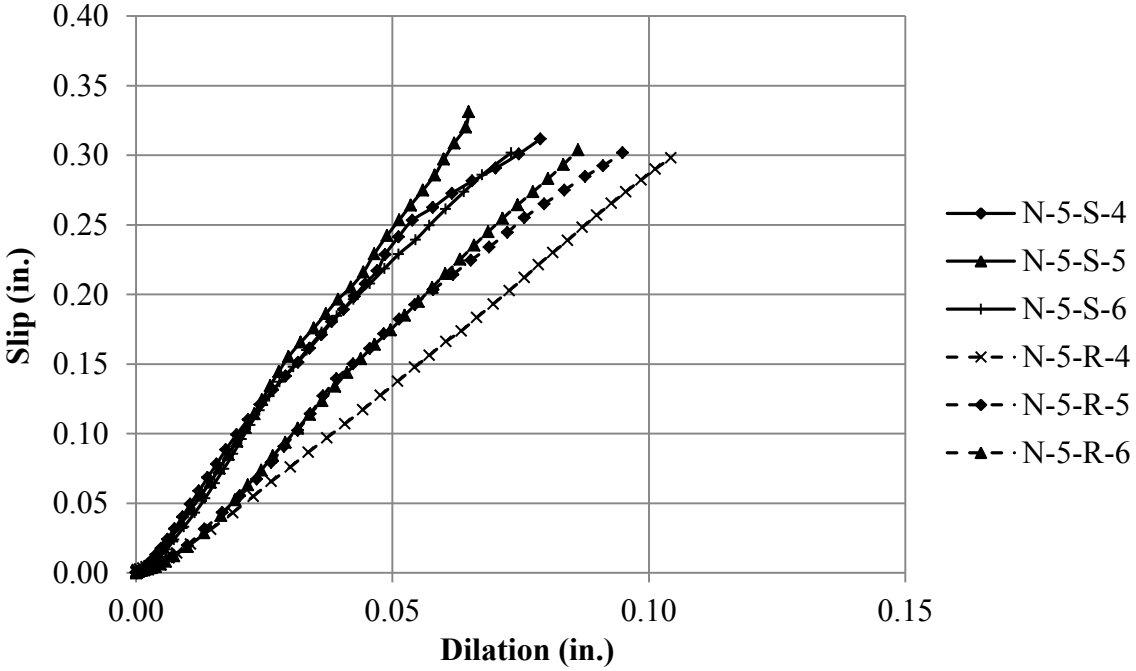

Figure 3.19. Slip vs. dilation for 5000 psi normalweight concrete specimens.

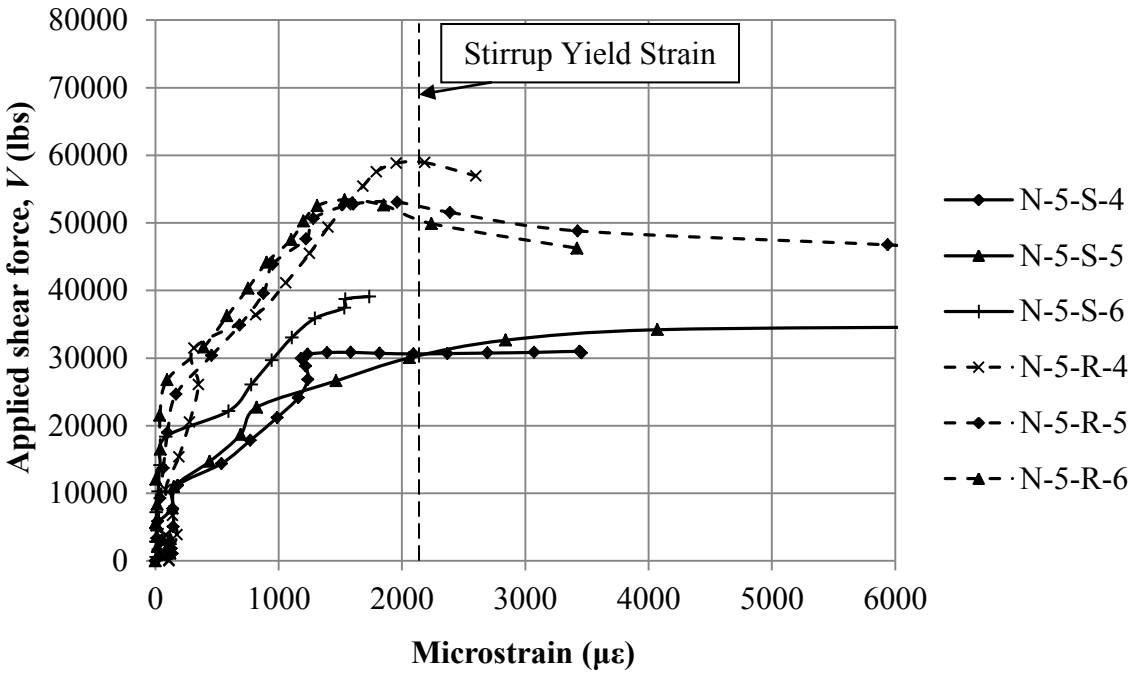

Figure 3.20. Applied shear force vs. interface steel strain for 5000 psi normalweight concrete specimens.

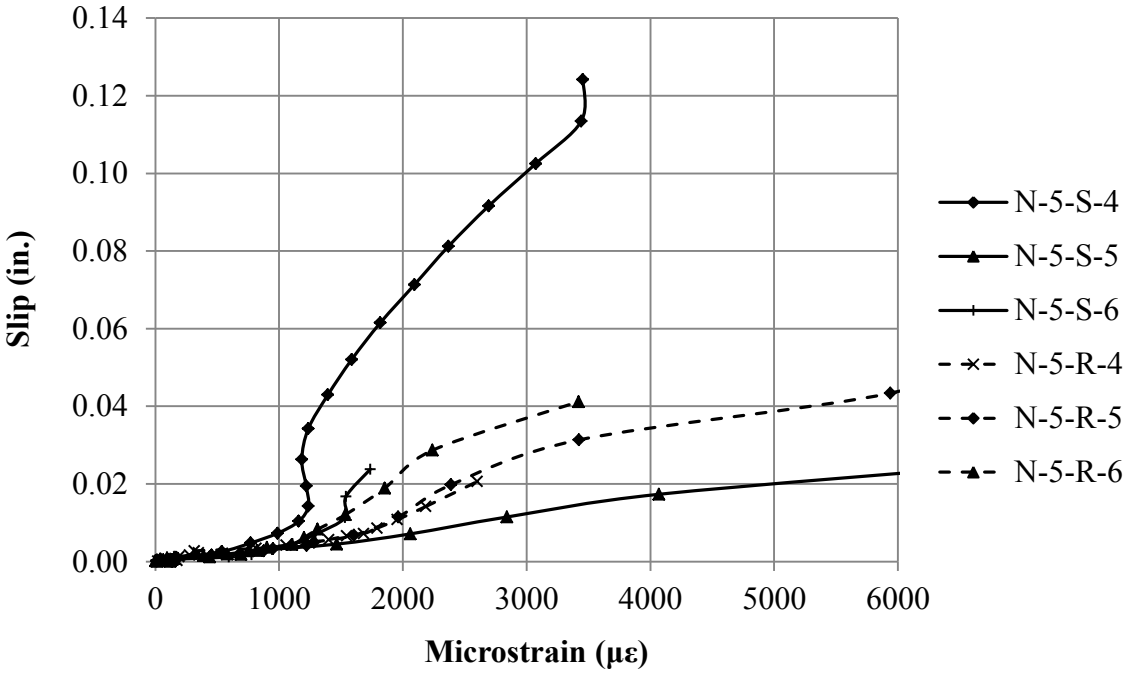

Figure 3.21. Slip vs. interface steel strain for 5000 psi normalweight concrete specimens.

3.6.1.2. 8000 psi specimens. Specimens presented in this section include series N-8-S and N-8-R. The testing was performed on 10/12/2012. All specimens exhibited the intended shear plane failure and expected post-peak behavior. Results are shown in Figure 3.22 through Figure 3.26. Figure 3.22 shows the applied shear versus slip relations. Figure 3.23 shows the applied shear versus interface dilation relations. Figure 3.24 shows the slip versus dilation relations. Figure 3.25 shows the applied shear versus steel strain relations. Figure 3.26 shows the slip versus interface steel relations.

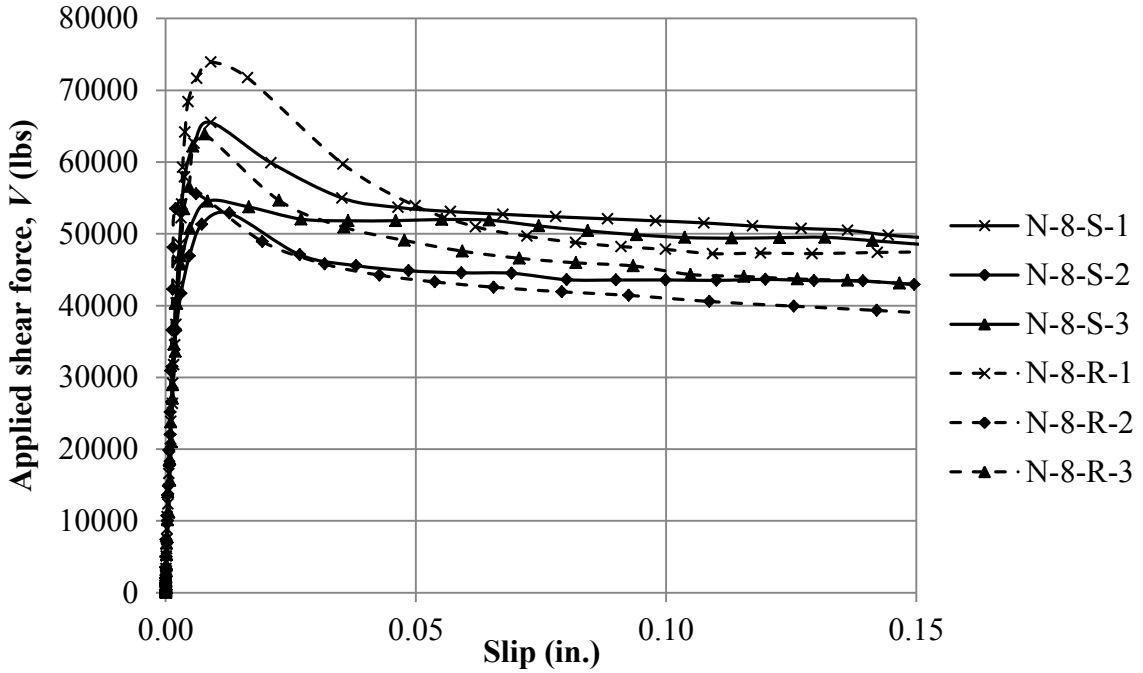

Figure 3.22. Applied shear force vs. slip relations for 8000 psi normalweight concrete specimens.

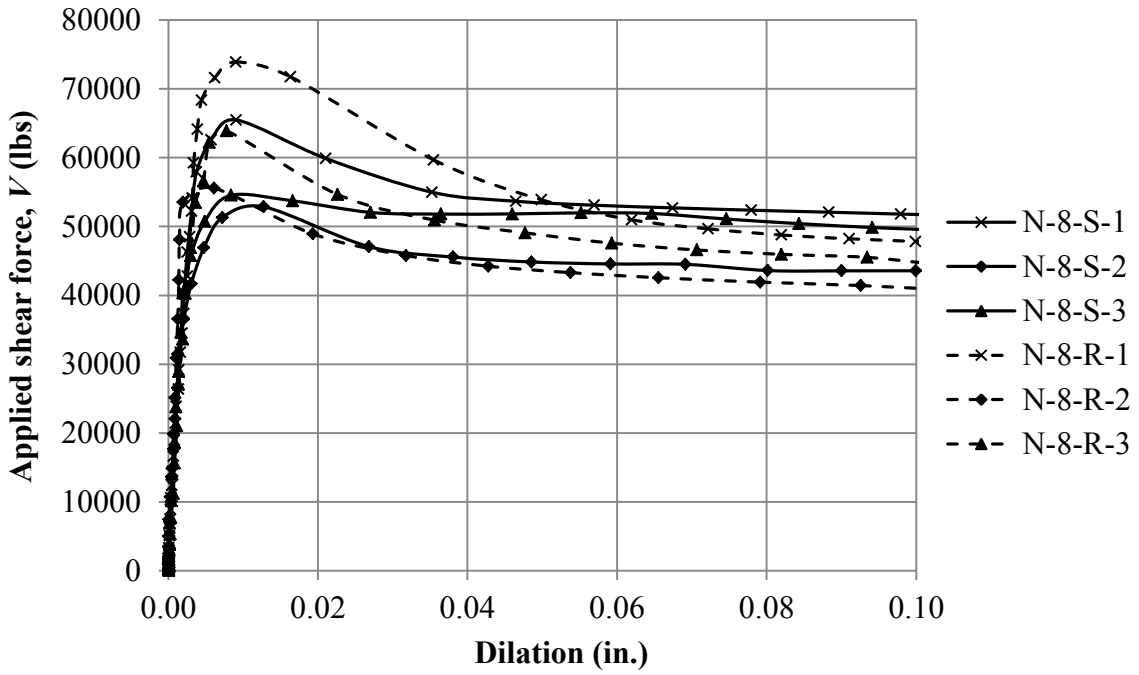

Figure 3.23. Applied shear force vs. interface dilation for 8000 psi normalweight concrete specimens.

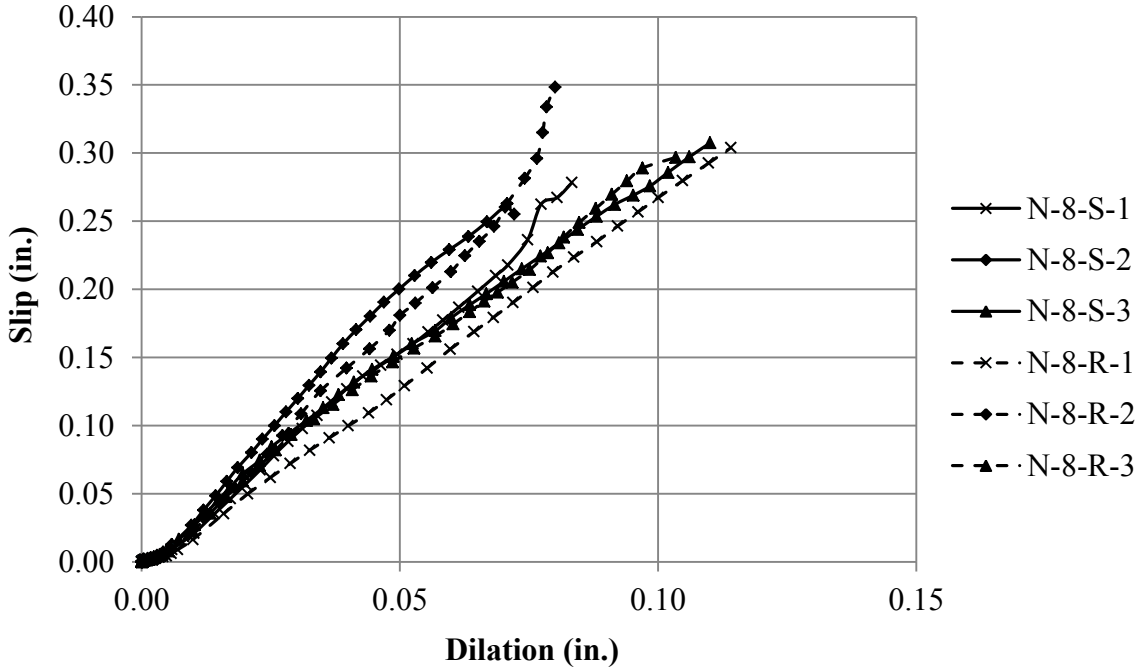

Figure 3.24. Slip vs. dilation for 8000 psi normalweight concrete specimens.

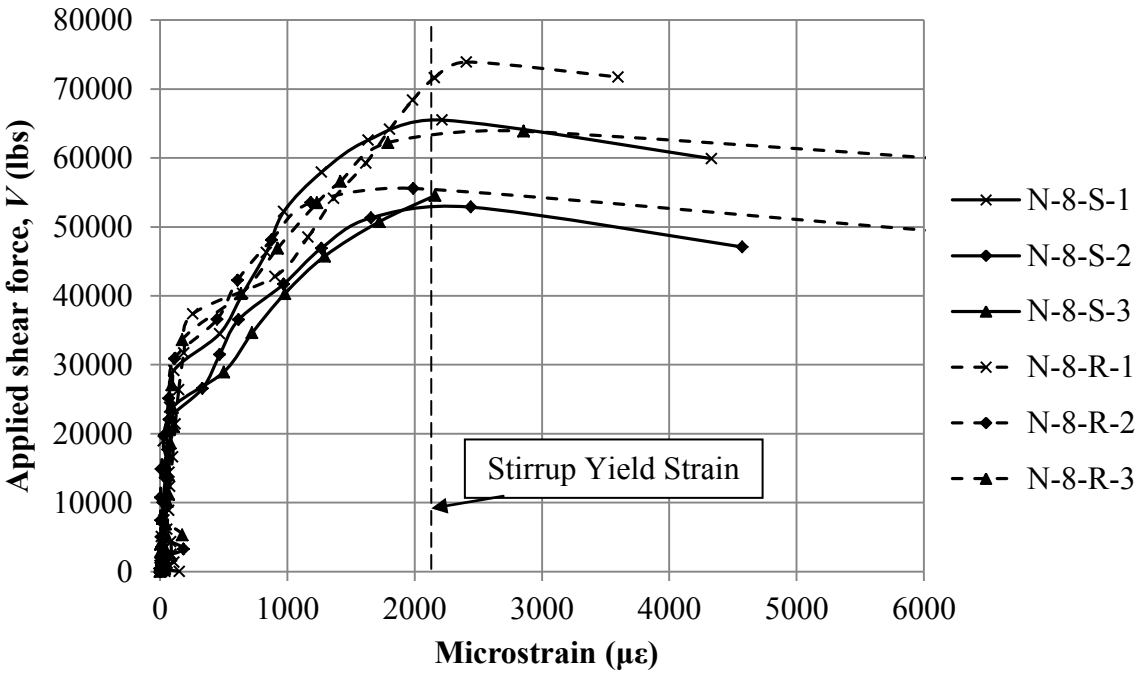

Figure 3.25. Applied shear force vs. interface steel strain for 8000 psi normalweight concrete specimens.

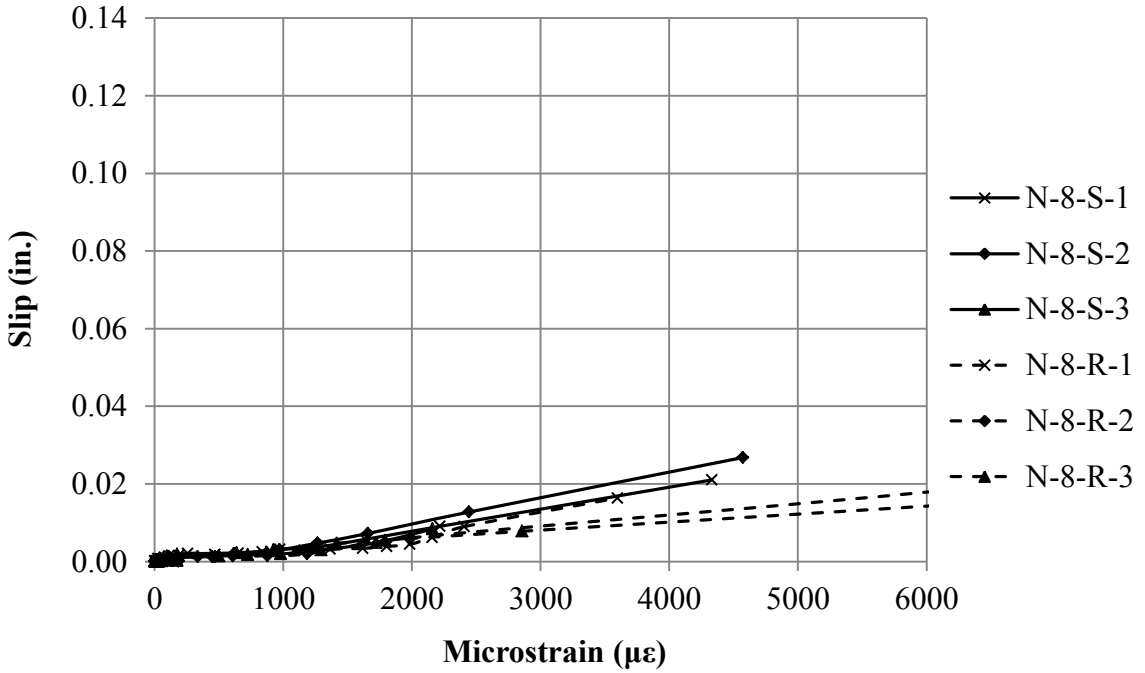

Figure 3.26. Slip vs. interface steel strain for 8000 psi normalweight concrete specimens.

3.6.2. Sand-lightweight Concrete Specimens.

3.6.2.1. 5000 psi specimens. Testing of the 5000 psi sand-lightweight specimens was performed on 8/22/2012. The behavior of the 5000 psi sand-lightweight concrete specimens is shown in Figure 3.27 through Figure 3.31. No unexpected failures or inconsistent results were observed except for specimen S-5-R-3. Specimen S-5-R-3 exhibited a softening of the section's response at the onset of shear interface cracking. As seen in Figure 3.27, at an applied shear force of approximately 30,000 lbs (applied shear stress of approximately 600 psi) the slope of the applied load versus slip plot decreased for this specimen, and the load dropped sharply after peak load. This behavior is attributed to cracking of the flange both parallel and perpendicular to the shear plane. The behavior is can also be observed in the slip versus dilation response shown in Figure 3.29. Figure 3.30 shows the applied shear versus steel strain relations. Figure 3.31 shows the slip versus interface steel relations.

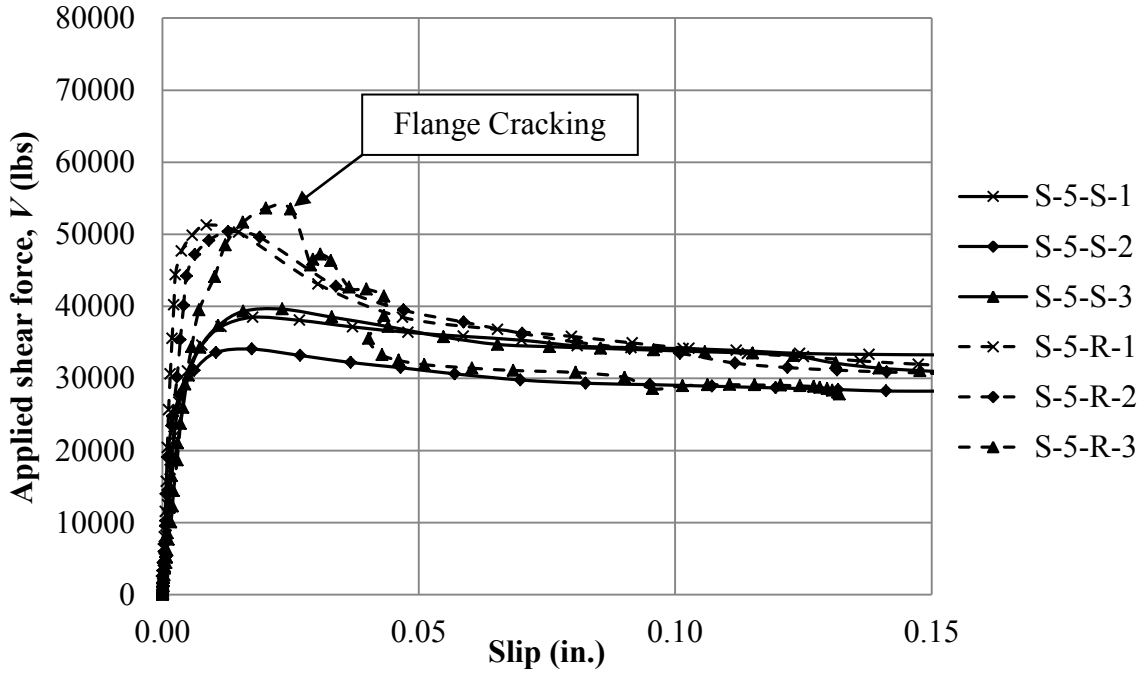

Figure 3.27. Applied shear force vs. slip relations for 5000 psi sand-lightweight concrete specimens.

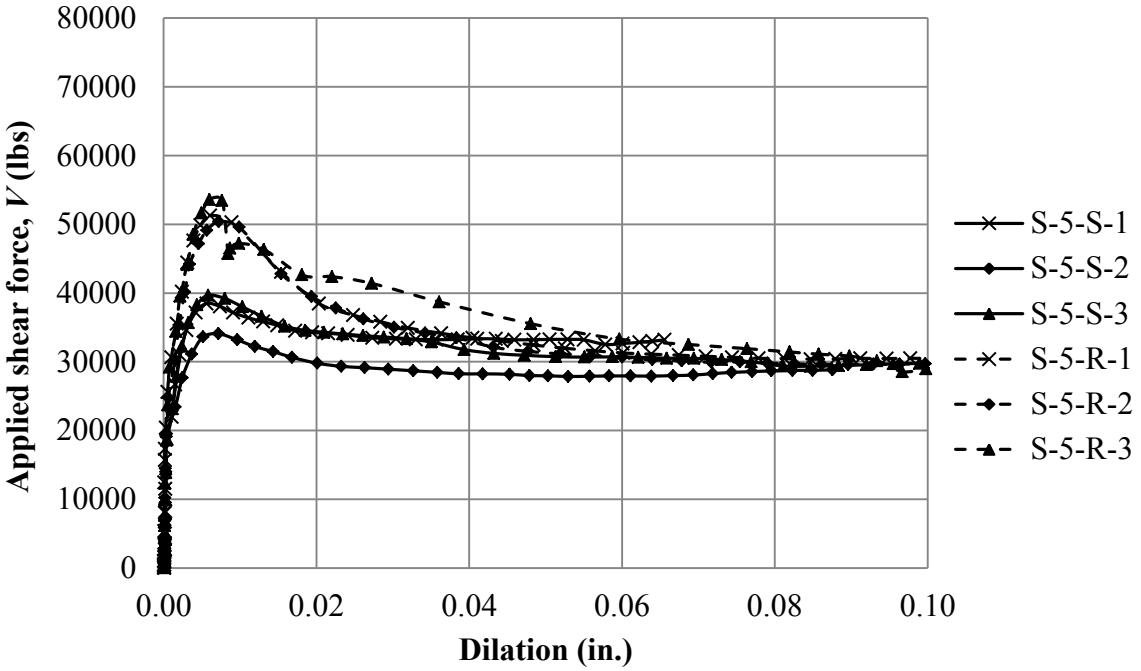

Figure 3.28. Applied shear force vs. interface dilation for 5000 psi sand-lightweight concrete specimens.

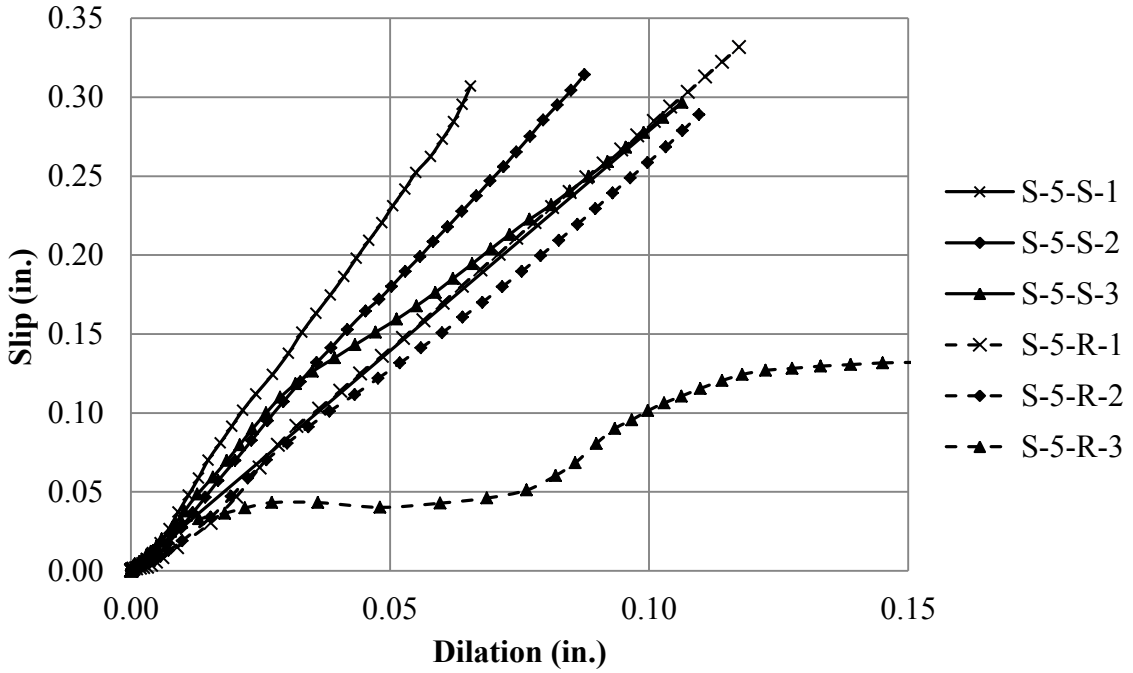

Figure 3.29. Slip vs. dilation for 5000 psi sand-lightweight concrete specimens.

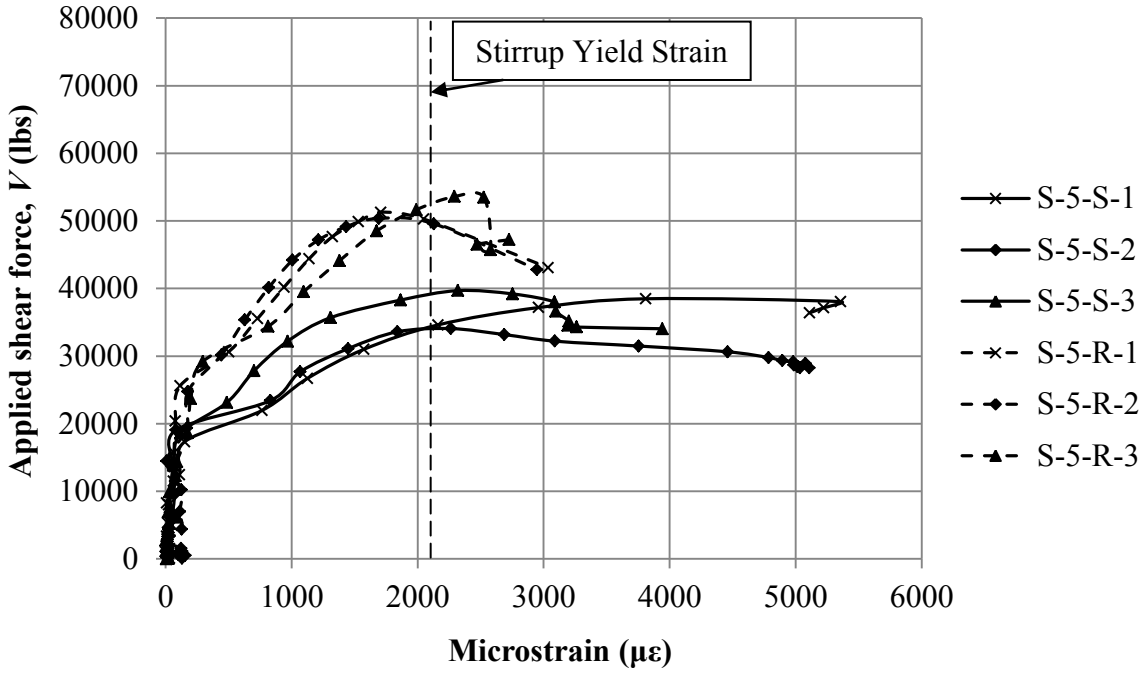

Figure 3.30. Applied shear force vs. interface steel strain for 5000 psi sand-lightweight concrete specimens.

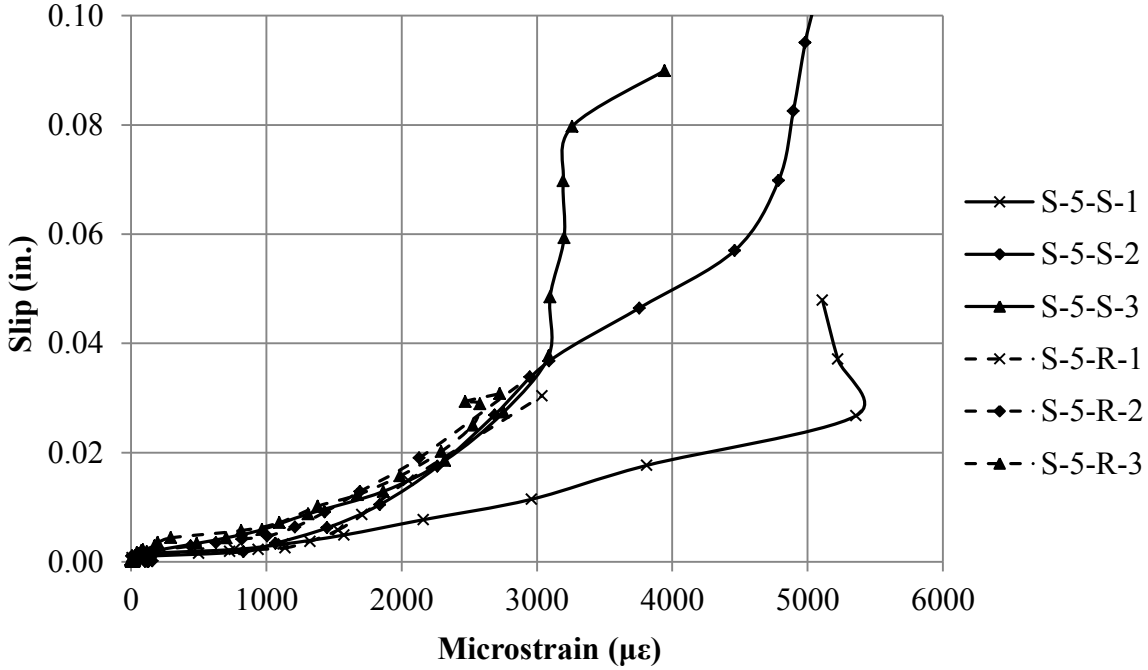

Figure 3.31. Slip vs. interface steel strain for 5000 psi sand-lightweight concrete specimens

3.6.2.2. 8000 psi specimens. Testing of the 8000 psi sand-lightweight specimens was performed on 12/18/2012. All specimens failed along the shear plane as expected. For specimens S-8-R-1 and S-8-R-3 failure of the flange occurred after the peak load was achieved. An example of the flange failure is shown in Figure 3.32. This failure is similar in nature to that discussed in section 3.6.2.1 for specimen S-5-R-3. The behavior of the 8000 psi sand-lightweight concrete

specimens is shown in Figure 3.33 through Figure 3.37. Figure 3.33 shows the applied shear versus slip relations. Figure 3.34 shows the applied shear versus interface dilation relations. Figure 3.35 shows the slip versus dilation relations. Figure 3.36 shows the applied shear versus steel strain relations. Figure 3.37 shows the slip versus interface steel relations.

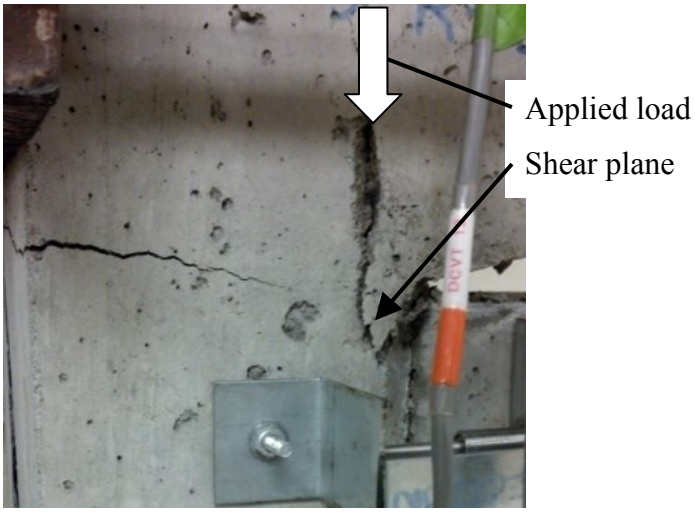

Figure 3.32. Flange failure of specimen S-8-R-1

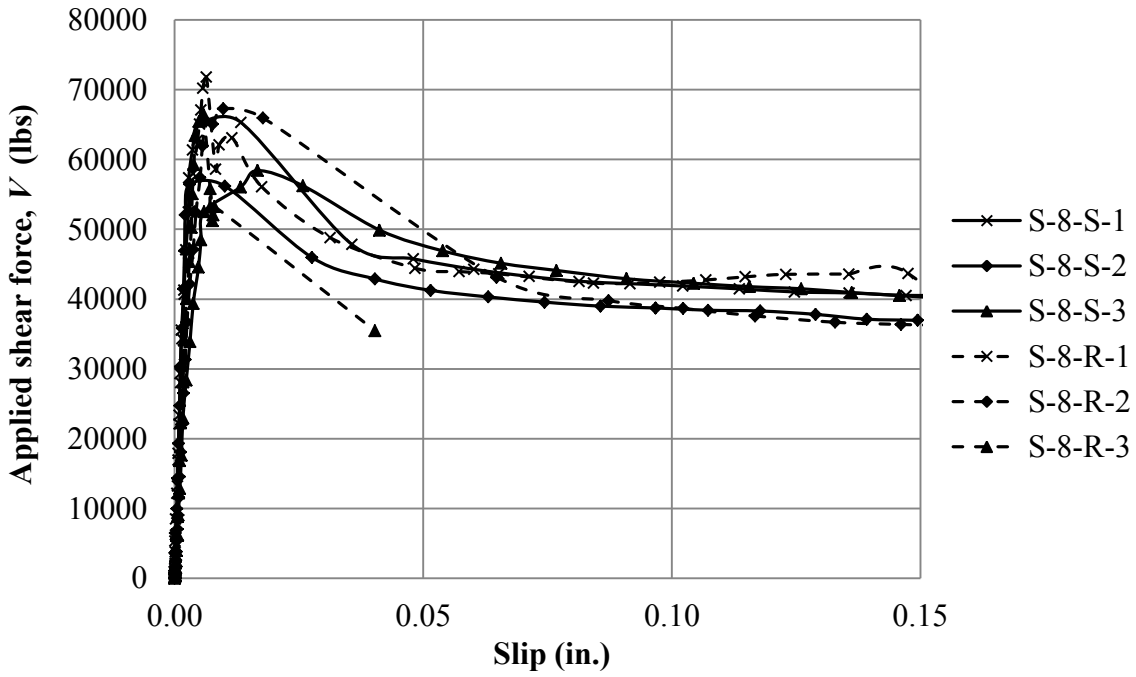

Figure 3.33. Applied shear force vs. slip relations for 8000 psi sand-lightweight concrete specimens.

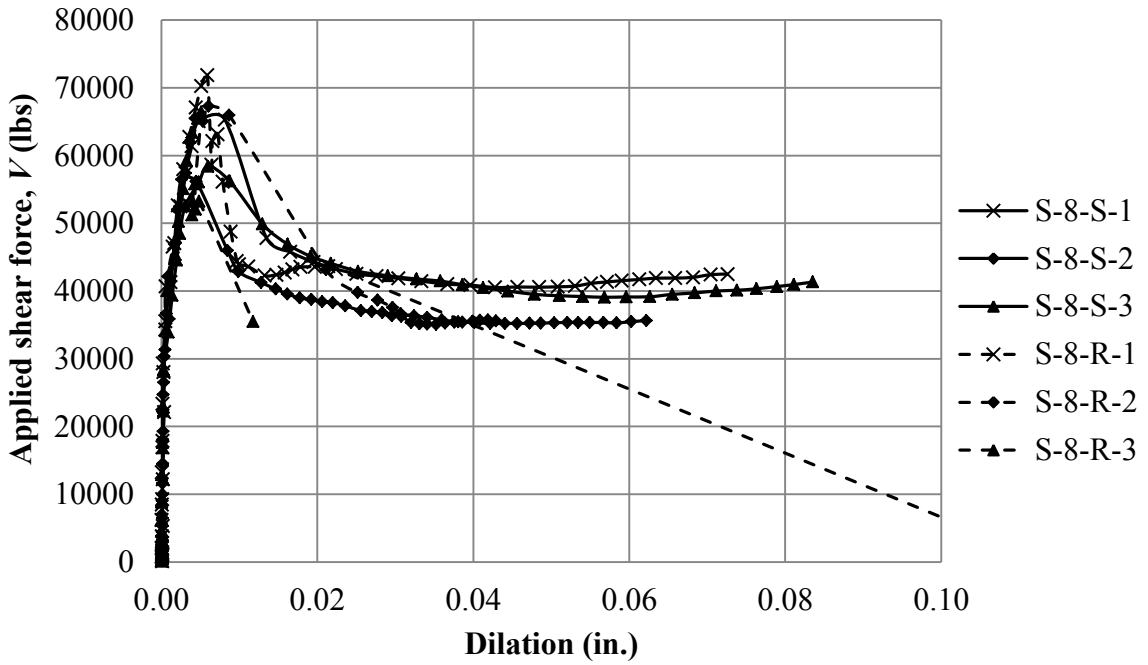

Figure 3.34. Applied shear force vs. interface dilation for 8000 psi sand-lightweight concrete specimens.

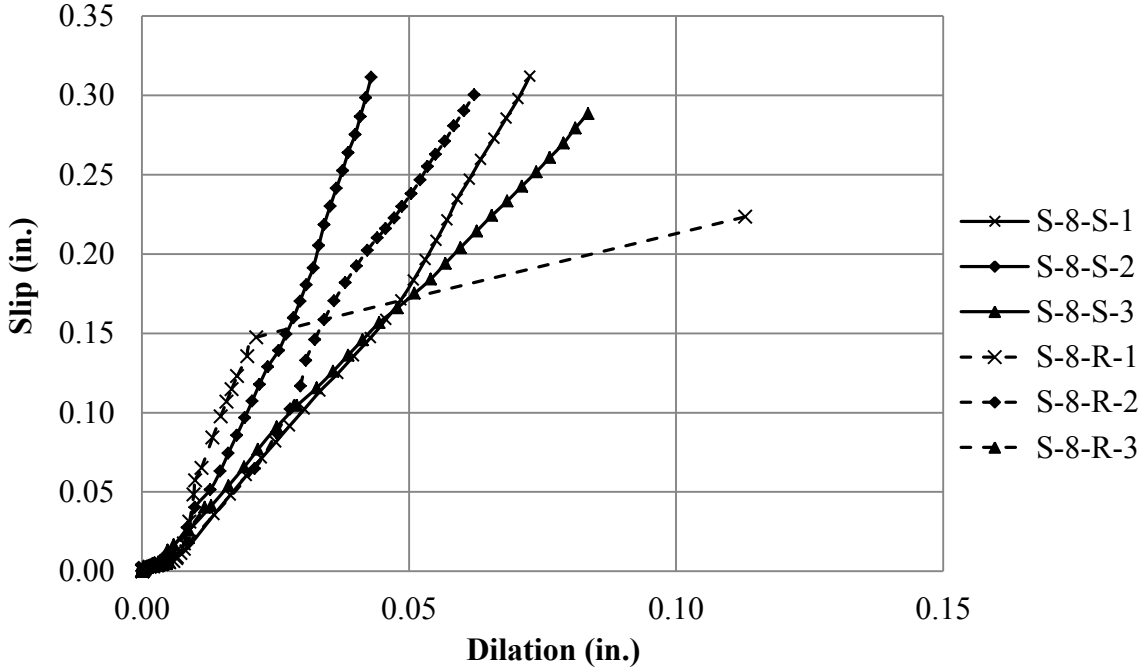

Figure 3.35. Slip vs. dilation for 8000 psi sand-lightweight concrete specimens.

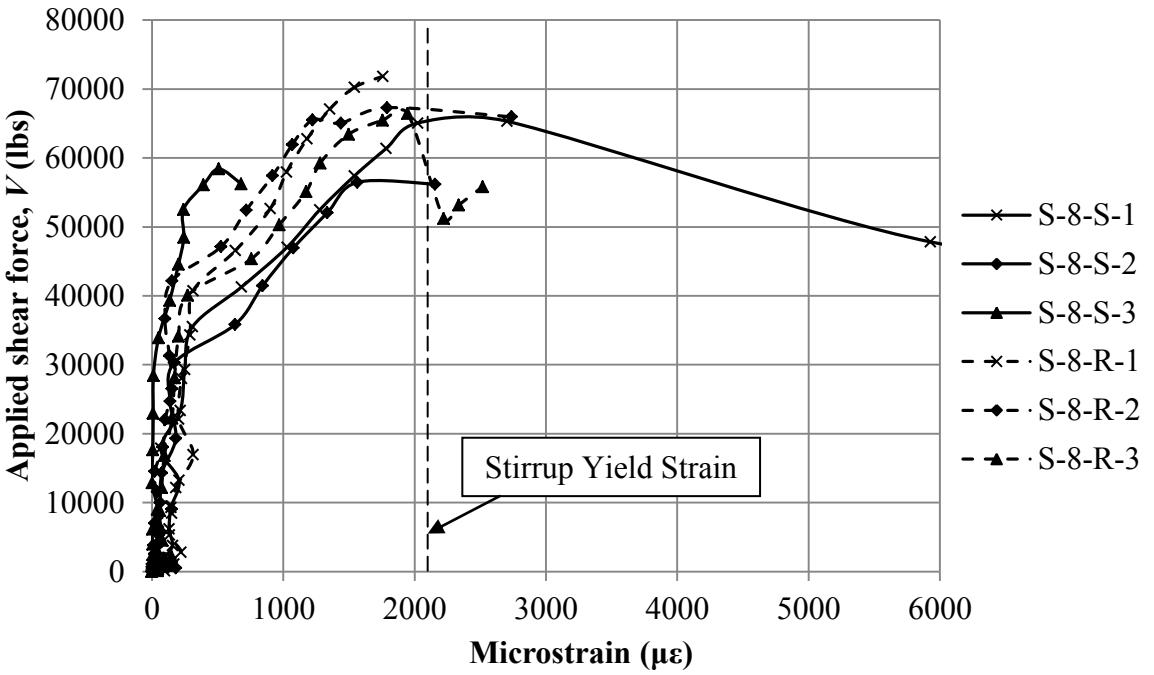

Figure 3.36. Applied shear force vs. interface steel strain for 8000 psi sand-lightweight concrete specimens.

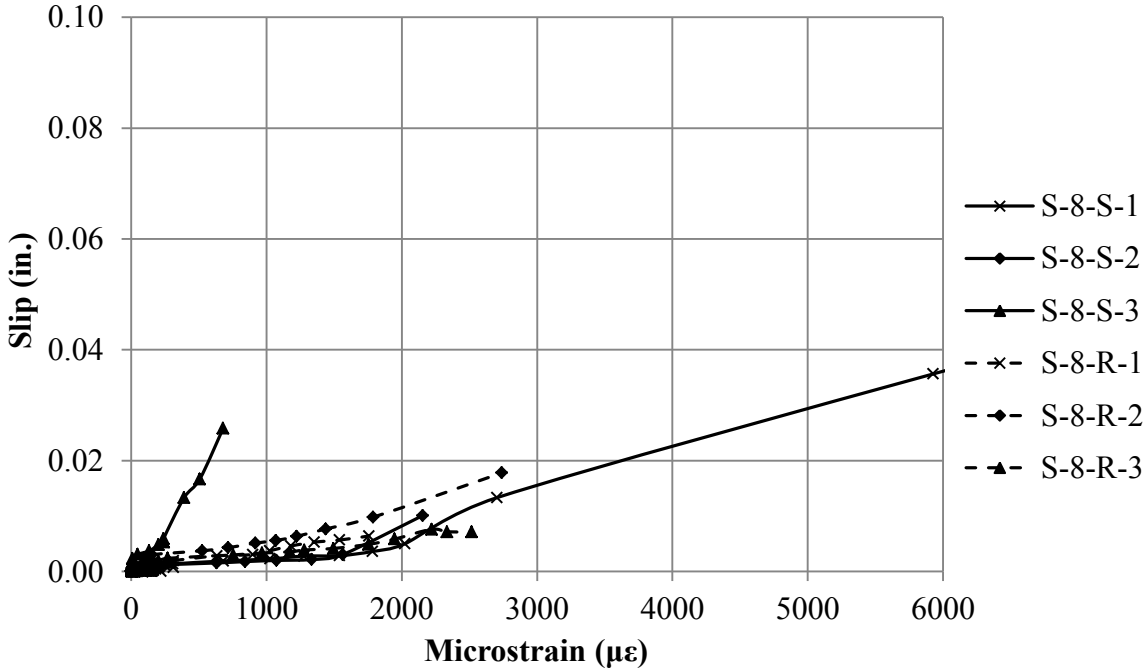

Figure 3.37. Slip vs. interface steel strain for 8000 psi sand-lightweight concrete specimens.

3.6.3. All-lightweight Concrete Specimens. This section presents information regarding the all-lightweight concrete specimens tested in this program.

3.6.3.1. 5000 psi specimens. Testing of the 5000 psi all-lightweight concrete specimens was completed on 9/24/2012. No unexpected failures were noted during testing. The behavior of the 5000 psi all-lightweight concrete specimens is shown in Figure 3.38 through Figure 3.42. Figure 3.38 shows the applied shear versus slip relations. Figure 3.39 shows the applied shear versus interface dilation relations. Figure 3.40 shows the slip versus dilation relations. Figure 3.41 shows the applied shear versus steel strain relations. Figure 3.42 shows the slip versus interface steel relations. Specimen A-5-S-2 has been removed from Figures 3.41 and 3.42 as strain data were unavailable because of problems with the data acquisition system.

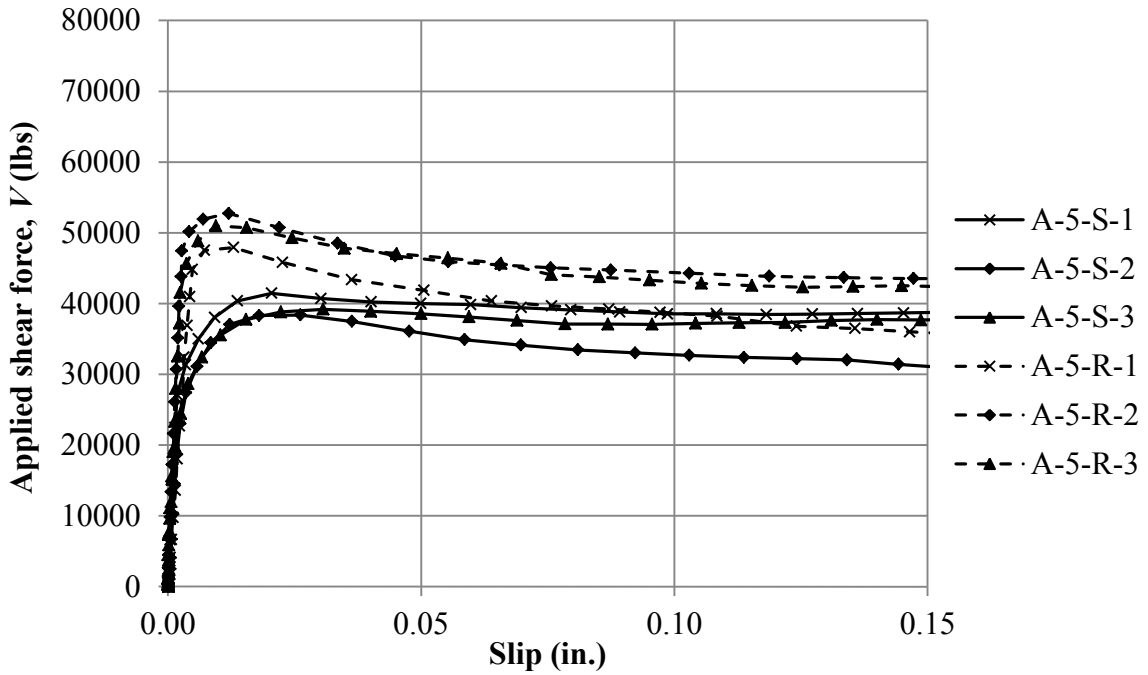

Figure 3.38. Applied shear force vs. slip relations for 5000 psi all-lightweight concrete specimens.

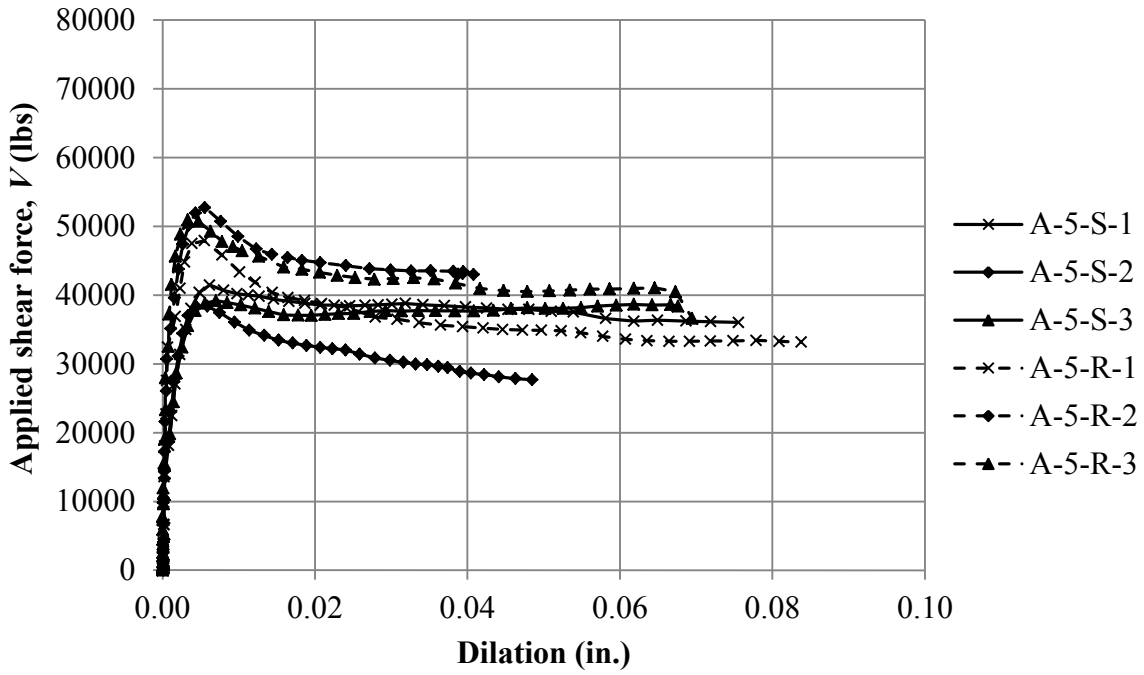

Figure 3.39. Applied shear force vs. dilation of 5000 psi all-lightweight concrete specimens.

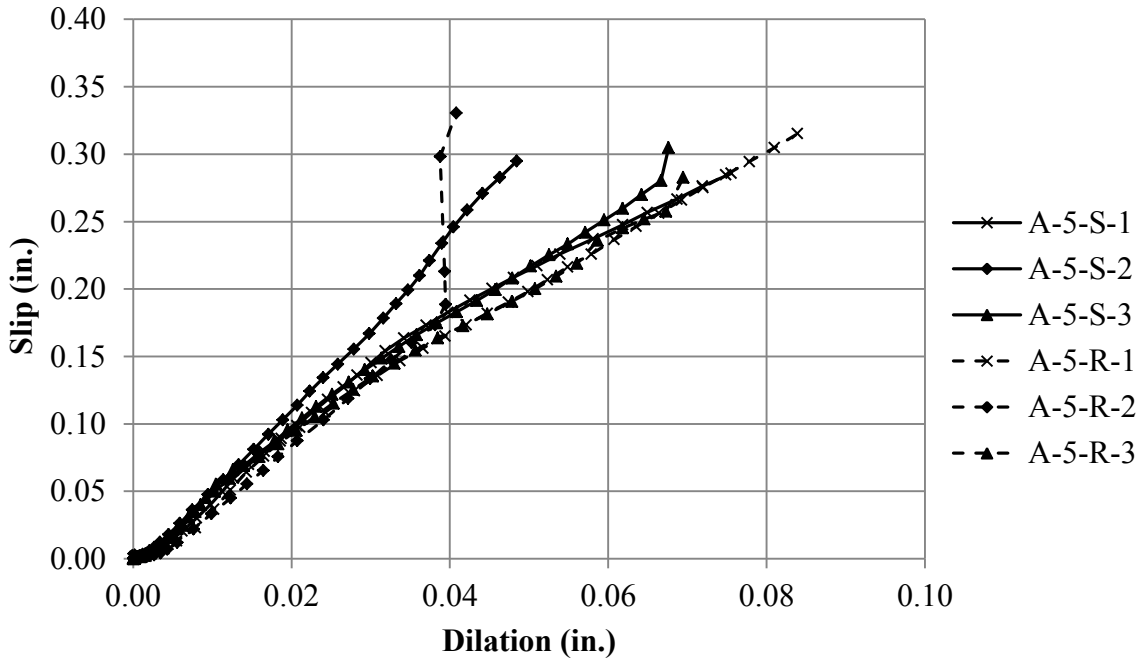

Figure 3.40. Slip vs. dilation for 5000 psi all-lightweight concrete specimens.

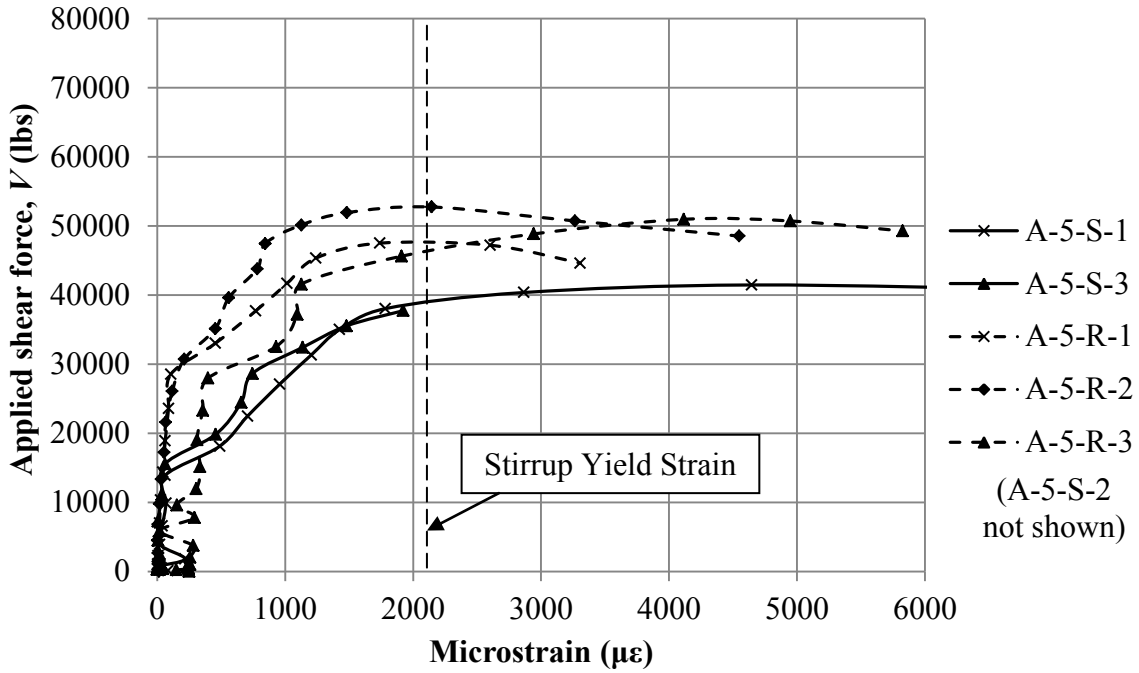

Figure 3.41. Applied shear force vs. interface steel strain for 5000 psi all-lightweight concrete specimens.

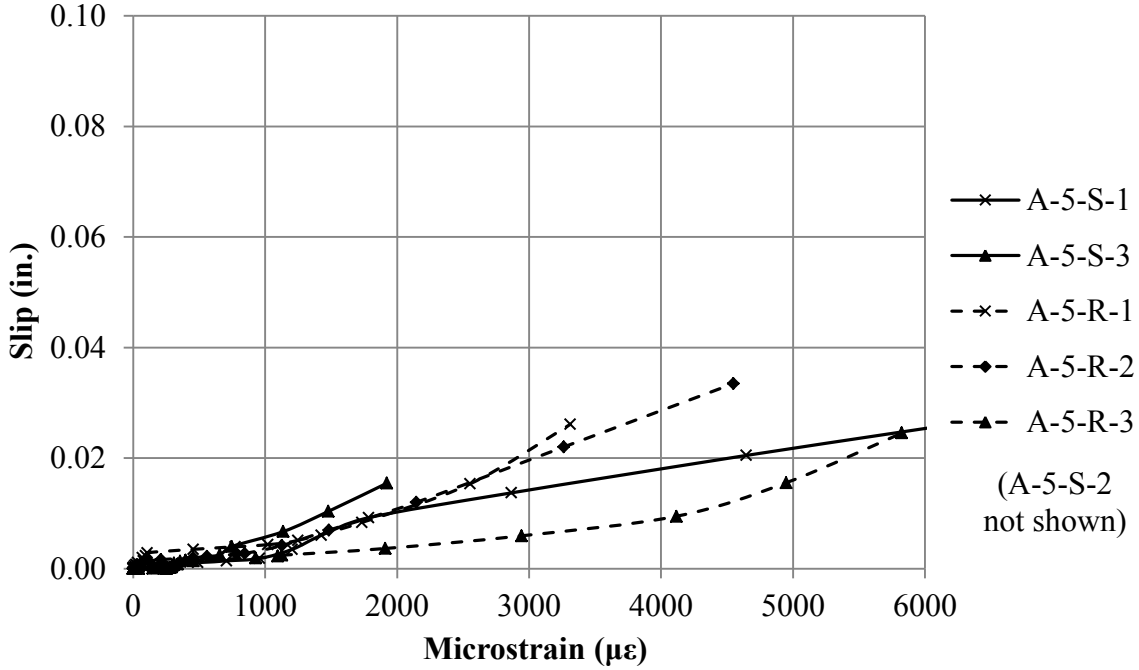

Figure 3.42. Slip vs. interface steel strain for 5000 psi all-lightweight concrete specimens.

3.6.3.2. 8000 psi specimens. Testing of the 8000 psi all-lightweight concrete specimens, the A-8-S and A-8-R series, was completed on 1/7/2012. The 8000 psi specimens were the first tests to use the secondary prestressing system discussed in Section 3.5.3.2. The application of the secondary system allowed testing of the roughened interface specimens beyond peak load and to the target slip of 0.3 in. discussed in Section 3.5.2. Strain in the reinforcing steel across the shear plane was monitored during the application of the prestressing system. The application of this system was determined to have no effect on the behavior of the specimens exhibited in this section, as was expected since the secondary prestressing system was a passive system. The behavior of the 8000 psi all-lightweight concrete specimens is shown in Figure 3.43 through Figure 3.45. Figure 3.43 shows the applied shear versus slip relations. Figure 3.44 shows the applied shear versus interface dilation relations. Figure 3.45 shows the slip versus dilation relations. Due to failure of the data acquisition system during testing of these specimens, strain data is unavailable for these specimens. Therefore, plots of applied shear vs. strain and slip vs. strain could not be produced.

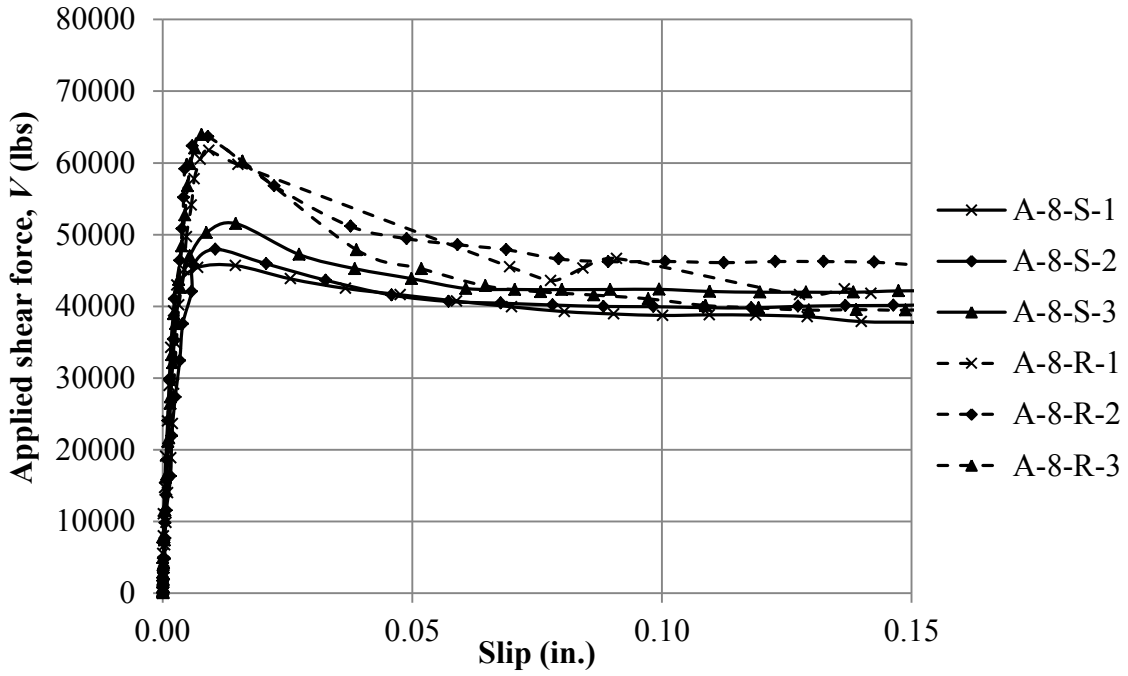

Figure 3.43. Applied shear force vs. slip relations for 8000 psi all-lightweight concrete specimens.

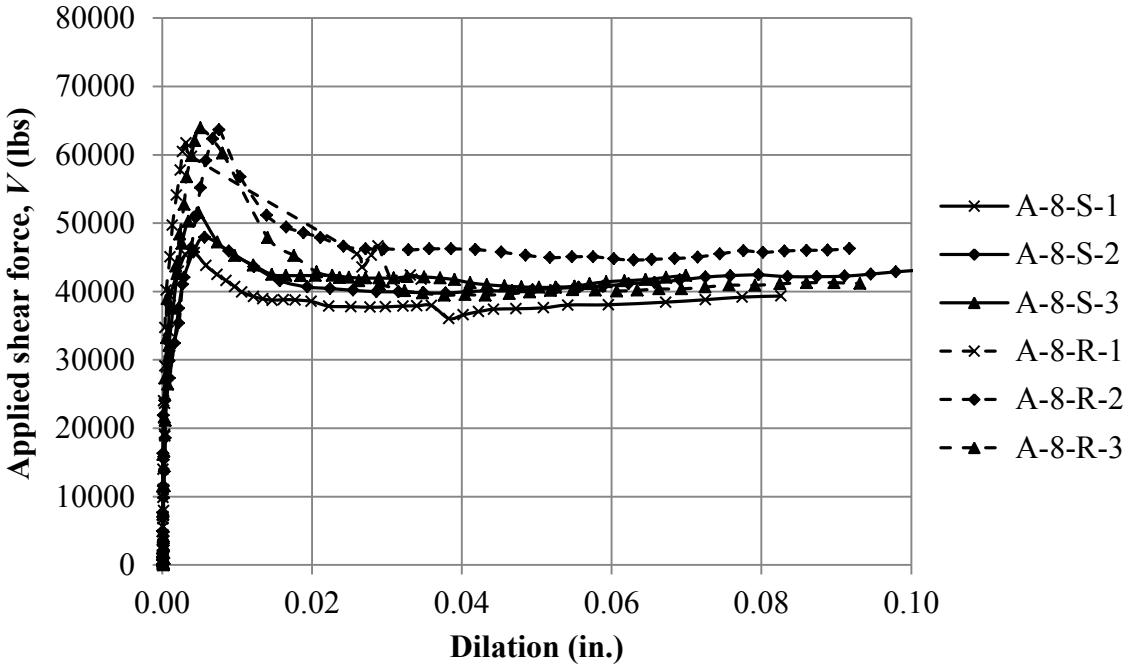

Figure 3.44. Applied shear force vs. dilation relations for 8000 psi all-lightweight concrete specimens.

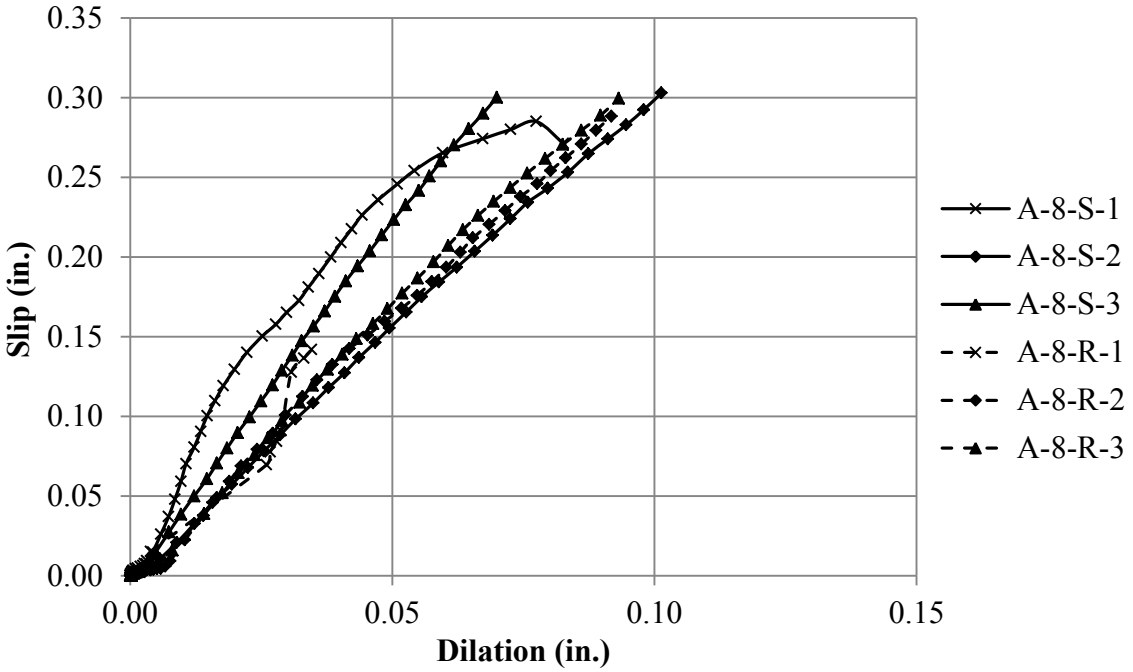

Figure 3.45. Slip vs. dilation for 8000 psi all-lightweight concrete specimens.

4. ANALYSIS AND DISCUSSION

4.1. INTRODUCTION

This section discusses the results of the experiments and analysis of the test data presented in Section 3. The results of the experiments are discussed and compared in terms of general behavior, measured shear strength, measured interface reinforcement strain, and measured displacements in Section 4.2. Results are also compared to current design provisions in both the PCI Design Handbook and the ACI 318 code in Section 4.3. In Section 4.4, results are compared to previous studies reported in the literature (summarized in Section 2.4).

4.2. GENERAL BEHAVIOR

4.2.1. Cracking. The general cracking behavior of all specimens was similar. No cracks were observed during testing of the specimens in the region adjacent to the shear plane, similar to previous research conducted by Mattock et al. (1976) on monolithic lightweight concrete specimens with a precracked interface discussed in Section 2.4.7. For the specimens with a roughened interface, the peak shear force V_u was associated with noticeable separation of the crack interface surfaces. Strain measured in the interface reinforcement indicated that yielding of reinforcement occurred at the peak shear force. Specimens with a smooth interface exhibited similar cracks along the shear plane, but with lesser observed separation of the crack interface surfaces than the specimens with a roughened interface. Figure 4.1 shows examples of cracks observed at the peak load in the specimens with the different interface conditions. In addition to cracking of the shear interface, spalling of the concrete cover was observed adjacent to the shear plane crack for many specimens.

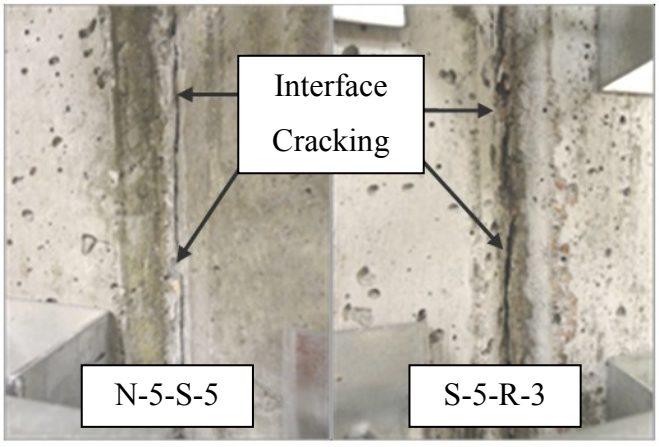

Figure 4.1. Typical failure crack along shear plane for specimens with smooth interface (left) and roughened interface (right)

4.2.2. Applied Shear Force – Slip Relations. Applied shear force-slip relations for the normalweight, sand-lightweight, and all-lightweight concrete series specimens are shown in Figures 3.17, 3.22, 3.27, 3.33, 3.38, and 3.43 in Section 3. The figures show that there is an

elastic region, shear plane "cracking", and followed by inelastic behavior upon loading for all specimens, and that the initial stiffness of the smooth and roughened interface specimens was similar. For the specimens with a smooth interface, the slip tended to increase at an increasing rate until the peak shear force V_u was achieved. After the peak shear force was achieved, the applied shear force reduced with increasing slip until a nearly constant value of applied shear force V_{ur} was reached for all specimens. Specimens with a roughened interface behaved in a more "quasi-brittle" manner than the corresponding smooth interface specimens, i.e., after the peak shear force was achieved, the shear force decreased more rapidly with increasing slip. However, the residual shear force V_{ur} was similar to that of the corresponding specimens with a smooth interface.

Comparison of the applied shear force-slip relations for specimens of the same concrete type (normalweight, sand-lightweight, or all-lightweight) and same interface condition indicates that the deformation behavior was more quasi-brittle (described above) for specimens with higher compressive strengths. This observation was also made by Mattock et al. (1976) as discussed in Section 2.4.8. Further discussion on the influence of concrete compressive strength is presented in Section 4.3.2. The applied shear force-slip relations also indicate that specimens with normalweight concrete tended to be more quasi-brittle than lightweight companion specimens with the same compressive strength of concrete and interface condition. These findings are different from those by Mattock et al. (1976), who observed that the post-peak response of lightweight concrete specimens was more quasi-brittle than companion normalweight concrete specimens. A possible explanation for this difference may be in aggregate used in the production of the lightweight concretes. This highlights the need to further study lightweight concrete mixtures with different types of aggregates. Further discussion on the influence of concrete type is presented in Section 4.3.1.

4.2.3. Applied Shear Force – Interface Strain Relations. The applied shear force-interface strain relations are shown in Figures 3.20, 3.25, 3.30, 3.36, and 3.42 of Section 3. The figures show an abrupt increase in measured strain at a level of force that can be associated with interface crack development and concrete cohesion. First cracking occurred at an applied shear stress v_{cr} in the range of 250 psi to 650 psi for specimens with a smooth interface. For specimens with a roughened interface, first cracking occurred at an applied shear stress v_{cr} between 550 psi to 880 psi. Figure 4.2 shows representative shear stress-interface strain plots for specimens N-8-S-2 and N-8-R-1, where the applied shear force V is plotted in terms of applied shear stress v ($v=V/A_{cr}$). The shear stress at interface cracking can be associated with a marked increase in strain measured in the interface reinforcement as indicated in Figure 4.2. Figure 4.3 and Table 4.1 summarize and compare the average value of the first cracking stress v_{cr} determined using this procedure for each series tested in this program. For all specimens, first cracking stress of the lightweight concrete specimens exceeded the corresponding normalweight concrete specimens with the exception of the A-8-S series.

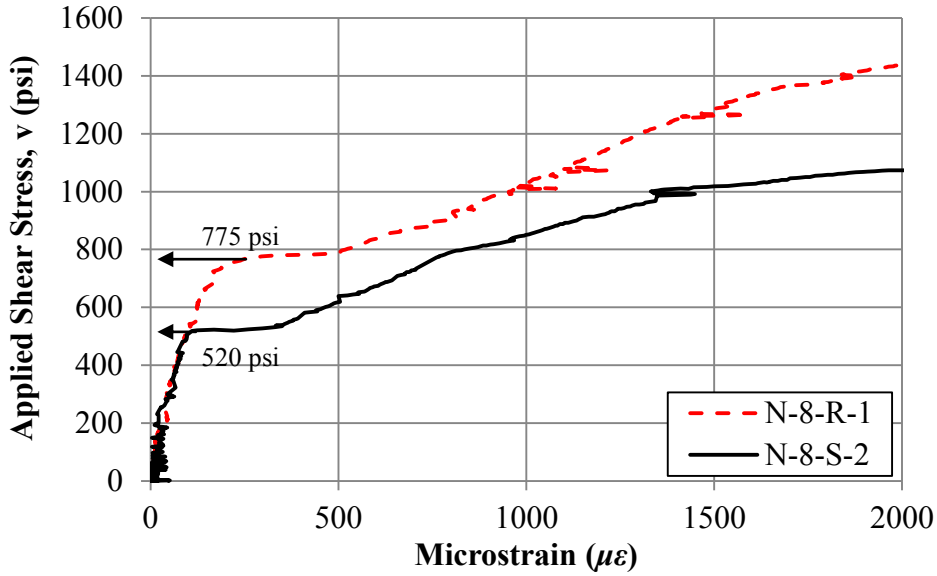

Figure 4.2. Typical shear stress-interface reinforcement strain plots for the determination of interface cracking stress (Specimens N-8-S-2 and N-8-R-1 shown)

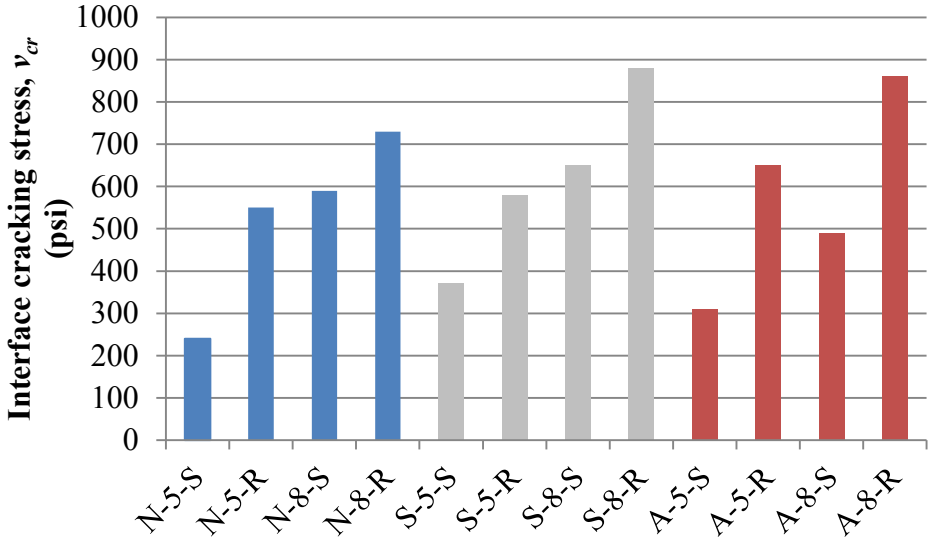

Figure 4.3. Average interface cracking stress, v_{cr} for all series

Table 4.1. Average Interface Cracking Stress for All Series

Concrete Type		Interface Condition	V_{cr} (Cohesion)	Concrete Type		Interface Condition	V_{cr} (Cohesion)
5000 psi	N	Smooth	230	8000 psi	N	Smooth	590
	S	Smooth	370		S	Smooth	550
	A	Smooth	305		A	Smooth	490
	N	Rough	550		N	Rough	720
	S	Rough	580		S	Rough	880
	A	Rough	650		A	Rough	860

4.3. INFLUENCE OF TEST VARIABLES

This section presents the results of the analysis conducted to study the influence of the test variables included in this study, namely, concrete unit weight, concrete compressive strength, and interface surface preparation, based on the test results reported in Section 3. Test results used in this analysis are summarized in Table 4.2. The measured values presented in Table 4.2 include the peak (ultimate) applied force V_u, slip at V_u, dilation at V_u, and residual force V_{ur}. The residual shear force V_{ur} is defined as the load corresponding to a slip of 0.15 in. as discussed in Section 3.6. Values of shear stresses v_u and v_{ur} , which are calculated as the corresponding applied shear force divided by the cross-sectional area of the shear plane (A_{cr} = 49.5 in^2), are also shown in the table for each specimen. Average values of shear stress v_u and v_{ur} for each series are also provided, as well as the average value of the peak-to-residual shear stress ratio (v_u/v_{ur}) for each series.

Table 4.2. Summary of Test Results and Analysis

Specimen ID	f'_c at test day (psi)	V_u (lbs)	v_u (psi)	$v_{u,\,avg}$ (psi)	Slip at V_u (in)	Dilation at V_u (in)	V_{ur} (lbs)	v_{ur} (psi)	$v_{ur,\,avg}$ (psi)	$\left(\frac{v_u}{v_{ur}}\right)_{avg}$
N-5-R-4	4860	59060	1190	1115	0.013	0.007	39470	800	790	1.41
N-5-R-5	4860	53420	1080		0.010	0.006	40140	810		
N-5-R-6	4860	53440	1080		0.012	0.007	38360	770		
N-5-S-4	4860	32705	660	680	0.057	0.015	38150	770	683	1.06
N-5-S-5	4860	34680	700		0.022	0.008	31150	630		
N-5-S-6	4860	39155	790		0.031	0.007	32000	650		
S-5-R-1	4550	51430	1040	1117	0.010	0.007	30500	620	603	1.85
S-5-R-2	4550	50395	1020		0.014	0.008	29600	600		
S-5-R-3	4550	63905	1290		0.022	0.007	29300	590		
S-5-S-1	4550	38530	780	757	0.019	0.006	33200	670	610	1.24
S-5-S-2	4550	34110	690		0.016	0.003	27900	560		
S-5-S-3	4550	39795	800		0.021	0.007	29500	600		
A-5-R-1	6080	48440	980	1030	0.010	0.005	35000	710	800	1.29
A-5-R-2	6080	52800	1070		0.011	0.005	43000	870		
A-5-R-3	6080	51410	1040		0.013	0.004	40500	820		
A-5-S-1	6080	41470	840	813	0.021	0.006	38500	780	727	1.13
A-5-S-2	6080	40080	810		0.023	0.005	32000	650		
A-5-S-3	6080	39250	790		0.032	0.007	37000	750		
N-8-R-1	7550	74040	1500	1310	0.010	0.008	47500	960	873	1.50
N-8-R-2	7550	56090	1130		0.008	0.005	39050	790		
N-8-R-3	7550	64140	1300		0.007	0.005	43000	870		
N-8-S-1	7550	65570	1320	1173	0.010	0.006	49500	1000	937	1.25
N-8-S-2	7550	53305	1080		0.010	0.005	42950	870		
N-8-S-3	7550	55330	1120		0.001	0.006	46695	940		
S-8-R-1	7210	72045	1460	1390	0.007	0.006	43660	880	805	1.76
S-8-R-2	7210	67380	1360		0.010	0.006	36300	730		
S-8-R-3	7210	66725	1350		0.006	0.005	N/A	N/A		
S-8-S-1	7210	67025	1350	1237	0.007	0.006	44480	900	820	1.51
S-8-S-2	7210	57880	1170		0.005	0.003	36970	750		
S-8-S-3[1]	7210	58865	1190		0.018	0.007	40340	810		
A-8-R-1	7845	61775	1250	1280	0.009	0.003	41330	830	853	1.51
A-8-R-2	7845	63935	1290		0.008	0.007	45800	930		
A-8-R-3	7845	64125	1300		0.009	0.006	39450	800		
A-8-S-1	7845	46090	930	983	0.011	0.004	37790	760	807	1.22
A-8-S-2	7845	48035	970		0.012	0.006	40185	810		
A-8-S-3	7845	51740	1050		0.012	0.004	42140	850		

[1] Flange failure during post-peak loading.

4.3.1. Effect of Concrete Unit Weight. Within this study three specific concrete types (normalweight, sand-lightweight, and all-lightweight) with three target unit weights were investigated. These target unit weights were 145 lb/ft^3, 120 lb/ft^3, and 108 lb/ft^3, respectively. Details and discussion of the concrete mixtures are presented in Section 3.3.2. This section examines the effect of concrete unit weight on the shear transfer for the specimens conducted in this study. To isolate this parameter, specimens with the same target compressive strength of concrete and interface condition were compared.

Figures 4.4 through 4.7 compare the ultimate shear strength v_u of the specimens with the same concrete compressive strength and interface condition versus unit weight. Figure 4.4 plots the ultimate shear stress v_u (not normalized) versus concrete unit weight for each specimen. The average values of the ultimate shear stress (not normalized) for each series are plotted versus concrete unit weight in Figure 4.5. Trendlines are also plotted in Figure 4.5 for each series with the same compressive strength and interface preparation. The trends shown in Figure 4.5 indicate that specimens with the same interface condition and the concrete compressive strength had nearly the same shear strength, irrespective of concrete unit weight. Figure 4.6 plots the normalized ultimate shear versus unit weight versus concrete unit weight for each specimen. Because the measured compressive strength of concrete varied for each series, the shear force has been normalized by the measured compressive strength at test day. The average values of the normalized ultimate shear stress for each series are plotted versus concrete unit weight in Figure 4.7. Trendlines are also plotted in Figure 4.7 for each series with the same compressive strength and interface preparation. Again, the trends shown in Figure 4.7 indicate that specimens with the same interface condition and concrete compressive strength had nearly the same ultimate shear strength, irrespective of concrete unit weight. Therefore, it can be concluded that for specimens in this study, unit weight had little effect on the ultimate shear capacity.

Similarly, Figures 4.8 through 4.11 compare the residual shear strength v_{ur} of the specimens with the same concrete compressive strength and interface condition versus unit weight. Figure 4.8 plots the residual shear stress v_{ur} (not normalized) versus concrete unit weight for each specimen. The average values of the ultimate shear stress (not normalized) for each series are plotted versus concrete unit weight in Figure 4.9. Trendlines are also plotted in Figure 4.9 for each series with the same compressive strength and interface preparation. Figure 4.10 plots the normalized ultimate shear (normalized by the compressive strength of concrete) versus unit weight versus concrete unit weight for each specimen. The average values of the normalized ultimate shear stress for each series are plotted versus concrete unit weight in Figure 4.11. Trendlines are also plotted in Figures 4.9 and 4.11 for each series with the same compressive strength and interface preparation. The trends shown in Figures 4.9 and 4.11 indicate that specimens with the same interface condition and concrete compressive strength had nearly the same residual shear strength, irrespective of concrete unit weight. Therefore, it can be concluded that for specimens in this study, unit weight had little effect on the residual shear capacity. It should be noted that limited conclusions can be drawn from this observation, however, because additional data from other research programs is limited regarding the residual shear force capacity.

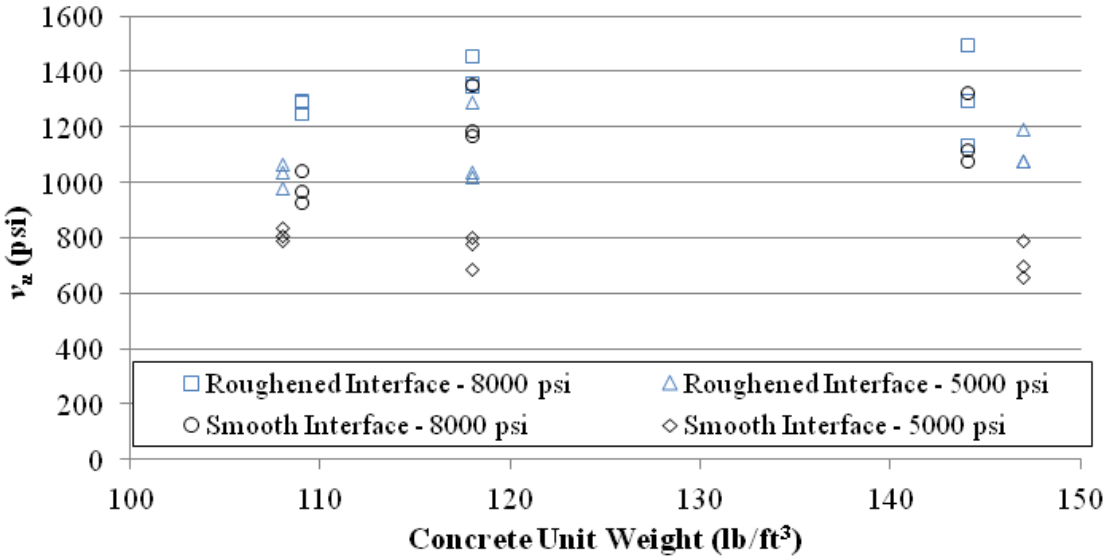

Figure 4.4. Shear strength v_u versus concrete unit weight for all specimens

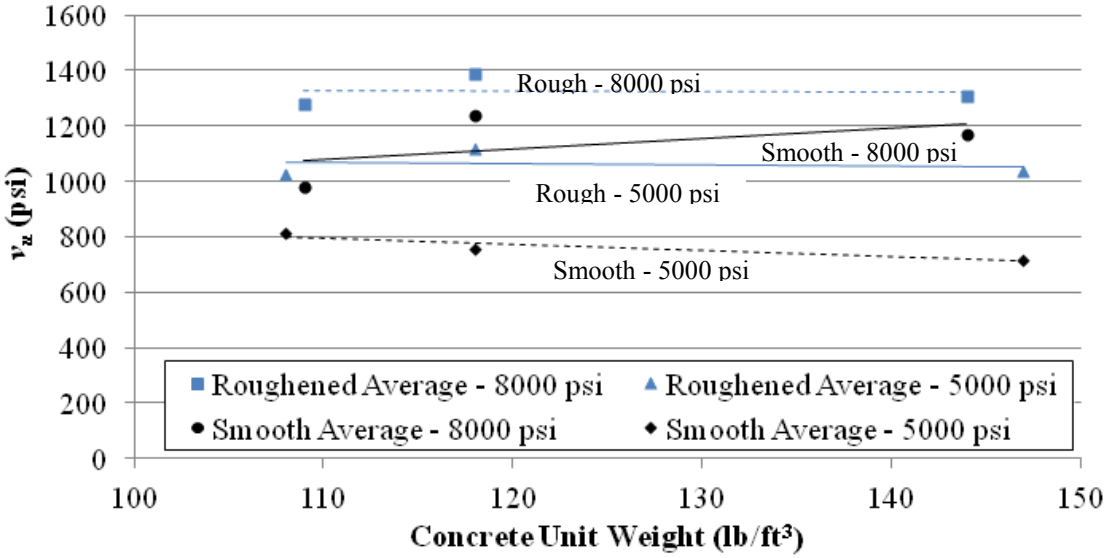

Figure 4.5. Average shear strength v_u versus concrete unit weight for each series

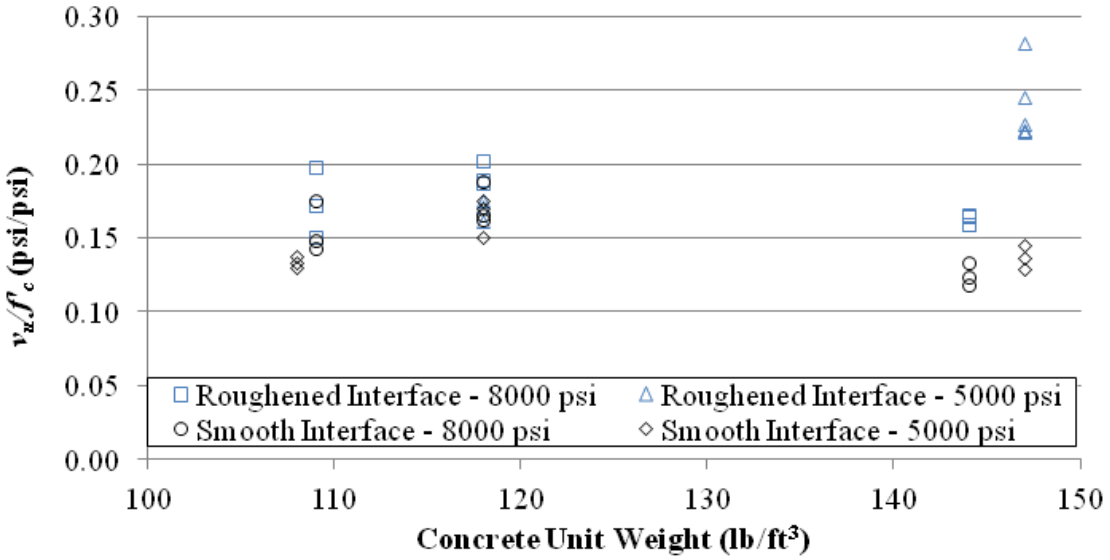

Figure 4.6. Normalized shear strength v_u versus concrete unit weight for all specimens

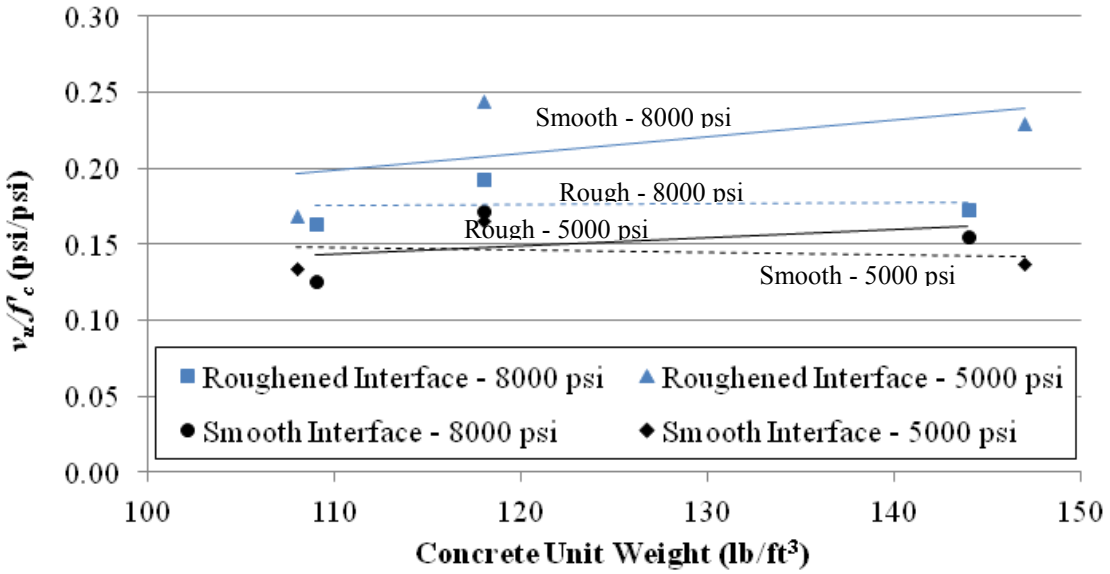

Figure 4.7. Normalized average shear strength v_u versus concrete unit weight for each series

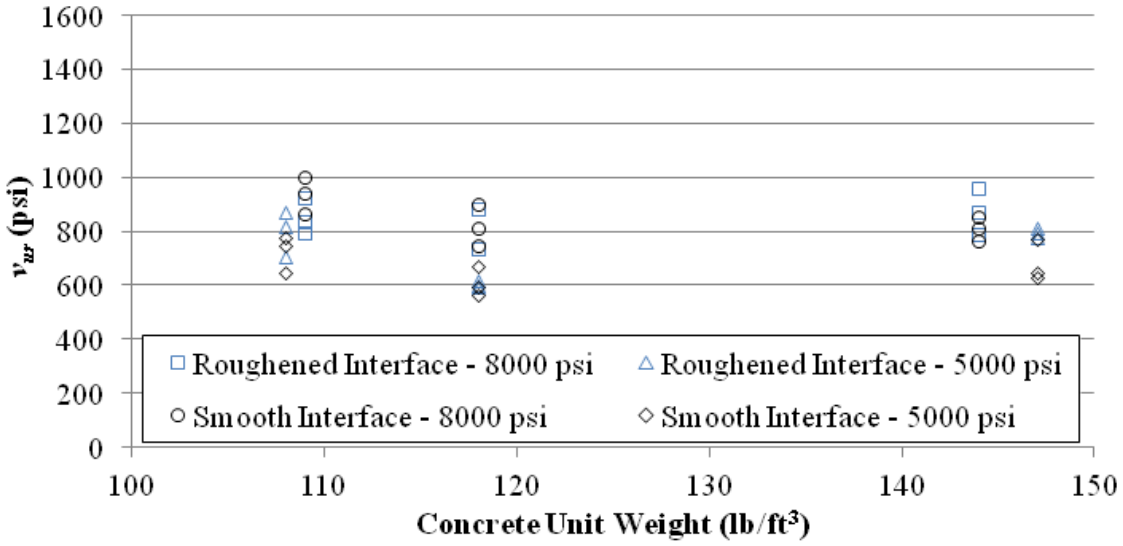

Figure 4.8. Residual shear strength v_{ur} versus concrete unit weight for all specimens

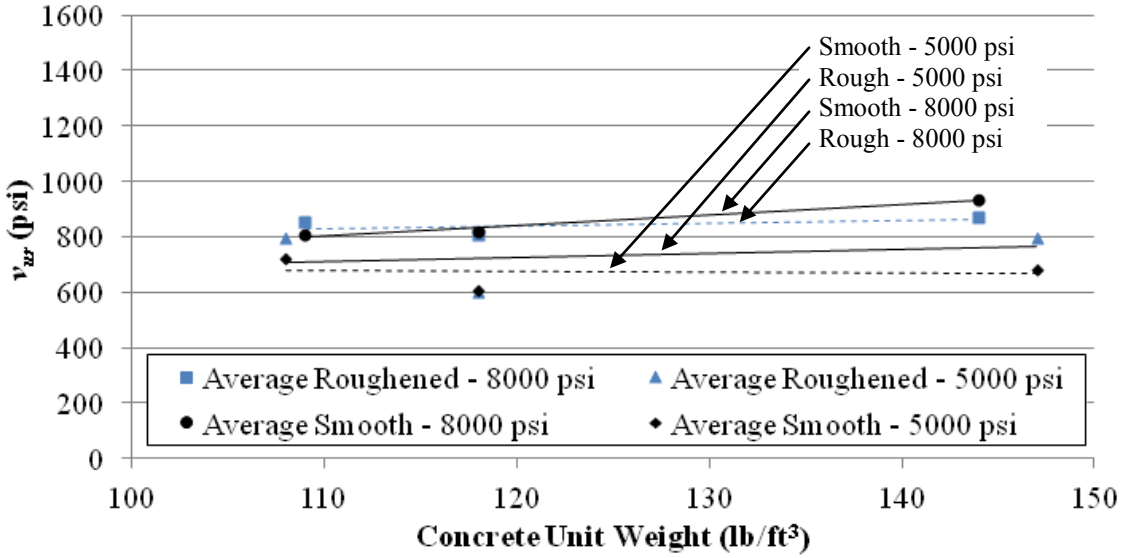

Figure 4.9. Average residual shear strength v_{ur} versus concrete unit weight for each series

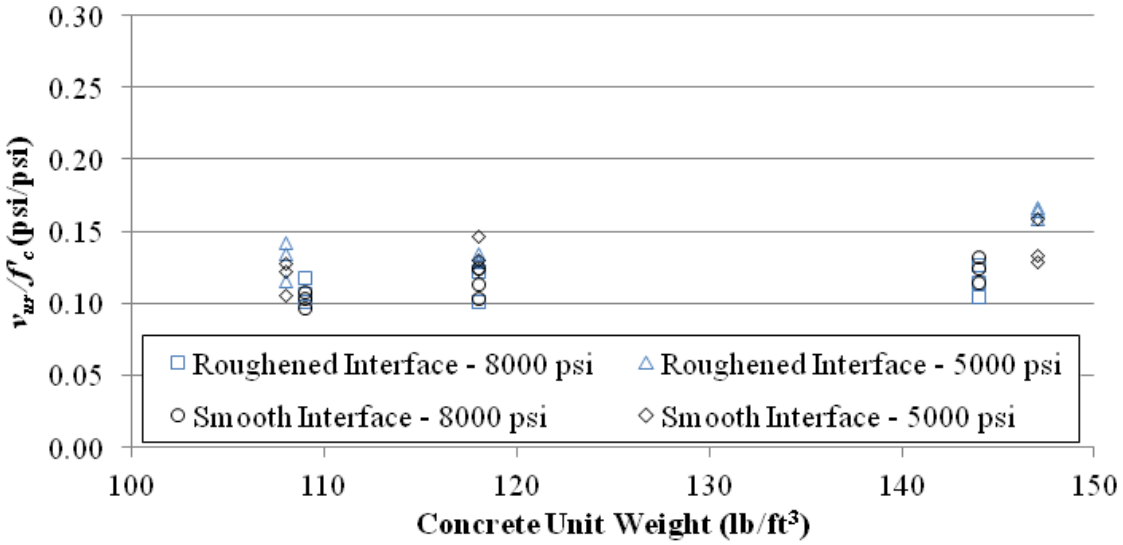

Figure 4.10. Normalized residual shear strength v_{ur} versus concrete unit weight for all specimens.

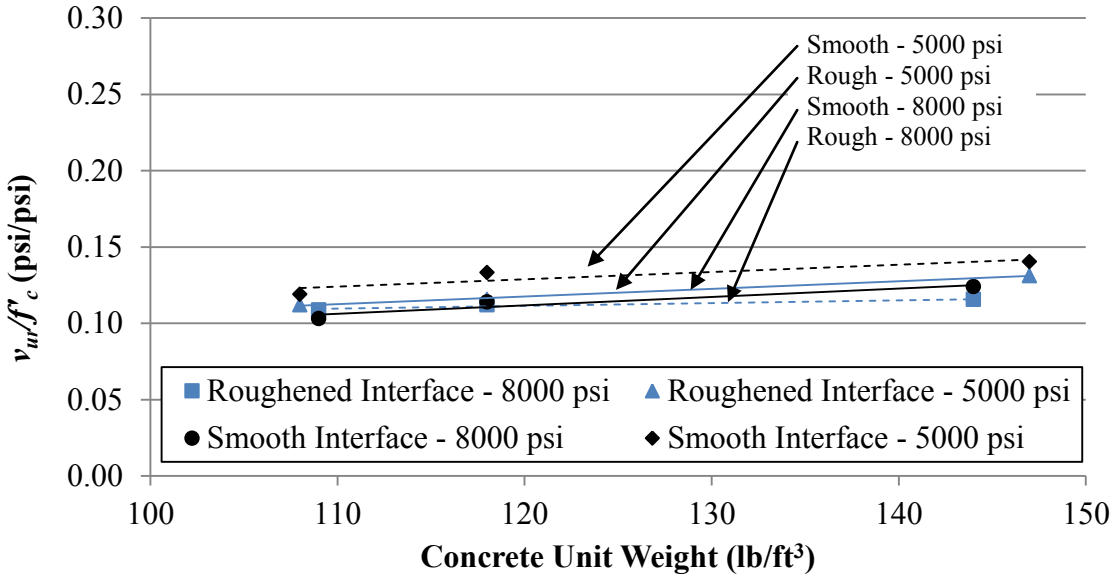

Figure 4.11. Normalized average residual shear strength v_{ur} versus concrete unit weight for each series.

4.3.2. Effect of Concrete Compressive Strength. Two target concrete compressive strengths (5000 psi and 8000 psi) were included in this study. The concrete mixture designs and material properties are presented in Section 3.3.2. To isolate the concrete compressive strength parameter, specimens with the same concrete type and interface condition were compared. Figure 4.12 through Figure 4.17 compare the applied shear force-slip relations for series with the same concrete type and interface condition. (It should be noted that the plots have not been normalized.) In each of the figures, the 5000 psi specimens are plotted with solid lines, and the 8000 psi specimens are plotted with dashed lines. Figure 4.12 through Figure 4.17 clearly show

that for a given concrete type and interface condition, specimens with a higher concrete compressive strength had a higher peak shear force. Figure 4.12 through Figure 4.17 also show that the magnitude of the peak shear force V_u and residual shear force V_{ur} were similar for the specimens with 5000 psi concrete, whereas the peak shear force V_u was higher than the residual shear force V_{ur} for specimens with 8000 psi concrete. In other words, the ratio V_u/V_{ur} (or v_u/v_{ur}) was higher for specimens with 8000 psi concrete than for specimens with 5000 psi concrete.

Table 4.3 summarizes the average ultimate shear stress v_u for each series and shows the percent difference and resulting percent increase between series of different concrete compressive strengths and with the same concrete type and interface condition. Results are also shown in the form of a bar graph in Figure 4.18, which includes average values presented in Table 4.3 shown as dashed lines in the graph. Table 4.3 shows that for specimens with a smooth interface, the increase in concrete compressive strength from 5000 psi to 8000 psi resulted in an increase in average ultimate shear stress that ranged from 22% to 73% for the different concrete types (unit weights). The average percent difference was 53%. For specimens with a roughened interface, the increase in concrete compressive strength resulted in an increase in average ultimate shear stress that ranged from 24% to 26%, with an average of 25%. These results suggest that the shear transfer strength of specimens with a smooth interface condition was more sensitive to concrete strength than specimens with a roughened interface. Results can also be interpreted as the shear interface preparation is more critical for lower concrete compressive strengths. These results also suggest that as concrete strength increases, the interface preparation becomes less critical, but it still has a significant influence on the shear strength of the section. The effect of interface condition is further discussed in Section 4.3.3.

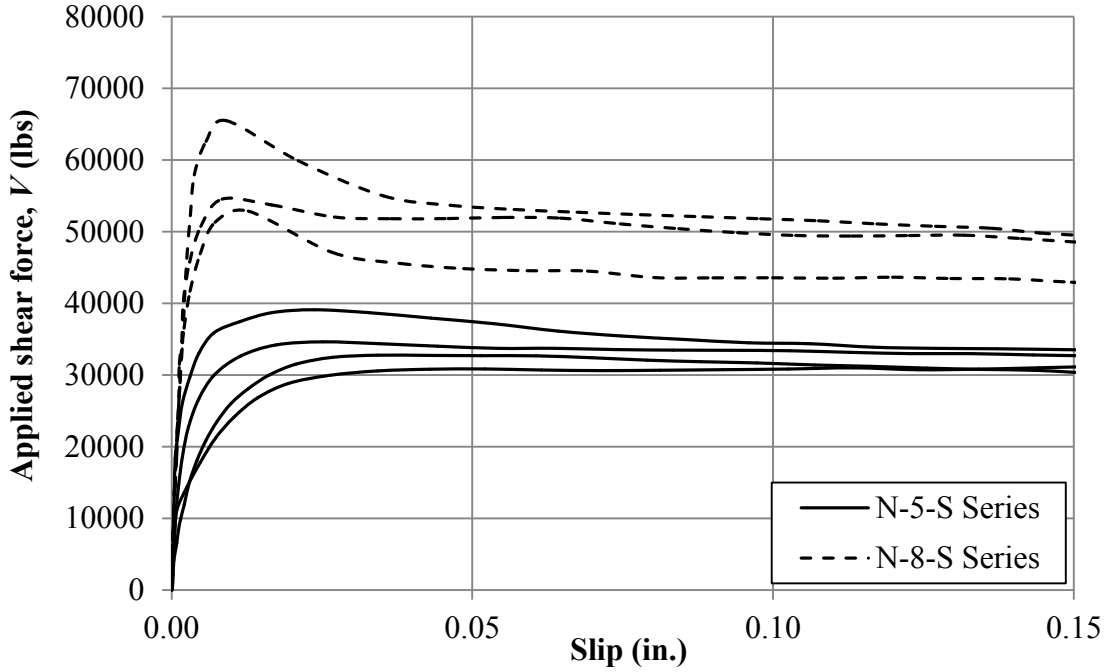

Figure 4.12. Effect of concrete strength for normalweight smooth interface specimens.

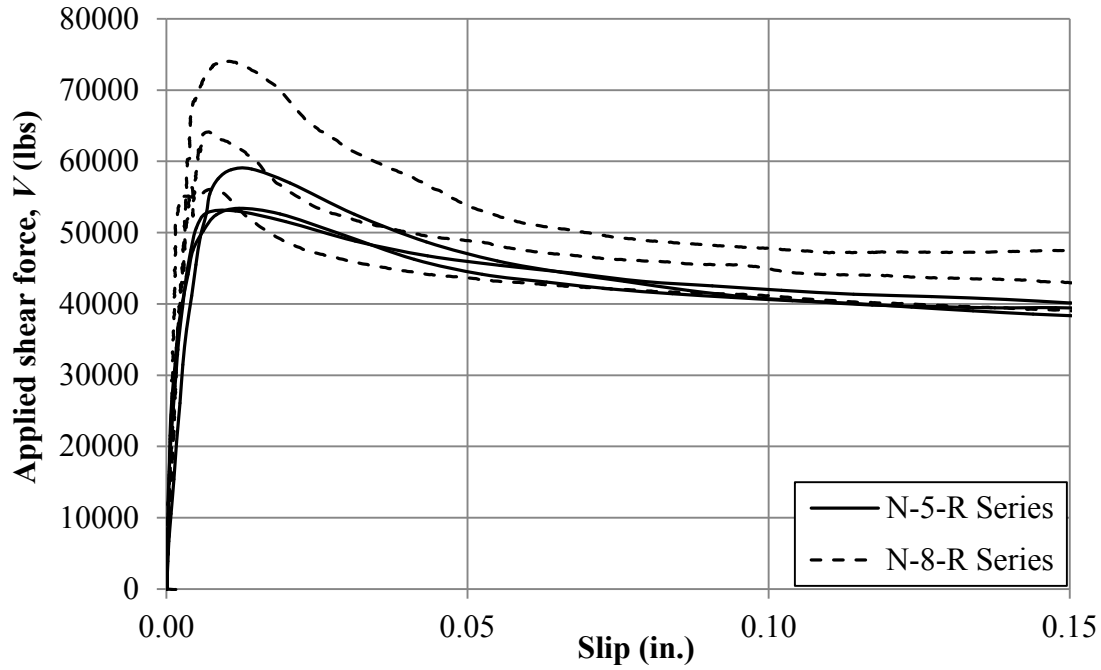

Figure 4.13. Effect of concrete strength for normalweight roughened interface specimens.

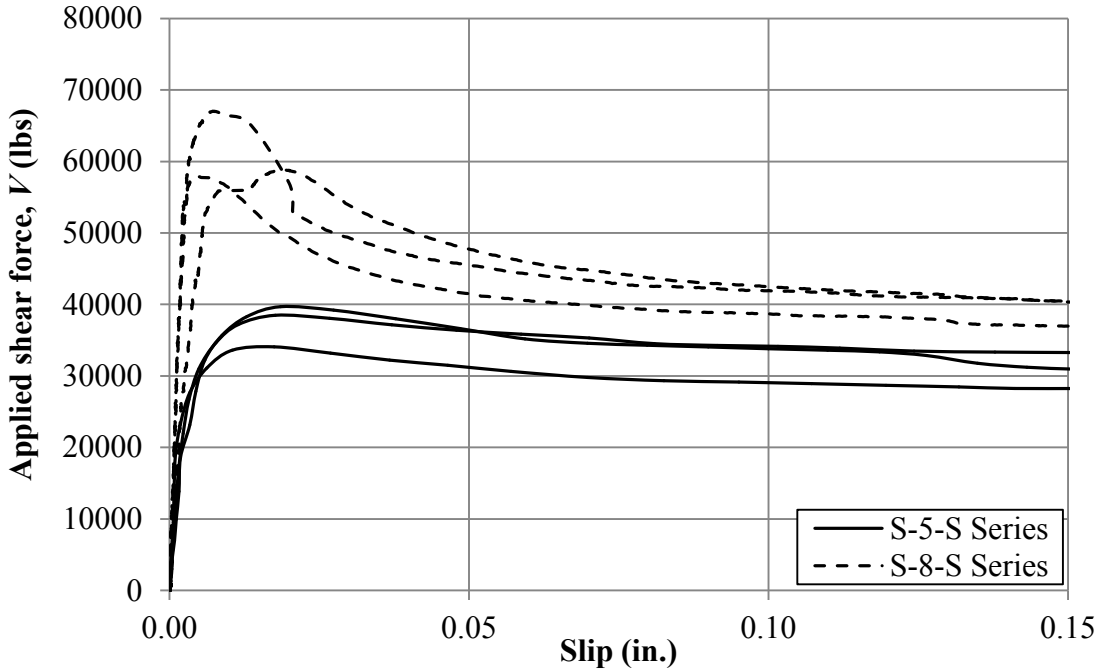

Figure 4.14. Effect of concrete strength for sand-lightweight smooth interface specimens.

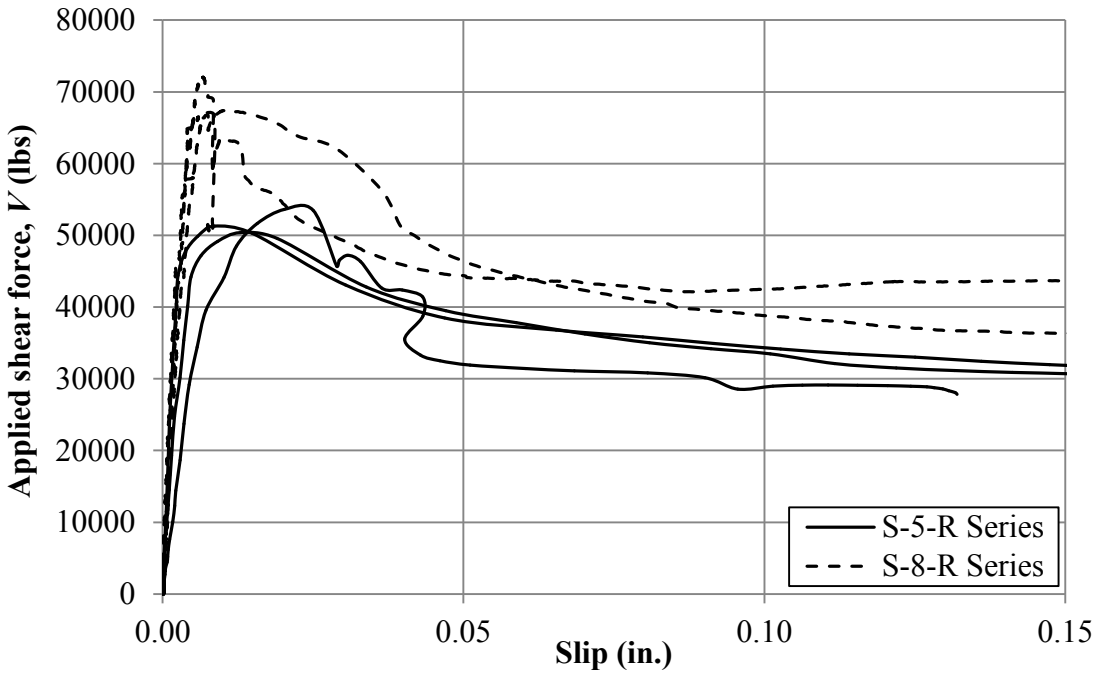

Figure 4.15. Effect of concrete strength for sand-lightweight roughened interface specimens.

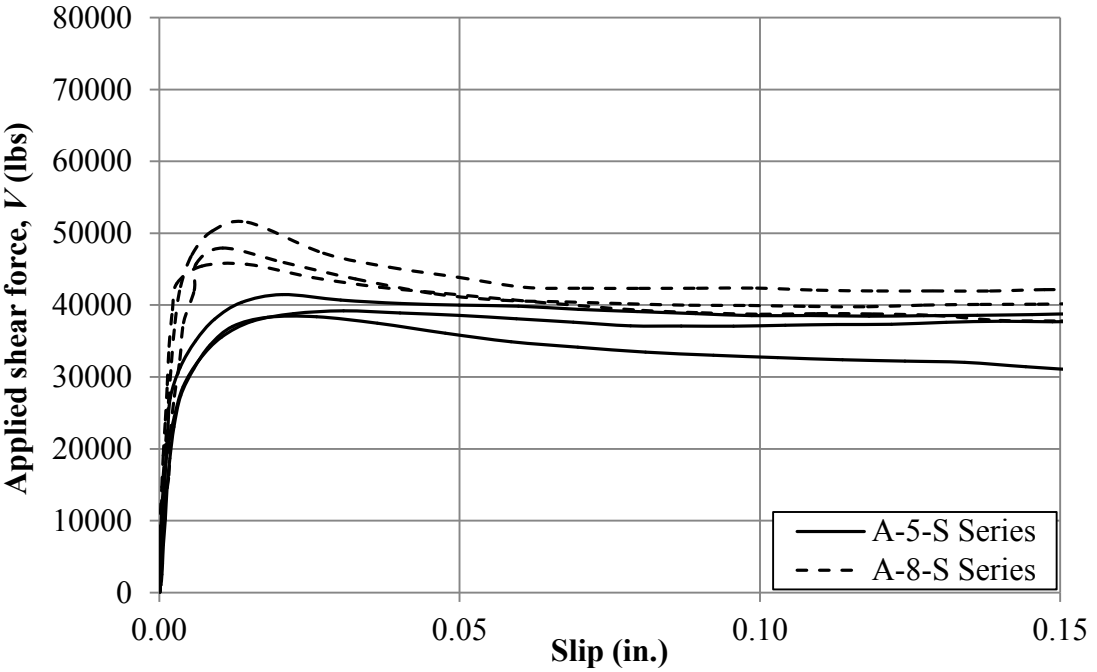

Figure 4.16. Effect of concrete strength for all-lightweight smooth interface specimens.

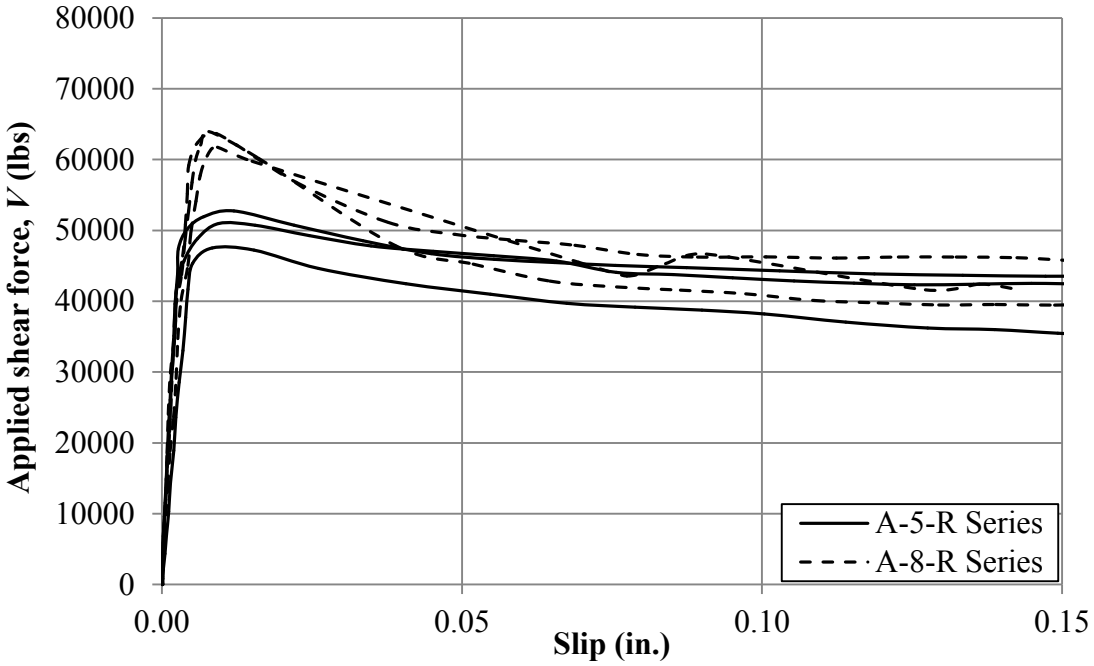

Figure 4.17. Effect of concrete strength for all-lightweight roughened interface specimens.

Table 4.3. Effect of Concrete Compressive Strength on the Average Ultimate Shear Stress for Each Specimen Series

Concrete Type	Smooth Interface				Roughened Interface			
	5000 psi (lb/in^2)	8000 psi (lb/in^2)	% Diff[1] (%)	% Increase[2] (%)	5000 psi (lb/in^2)	8000 psi (lb/in^2)	% Diff[1] (%)	% Increase[2] (%)
Normal-weight	680	1173	53%	73%	1037	1310	23%	26%
Sand-lightweight	757	1237	48%	63%	1117	1390	22%	24%
All-lightweight	813	983	19%	22%	1030	1280	22%	24%
Average	750	1131			1061	1327		

[1] Percent difference of the 5000 psi and 8000 psi specimens for a given concrete type and interface condition.
[2] Percent increase from 5000 psi to 8000 psi specimens for a given concrete type and interface condition.

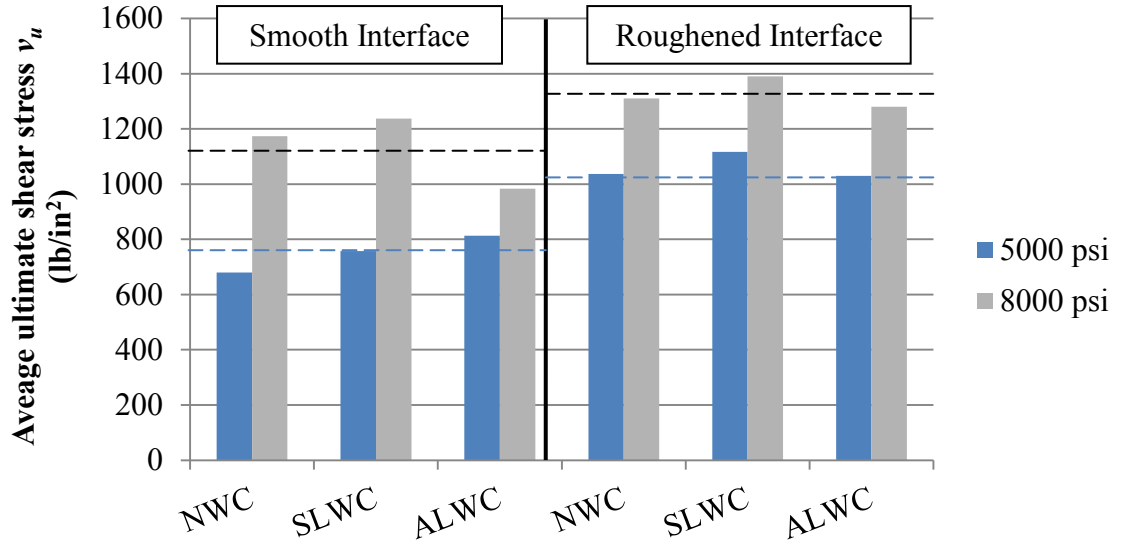

Figure 4.18. Effect of concrete compressive strength on the average ultimate shear stress for each specimen series

4.3.3. Effect of Shear Interface Preparation. Specimens tested in this program included non-monolithic interfaces that were either trowelled smooth or roughened to 0.25 in. amplitude as discussed in Section 3.4.3. This section compares the results of the experiments in terms of interface condition. To isolate this parameter, specimens with the same target compressive strength of concrete and concrete type (unit weight) were compared.

Figure 4.19 through Figure 4.24 compare the applied shear force-slip relations for series with the same concrete type and target compressive strength. The shear force has not been normalized since the compressive strength of concrete is the same for the series being compared. (The figures are similar to the figures presented in Section 3.6, but with a format similar to other figures in this section.) Figure 4.19 through Figure 4.24 show that, for specimens with the same concrete type and target compressive strength, the peak shear force is higher for specimens with a roughened interface than for those with a smooth interface. This can be explained as follows. For specimens with a smooth interface, the aggregate interlock is limited, and the initial load transfer capability is due to concrete cohesion at the interface. As discussed in Section 4.2, first cracking was found to occur at an applied shear stress v_{cr} in the range of approximately 250 psi to 650 psi for specimens with a smooth interface and between 550 psi to 880 psi for specimens with a roughened interface. The lack of surface roughness in the smooth interface specimens allows for limited restraint of motion, and limited increase in shear force, once the interfacial bond is eliminated. Table 4.3 compares the average ultimate shear stress v_u for specimens with a smooth and roughened interface in each series. Specimens with a roughened interface had an average ultimate shear stress 11% to 42% higher than corresponding specimens with a smooth interface.

As discussed in Section 4.2.2, the applied shear force-slip relations presented in Section 3.6 indicate that specimens with a roughened interface behaved in a more quasi-brittle manner than the corresponding smooth interface specimens. Figure 4.19 through Figure 4.24 show that the

residual shear force is similar for specimens of the same concrete type and compressive strength, but different interface condition. For the specimens with 5000 psi concrete and a smooth interface, Figures 4.19, 4.21, and 4.23 show that the peak shear force that was similar in magnitude to the residual shear force. In other words, the ratio V_u/V_{ur} (or v_u/v_{ur}) is close to 1.0. In the case of the 8000 psi concrete specimens with a smooth interface, however, Figures 4.20, 4.22, and 4.24 show that the peak shear force was higher than the residual shear force resulting in a higher peak force-to-residual force ratio V_u/V_{ur} (or v_u/v_{ur}). In fact, the response of the 8000 psi smooth interface specimens with normalweight or sand-lightweight concrete is similar, in terms of load-slip behavior, to that the corresponding specimens with a roughened interface. This observation suggests interface condition may be less significant at higher concrete compressive strengths for the case of normalweight concrete. Comparison of Figure 4.23 and 4.24 indicates that increased concrete compressive strength did not influence the general shape of the response for the all-lightweight concrete specimens.

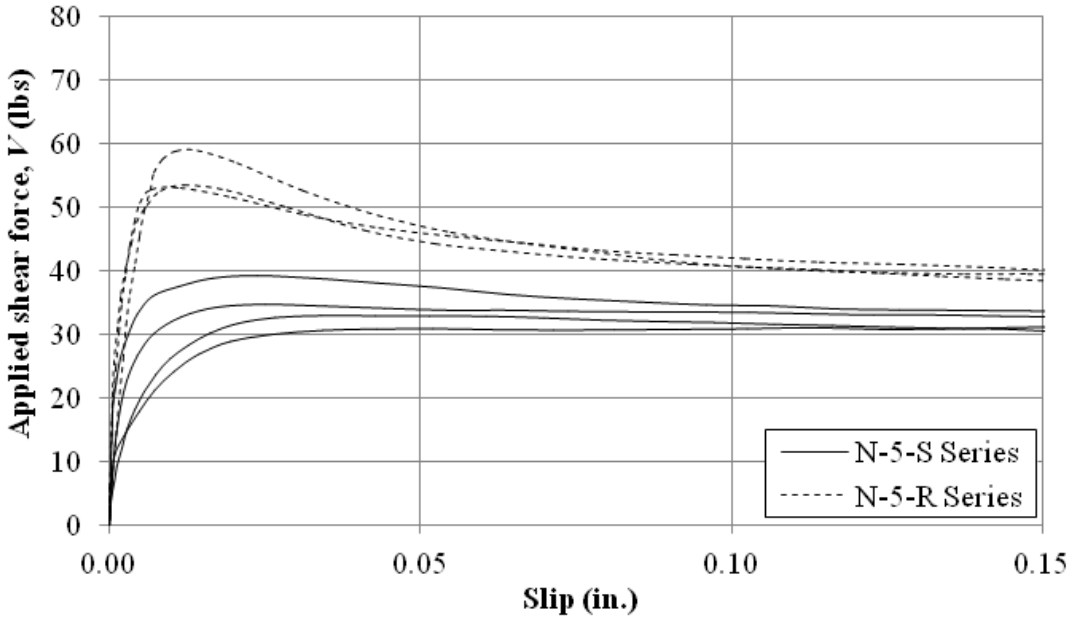

Figure 4.19. Effect of interface roughness on the applied shear force for 5000 psi normalweight concrete specimens

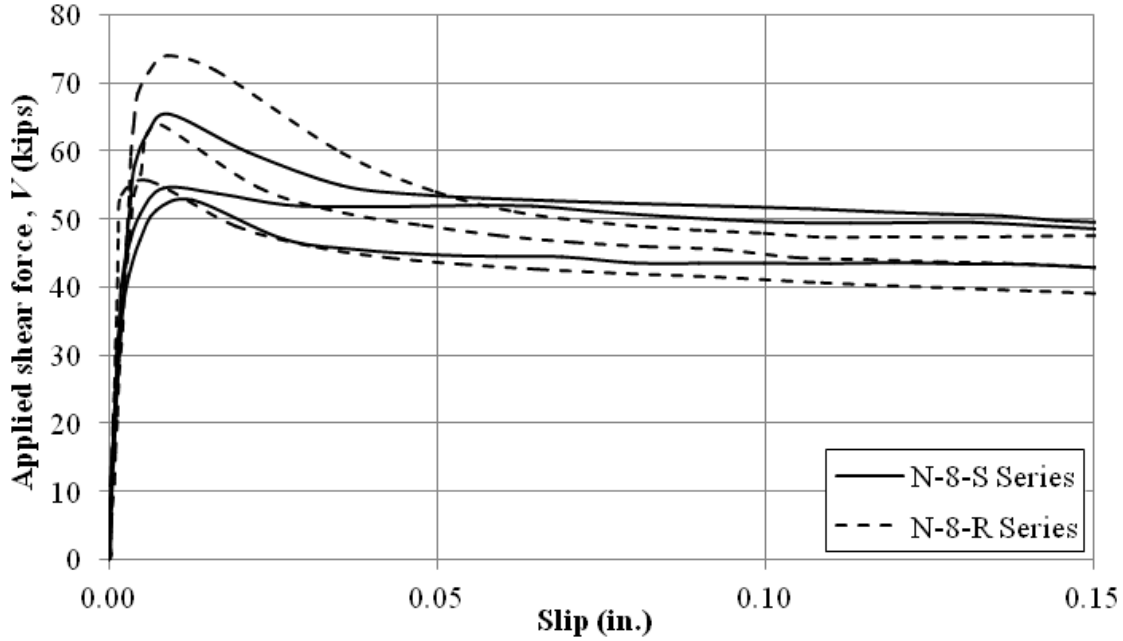

Figure 4.20. Effect of interface roughness on the applied shear force for 8000 psi normalweight concrete specimens

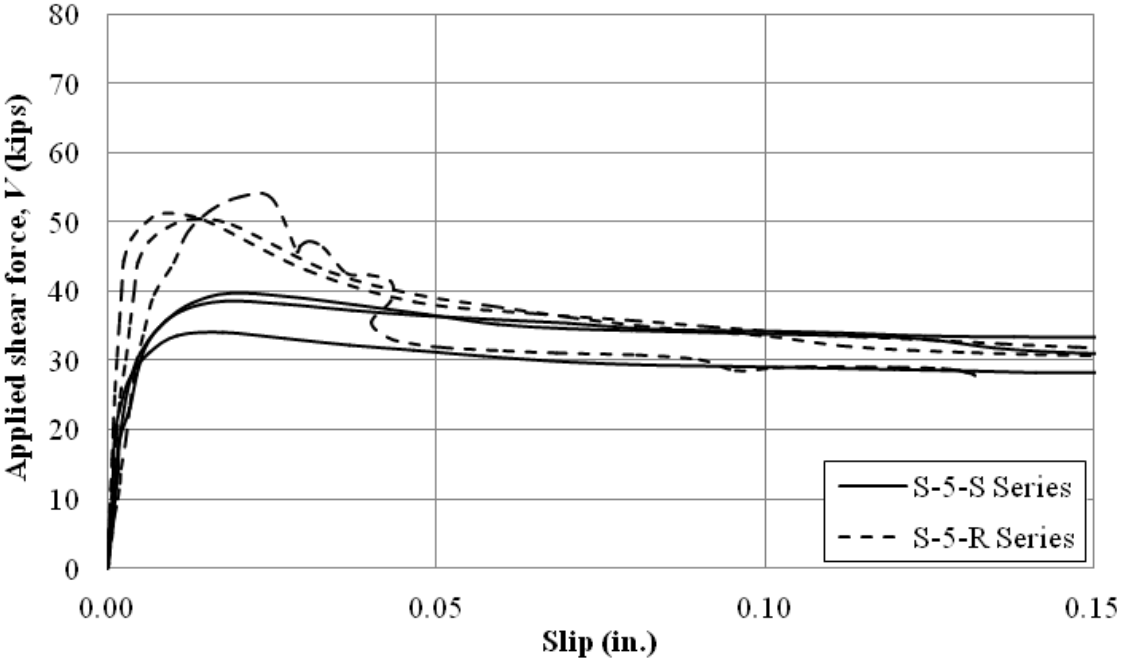

Figure 4.21. Effect of interface roughness on the applied shear force for 5000 psi sand-lightweight concrete specimens

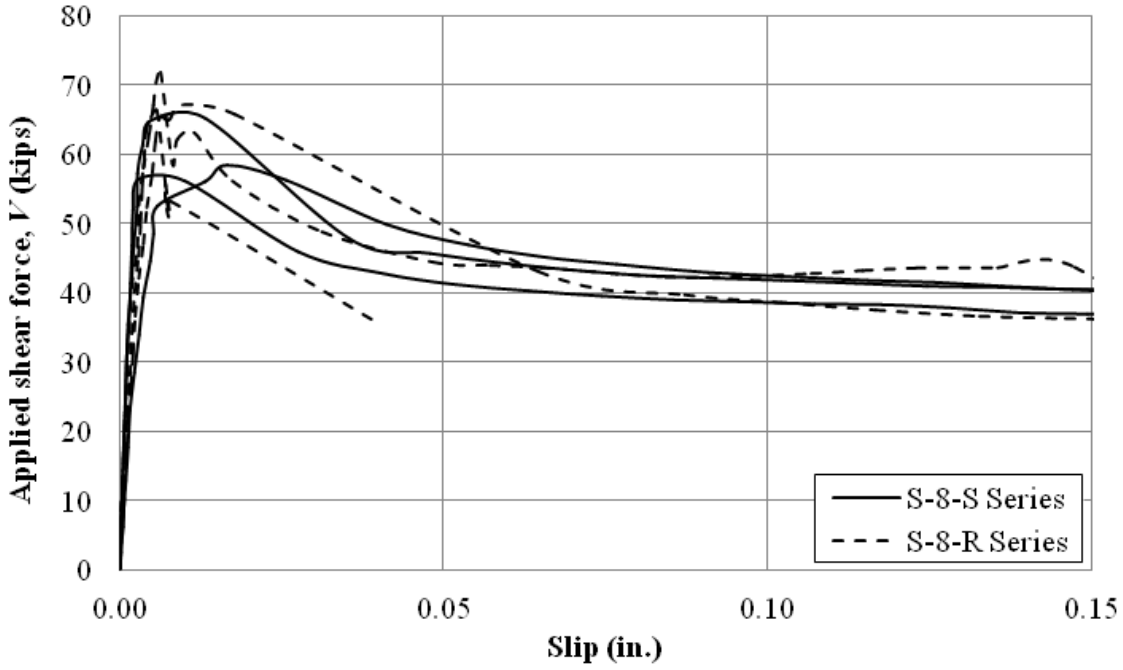

Figure 4.22. Effect of interface roughness on the applied shear force for 8000 psi sand-lightweight concrete specimens

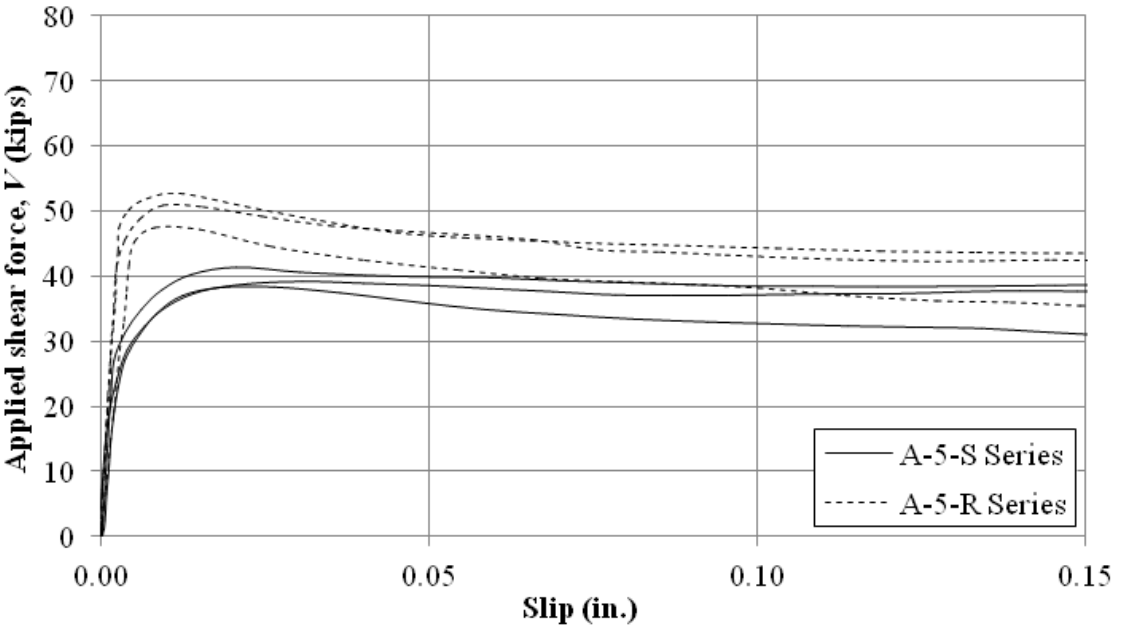

Figure 4.23. Effect of interface roughness on the applied shear force for 5000 psi all-lightweight concrete specimens

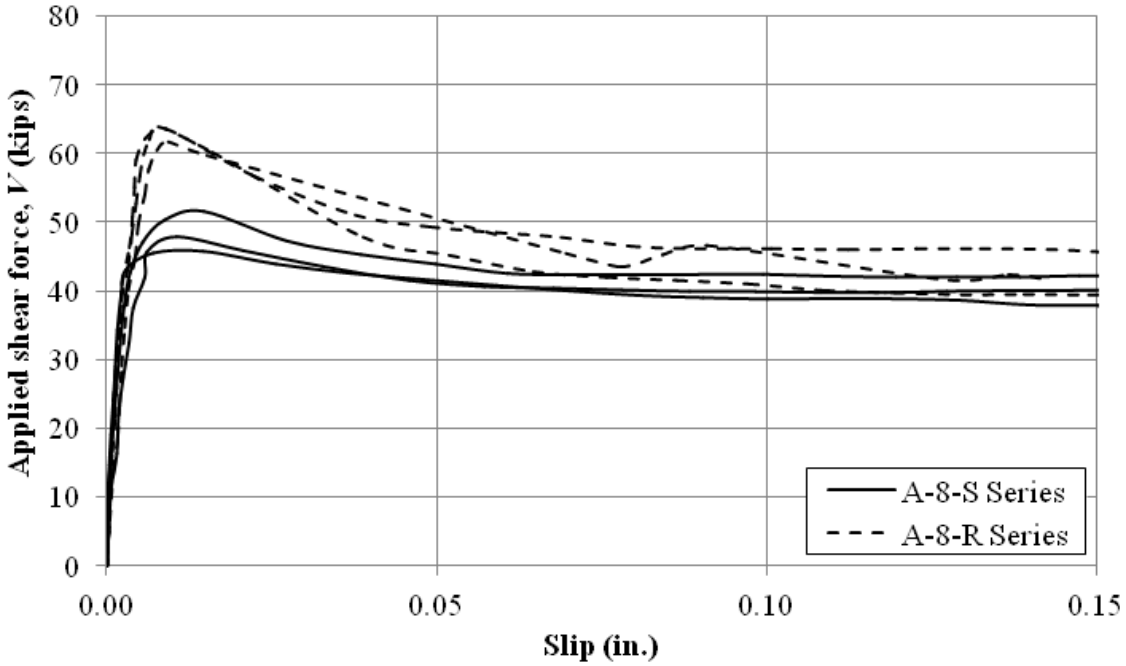

Figure 4.24. Effect of interface roughness on the applied shear force for 8000 psi all-lightweight concrete specimens

Table 4.4. Effect of Interface Preparation on the Ultimate Shear Capacity

Specimen Series	Average Ultimate Shear Capacity (lb/in^2)		
	Smooth Interface	Roughened Interface	% Increase
N-5	680	1037	42%
N-8	1173	1310	11%
S-5	757	1117	38%
S-8	1237	1390	12%
A-5	813	1030	24%
A-8	983	1280	26%

4.4. COMPARISON TO PCI AND ACI DESIGN PROVISIONS

In this section the design provisions discussed in Section 2.3 are evaluated with respect to the results of the specimens tested in this program. Section 4.4.1 summarizes the equations and limits used in the evaluation. In Section 4.4.2, results are compared in terms of the effective coefficient of friction μ_e computed using the PCI Design Handbook. In Section 4.4.3, results are compared in terms of the nominal shear strength V_n (or v_n) computed using the PCI Design Handbook and the ACI 318 code.

4.4.1. Shear Friction Design Provisions. This section summarizes the equations and limits in the 6th and 7th Editions of the PCI Design Handbook (2004 and 2011) and the ACI 318

code (2011) shear friction design provisions used in comparing the results of the test data. The limitations on the application of design provisions are summarized in Table 4.5 to Table 4.7. The design provisions are discussed in detail in Section 2.3.

Table 4.5. Limits for Applied Shear of Shear Friction Elements.

Case	PCI 6th Edition Max $V_u = \phi V_n$	PCI 7th Edition Max V_u/ϕ	ACI 318-11 Max V_n
1	$0.30\lambda^2 f'_c A_{cr} \leq 1000\lambda^2 A_{cr}$	$0.30\lambda f'_c A_{cr} \leq 1000\lambda A_{cr}$	For normalweight concrete: $0.2f'_c A_c < (480 + 0.08f'_c)A_c < 1600A_c$ For all other cases: $0.2f'_c A_c \leq 800A_c$
2	$0.25\lambda^2 f'_c A_{cr} \leq 1000\lambda^2 A_{cr}$	$0.25\lambda f'_c A_{cr} \leq 1000\lambda A_{cr}$	
3	$0.20\lambda^2 f'_c A_{cr} \leq 800\lambda^2 A_{cr}$	$0.20\lambda f'_c A_{cr} \leq 800\lambda A_{cr}$	$0.2f'_c A_c \leq 800A_c$
4	$0.30\lambda^2 f'_c A_{cr} \leq 800\lambda A_{cr}$	$0.30\lambda f'_c A_{cr} \leq 800\lambda A_{cr}$	

Table 4.6. Shear Friction Coefficients Recommended for Design

		PCI 6th Edition		PCI 7th Edition		ACI 318-11
Case	Crack Interface Condition	μ	Max μ_e	μ	Max μ_e	μ
1	Concrete to concrete, cast monolithically	1.4λ	3.4	1.4λ	3.4	1.4λ
2	Concrete to hardened concrete, with roughened surface	1.0λ	2.9	1.0λ	2.9	1.0λ
3	Concrete placed against hardened concrete not intentionally roughened	0.6λ	2.2	0.6λ	Not applicable	0.6λ
4	Concrete to steel	0.7λ	2.4	0.7λ	Not applicable	0.7λ

Table 4.7. Values for μ and λ with Respect to Concrete Type and Interface Condition

Factor	Normalweight		Sand-lightweight		All-lightweight	
	Smooth	Rough	Smooth	Rough	Smooth	Rough
μ	0.60	1.00	0.51	0.85	0.45	0.75
λ	1.00	1.00	0.85	0.85	0.75	0.75

4.4.1.1. PCI Design Handbook 6th Edition (2004). Equations 4.1 and 4.2 are presented in the 6th Edition of the PCI Design Handbook as discussed in Section 2.3.1.1.

$$A_{vf} = \frac{V_u}{\phi f_y \mu_e} \tag{4.1}$$

$$\mu_e = \frac{1000 \lambda A_{cr} \mu}{V_u} \tag{4.2}$$

Equations 4.1 and 4.2 apply to all four interface conditions, Cases 1-4, defined in Section 1.1. Substituting the term V_n for V_u/ϕ, and recognizing that $V_n=v_nA_{cr}$, Equations 4.1 and 4.2 can be expressed in terms of in v_n in Equation 4.3:

$$v_n = 31.62\sqrt{\phi \rho f_y \lambda \mu} \tag{4.3}$$

Equation 4.1 can be rewritten in terms of μ_e as in Equation 4.4:

$$\mu_e = \frac{v_n}{\rho f_y} \tag{4.4}$$

The maximum value of ϕV_n is limited to the values shown in Table 4.5. f_y is limited to 60 ksi. The maximum value of μ_e is limited to the values shown in Table 4.6. Values of λ and μ are given in Table 4.6.

4.4.1.2. PCI Design Handbook 7th Edition (2011). In the current edition of the PCI Design Handbook (7th Edition), two approaches can be used to determine the required shear reinforcement as discussed in Section 2.3.1.2. The first approach includes the coefficient of friction, μ, while the second approach includes the effective coefficient of friction, μ_e. The first approach is shown in Equation 4.5 and can be used for all four crack interface conditions (Cases 1-4 Table 4.5).

$$A_{vf} = \frac{V_u}{\phi f_y \mu} \tag{4.5}$$

Substituting the term V_n for V_u/ϕ, and recognizing that $V_n=v_nA_{cr}$, Equation 4.5 can be expressed in terms of in v_n in Equation 4.6:

$$v_n = \rho f_y \mu \tag{4.6}$$

Equation 4.5 can be rewritten in terms of μ as in Equation 4.7:

$$\mu = \frac{v_n}{\rho f_y} \tag{4.7}$$

The second approach to determining the required shear reinforcement is shown in Equation 4.8, where μ_e is given in Equation 4.9. Use of Equation 4.8 is limited to situations where load reversal does not occur, and the interface of consideration is either monolithic or has an intentionally roughened surface (Cases 1 and 2 in Table 4.5). Equations 4.8 and 4.9 are similar to Equations 4.1 and 4.2 from the 6th Edition of the PCI Handbook except for the inclusion of ϕ in Equation 4.9.

$$A_{vf} = \frac{V_u}{\phi f_y \mu_e} \tag{4.8}$$

$$\mu_e = \frac{\phi 1000 \lambda A_{cr} \mu}{V_u} \tag{4.9}$$

Substituting the term V_n for V_u/ϕ and recognizing that $V_n=v_nA_{cr}$ leads to Equation 4.10:

$$v_n = 31.62\phi\sqrt{\rho f_y \lambda \mu} \tag{4.10}$$

Equation 4.8 can be rewritten in terms of μ_e as in Equation 4.11:

$$\mu_e = \frac{v_n}{\rho f_y} \tag{4.11}$$

The maximum value of V_u/ϕ (=V_n) is limited to the values shown in Table 4.5. f_y is limited to 60 ksi. The maximum value of μ_e is limited to the values shown in Table 4.6. Values of μ and λ are given in Table 4.7.

4.4.1.3. ACI 318-11. Equation 4.12 is presented in the ACI 318 code as discussed in Section 2.3.1.

$$V_n = \mu A_{vf} f_y \tag{4.12}$$

Substituting the term V_n for V_u/ϕ, and recognizing that $V_n=v_nA_{cr}$ leads to Equation 4.13:

$$v_n = \rho f_y \mu \tag{4.13}$$

Equation 4.12 can be rewritten in terms of μ as in Equation 4.14:

$$\mu = \frac{v_n}{\rho f_y} \tag{4.14}$$

The maximum value of V_n is limited to the values shown in Table 4.5. f_y is limited to 60 ksi. Values of μ and λ are given in Table 4.7.

4.4.2. Shear Strength. In this section, the peak shear stress v_u of the specimens tested in Section 3 is compared with the values predicted using the current (7th Edition) PCI Design Handbook (2011) and ACI 318 code (2011) provisions for designing the required shear interface reinforcement. The predicted value of the shear strength v_n is computed using two approaches: 1) the coefficient of friction μ approach, which is permitted in both the current (7th Edition) PCI Design Handbook and the ACI 318 code and is applicable to all interface conditions, and 2) the effective coefficient of friction μ_e approach, which is permitted in the current PCI Design Handbook (7th Edition) for roughened interface (Case 2) conditions. It should be noted that the μ_e approach is applicable to non-monolithic interface conditions with either a roughened or smooth interface condition (Case 2 and 3 respectively) in the 6th Edition of the PCI Design Handbook, but it is not applicable to non-monolithic interface conditions with a smooth interface condition (Case 3) in the 7th Edition. However, the predictive equation for μ_e is examined herein to determine whether its application is conservative for the specimens in this study. Values of μ_e are taken from the 6th Edition in this comparison.

Using the coefficient of friction μ approach, the predicted value of the shear strength v_n is computed using Equations 4.6 (PCI Design Handbook) and 4.13 (ACI 318 code), which are the same equation. The value of μ is a function of the interface condition and concrete type as given in Table 4.6. Using the effective coefficient of friction μ_e approach in the PCI Design Handbook, the predicted value of v_n is computed using Equation 4.10. Equations 4.6 (and 4.13) and 4.10 are plotted in Figure 4.25 to Figure 4.30 for the different concrete types and interface conditions. The upper limit on the shear strength for each approach is given in Table 4.5. f_y is limited to 60 ksi. The data are presented in this way as it results in the least conservative condition. Values of the peak shear stress v_u for the corresponding test specimens are plotted on the graphs for comparison.

In Figure 4.25 to Figure 4.30, good correlation is observed for specimens with 5000 psi concrete compressive strength (regardless of interface condition) using the μ_e approach of Equation 4.10 (dashed line in the figures). As concrete compressive strength increases, the results are increasingly conservative. In all cases, the μ approach of Equations 4.6 and 4.13 (solid line in the figures) is conservative.

Figure 4.25, 4.27, and 4.29 pertain to specimens with a smooth interface condition. As mentioned previously, the μ_e approach in the current (7th Edition) PCI Design Handbook is not applicable for Case 3 interface conditions. However, the results indicate that using this approach, a similar level of conservatism is achieved as for the specimens with the same concrete type and a roughened interface condition shown in Figures 4.26, 4.28, and 4.30. These test results support

the previous version of the PCI Design Handbook (6th Edition) that allowed the application of the effective coefficient of friction for non-monolithic smooth interface conditions (Case 3).

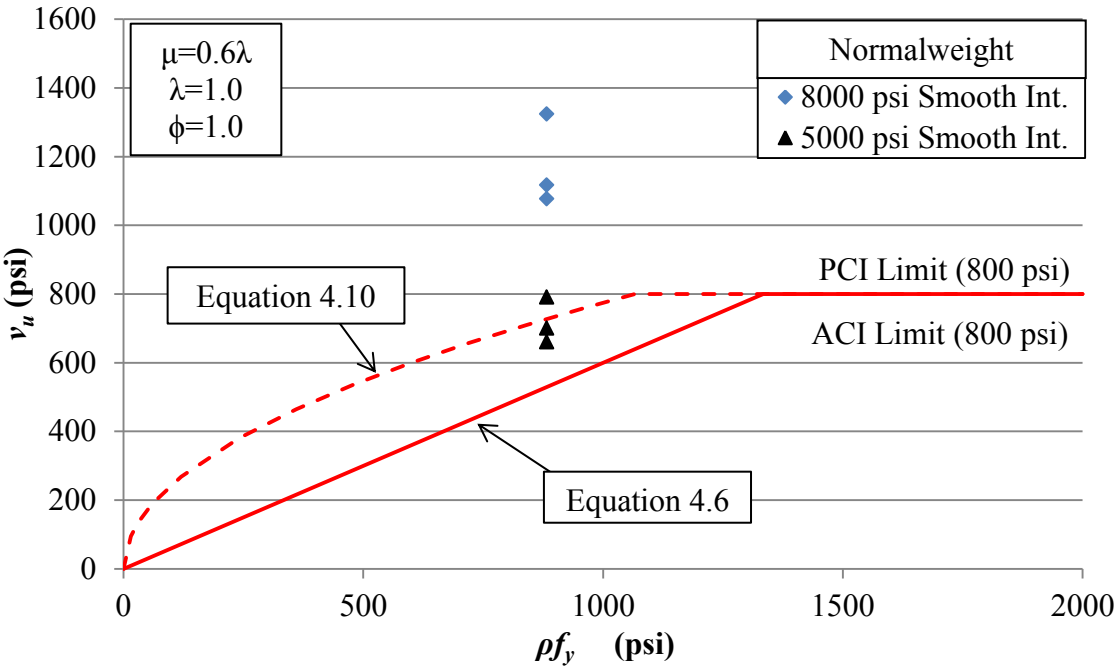

Figure 4.25. Comparison of shear strength v_u with Equations 4.6 and 4.10 for normalweight concrete specimens with a smooth interface

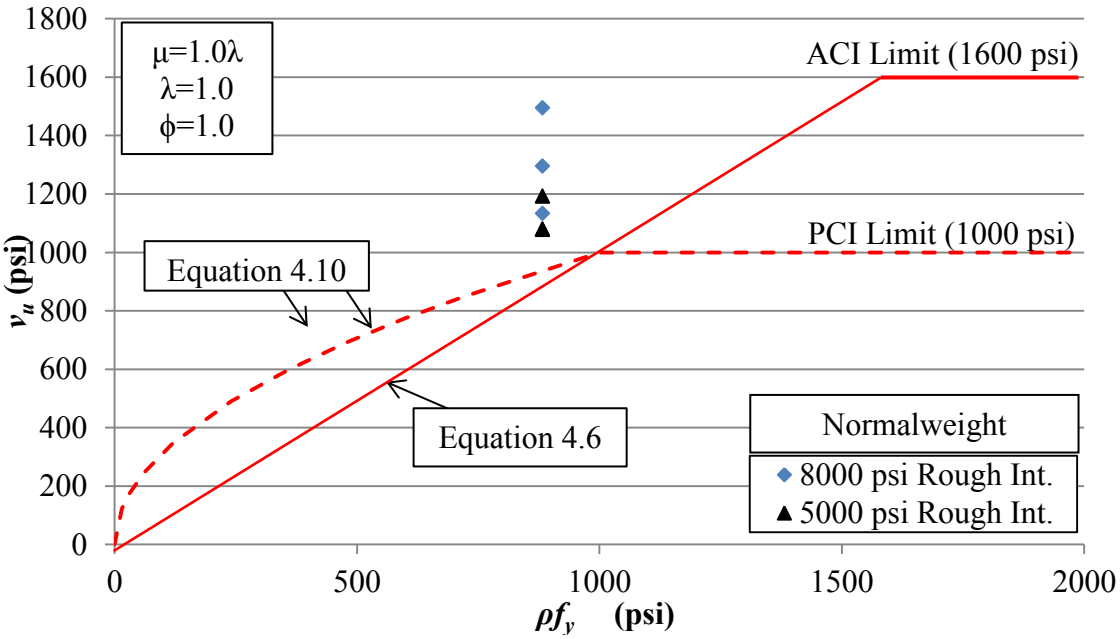

Figure 4.26. Comparison of shear strength v_u with Equations 4.6 and 4.10 for normalweight concrete specimens with a roughened interface

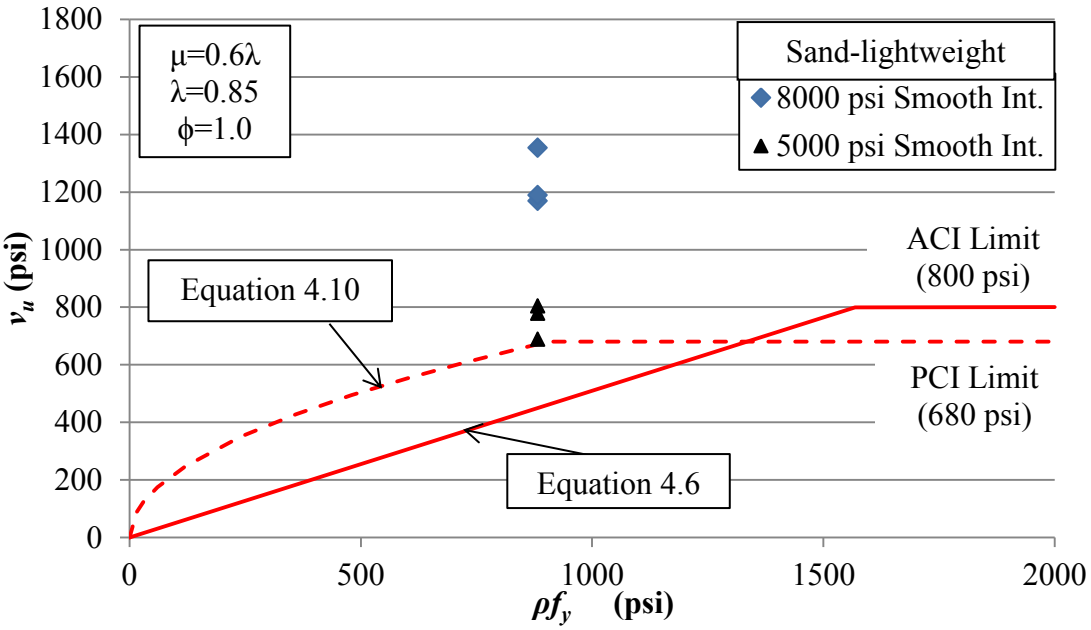

Figure 4.27. Comparison of shear strength v_u with Equations 4.6 and 4.10 for sand-lightweight concrete specimens with a smooth interface

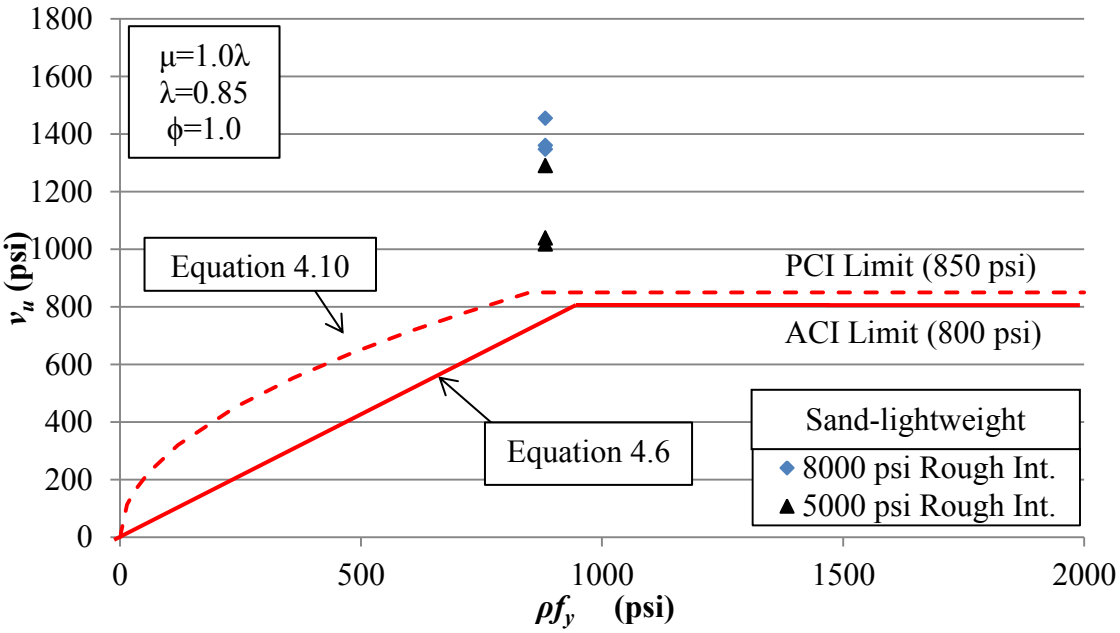

Figure 4.28. Comparison of shear strength v_u with Equations 4.6 and 4.10 for sand-lightweight concrete specimens with a roughened interface

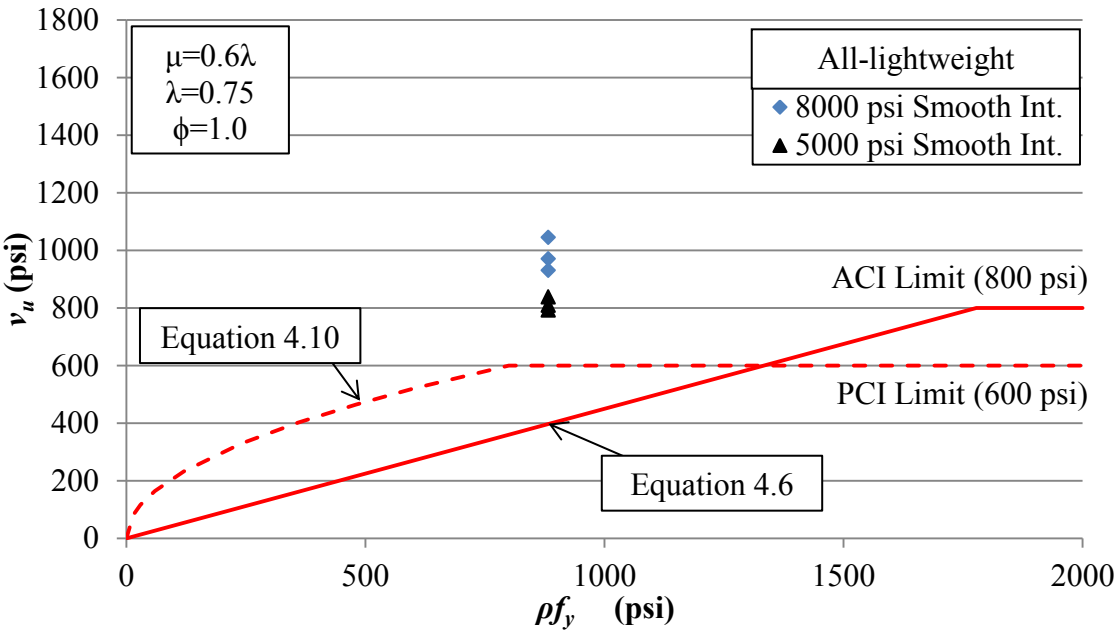

Figure 4.29. Comparison of shear strength v_u with Equations 4.6 and 4.10 for all-lightweight concrete specimens with a smooth interface

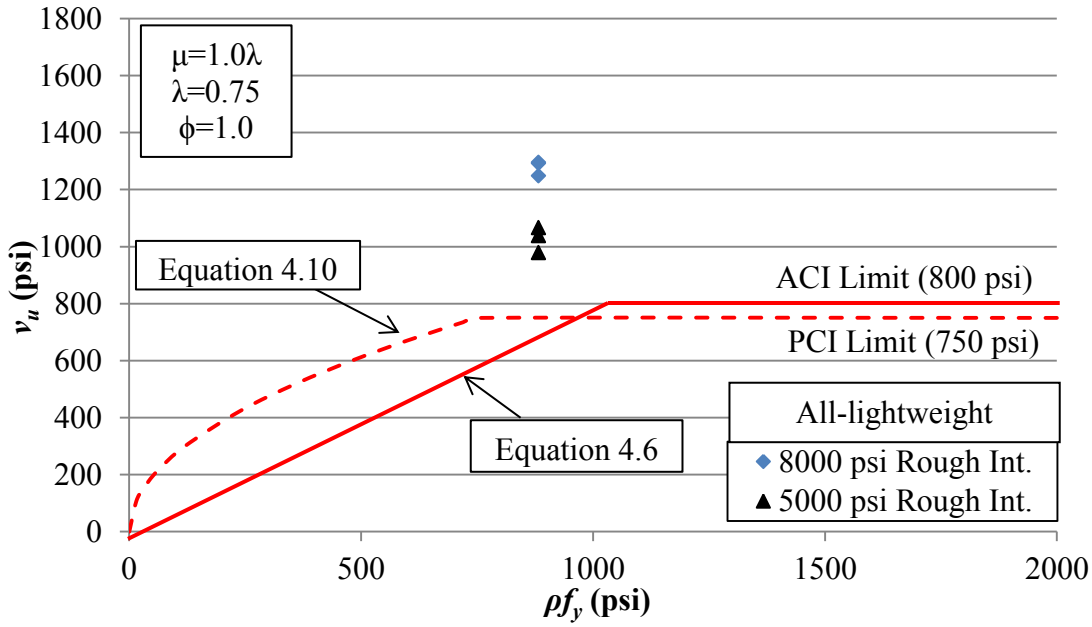

Figure 4.30. Comparison of shear strength v_u with Equations 4.6 and 4.10 for all-lightweight concrete specimens with a roughened interface

4.4.3. Effective Coefficient of Friction, μ_e. In this section, the results of the Section 3 experiments are compared to predicted values of the effective coefficient of friction μ_e using the equations and limits on shear strength from the current PCI Design Handbook (7th Edition). As discussed in Section 4.4.1, the μ_e approach is applicable to non-monolithic interface conditions with either a roughened or smooth interface condition (Case 2 and 3 respectively) in the 6th Edition, but it is not applicable to non-monolithic interface conditions with a smooth interface condition (Case 3) in the 7th Edition. However, the predictive equation for μ_e is examined herein to determine whether its application is conservative for the specimens in this study. Values of μ_e are taken from the 6th Edition in this comparison.

Figures 4.31 through 4.36 compare the measured and predicted values of μ_e for each concrete type and interface condition. The predicted value of μ_e is determined from Equation 4.9. Equation 4.9 is the same as Equation 4.2 from the 6th Edition of the PCI Handbook with the exception of the strength reduction factor ϕ in Equation 4.9. Since material strengths are known values, ϕ=1.0, and therefore the results of Equations 4.2 and 4.9 are the same for this comparison. The upper limit on v_n in each figure is the result of the limits shown in Table 4.5 for the 7th Edition. Since all of the specimens in this study had a concrete compressive strength greater than 4000 psi, the quantities $1000\lambda A_{cr}$ and $800\lambda A_{cr}$ govern. The upper limit on μ_e is based maximum values indicated in Table 4.6 from the 6th Edition, since the μ_e approach is applicable to specimens with a smooth interface condition (Case 3). The measured value of μ_e is computed from the shear strength using Equation 4.11 from the 7th Edition with $V_u=\phi V_n$, which yields the same results as Equation 4.4 from the 6th Edition. The value of f_y is the measured yield stress of the interface steel reinforcement. Load and strength reduction factors are taken as 1.0 since the magnitude of the applied load and the material properties are known. In the figures, measured values above and right of the lines indicate conservative values of the effective coefficient of friction, while values to the left and inside the lines indicate unconservative values.

Figure 4.31 and 4.32 for normalweight concrete indicate good correlation between the test results and the predicted value of μ_e for specimens with a smooth or roughened interface condition and a compressive strength of concrete near 5000 psi (N-5-S and N-5-R series, respectively). Comparing series with 5000 psi and 8000 psi concrete indicates that increases in concrete compressive strength result in increasing levels of conservatism for the same interface condition. Similarly, Figures 4.33 and 4.34 compare the results of the sand-lightweight concrete specimens, and Figures 4.35 and 4.36 compare the results of the all-lightweight concrete specimens. All points reported in Figures 4.31 through 4.36 are average values for each series to facilitate discussion. All results are tabulated in Table 4.2. From these figures, it can be seen that the predicted value of effective coefficient of friction μ_e is conservative, and in some cases very conservative, for concretes containing lightweight aggregates. It should be noted however, that the predicted value of the effective coefficient of friction μ_e was slightly unconservative for the normalweight concrete specimens with compressive strengths near 5000 psi and a smooth interface condition. Further study is needed to investigate this condition.

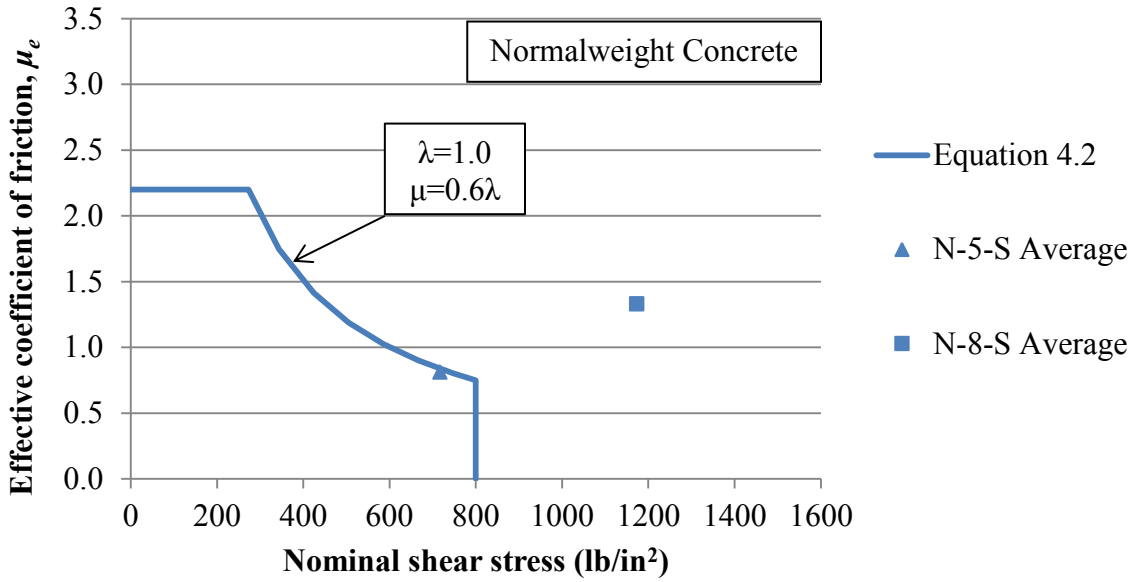

Figure 4.31. Evaluation of the effective coefficient of friction for normalweight smooth interface concrete

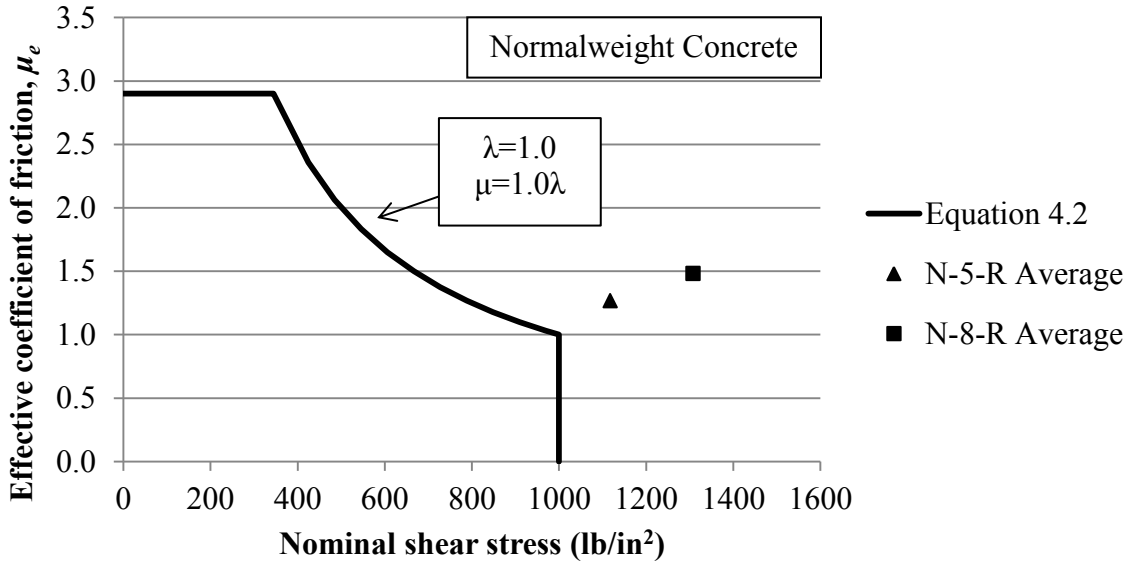

Figure 4.32. Evaluation of the effective coefficient of friction for normalweight roughened interface concrete

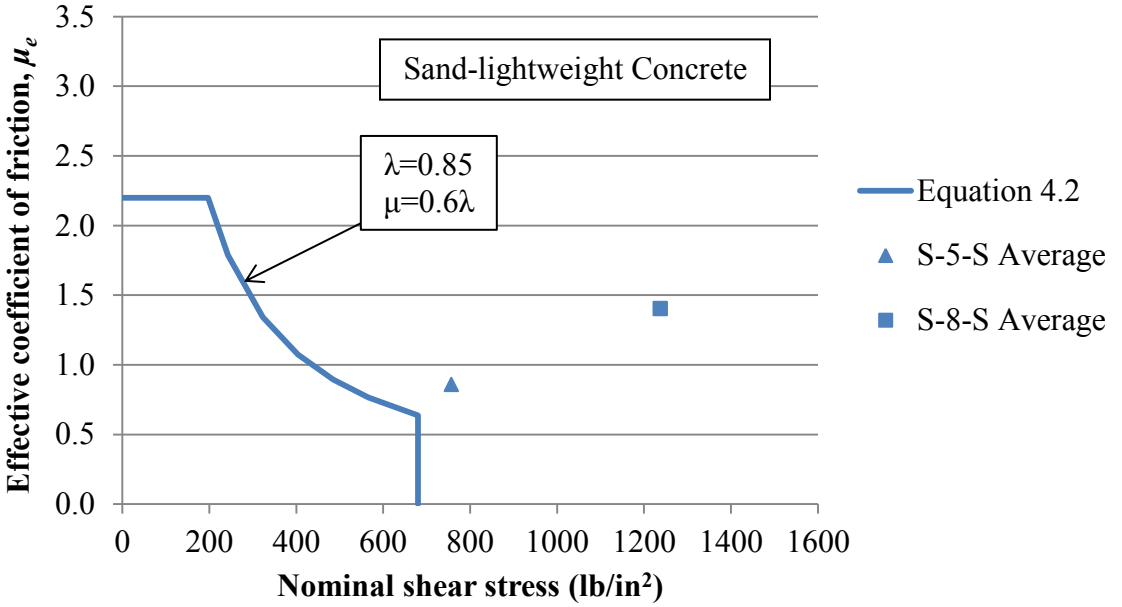

Figure 4.33. Evaluation of the effective coefficient of friction for sand-lightweight smooth interface concrete

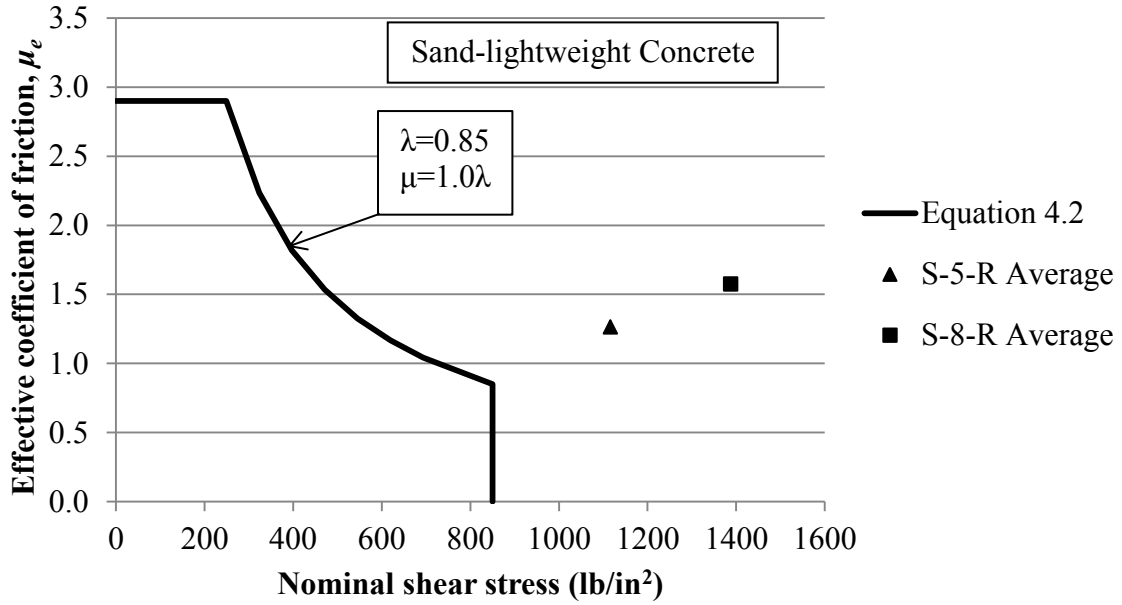

Figure 4.34. Evaluation of the effective coefficient of friction for sand-lightweight roughened interface concrete

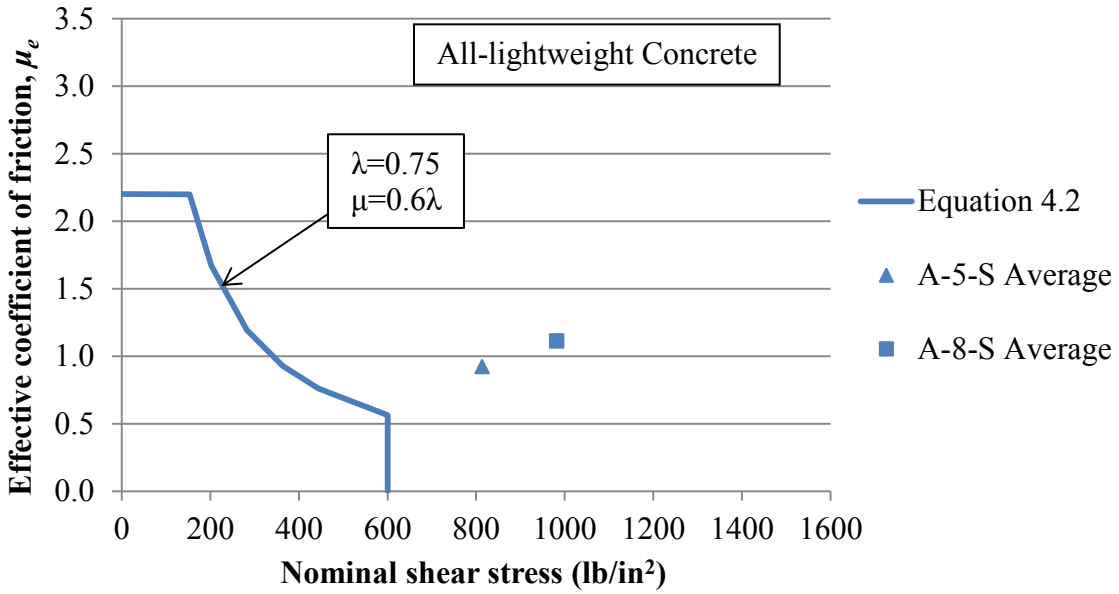

Figure 4.35. Evaluation of the effective coefficient of friction for all-lightweight smooth interface concrete

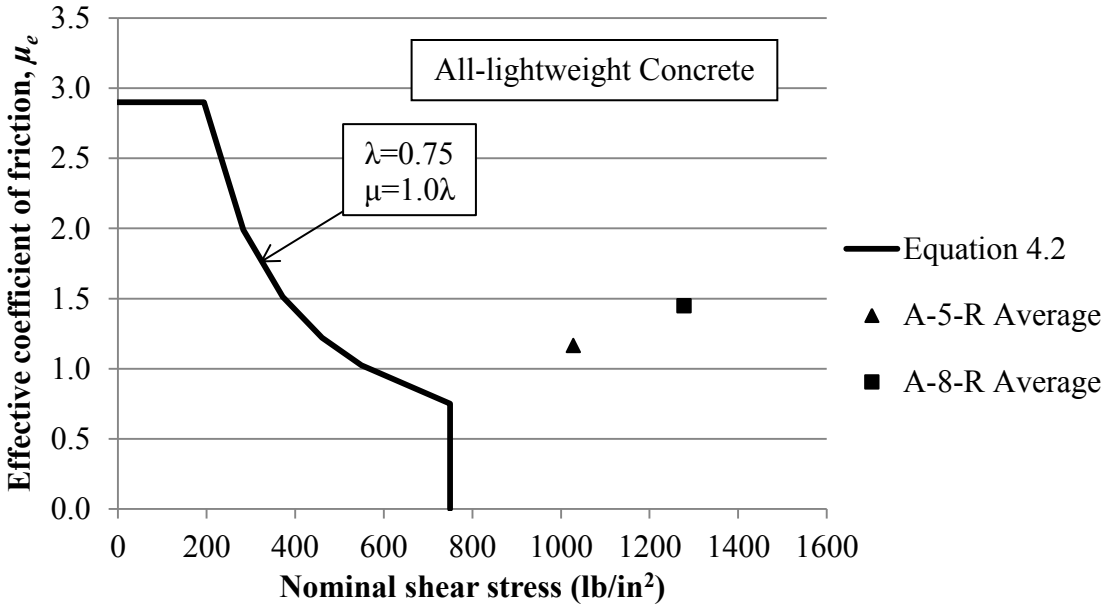

Figure 4.36. Evaluation of the effective coefficient of friction for all-lightweight roughened interface concrete

In the calculation of the predictive value of μ_e (Equation 4.9) the lightweight modification factor λ, which is intended to account for reduced mechanical properties of lightweight concretes relative to normalweight concrete of the same compressive strength, is included explicitly and in the value for the coefficient of friction, μ. As a result, the calculation of μ_e includes the term λ^2, which results in a significant reduction in μ_e for lightweight concretes. As discussed in the

previous paragraph, results for the sand-lightweight and all-lightweight concrete specimens in this study were quite conservative with respect to predicted values of μ_e. As discussed in Section 4.3.1, unit weight (concrete type) did not significantly influence the shear strength of the specimens in this study, and as a result, the need for including the term λ^2 (or even λ) may be questioned. To examine this issue further, the average values for all series with the same interface condition are plotted on the same graph with $\lambda = 1.0$ (i.e., no reduction in mechanical properties) in Figures 4.37 and 4.38. From these figures it can be see that all 5000 psi specimen averages show good correlation to predicted values, and for the 8000 psi specimens, the results are more conservative. This result suggests that concrete compressive strength (f'_c) should be considered in design for shear friction, and the term λ^2 may not be required.

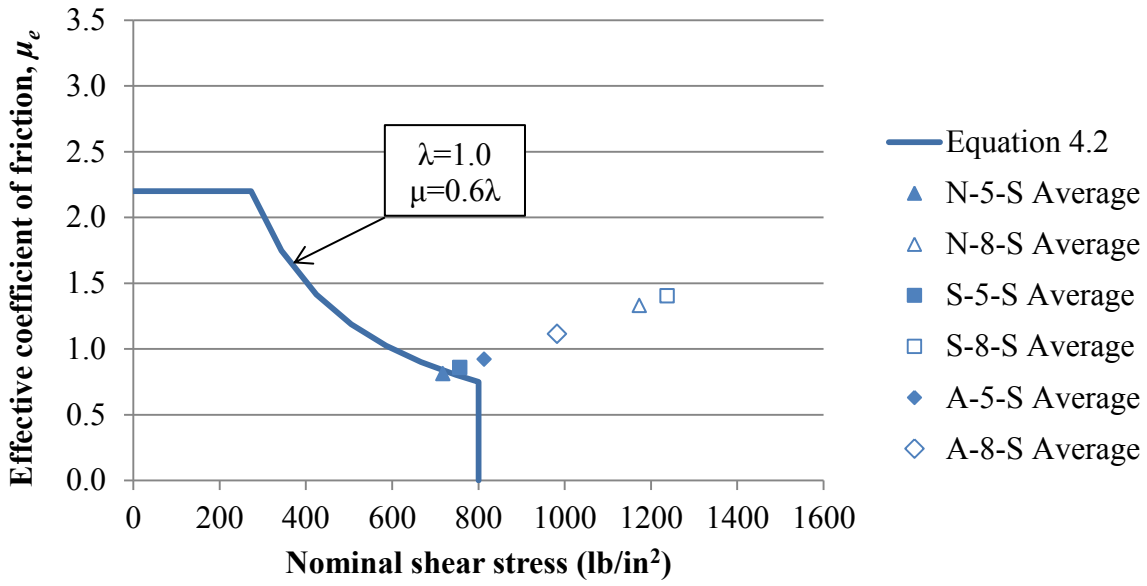

Figure 4.37. Evaluation of the effective coefficient of friction for smooth interface specimens (μ=0.6) where λ=1.0 for all concrete types.

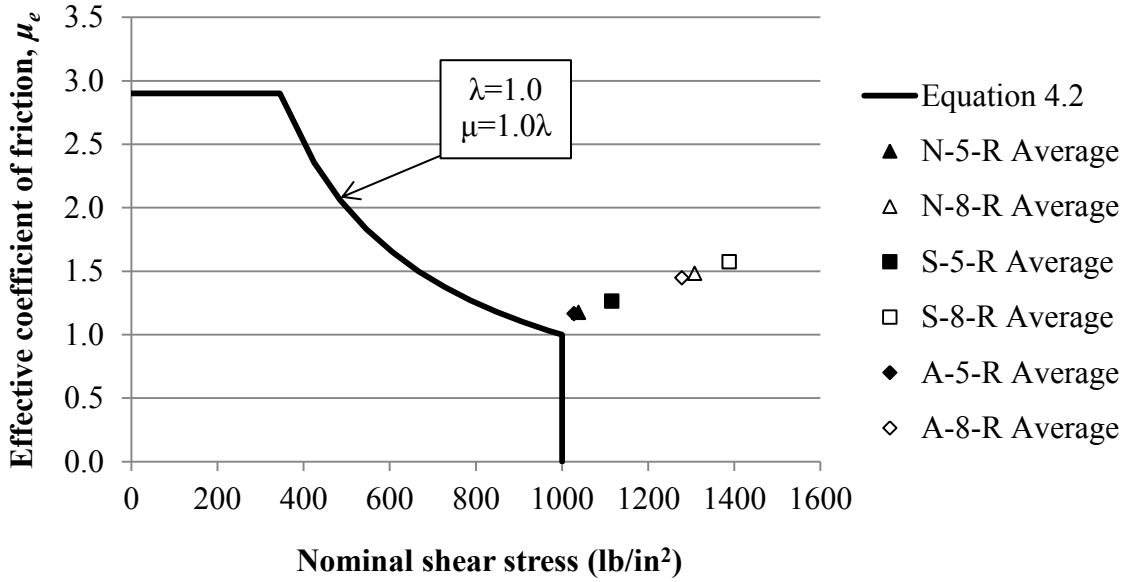

Figure 4.38. Evaluation of the effective coefficient of friction for roughened interface specimens (μ=1.0) where λ=1.0 for all concrete types.

4.5. COMPARISON TO PREVIOUS STUDIES

The shear strength v_u for the specimens in this study is compared with previous data from the literature on sand-lightweight and all-lightweight concrete (Mattock et al. 1976) in Figures 4.39 and 4.40, respectively. It should be noted that the specimens tested by Mattock at al. were cast monolithically, and some specimens were precracked prior to testing (indicated in the figures). Also, the specimens by Mattock et al. had a compressive strength of concrete between 2500 to 8000 psi, which is similar to those tested in this study (approximately 4600 to 8000 psi). Results show that the shear strength of the sand-lightweight and all-lightweight specimens in this study is consistent with specimens by Mattock et al. Interestingly, the cold-joint specimens in this study with a smooth interface had a shear strength v_u similar to specimens that were monolithic and precracked. Similarly, the cold-joint specimens with a roughened interface had a shear strength v_u similar to specimens that were monolithic and uncracked.

In Figure 4.39, it is important to note that the Mattock et al. (1976) series includes lower strength specimens (approx. 2500 psi) with all other specimens exceeding 4000 psi compressive strength. The trendlines show an increasing trend in shear strength v_u with increasing clamping stress ρf_y. Mattock et al. also found that the rate of increase of v_u with increasing ρf_y was similar for different aggregate types, although the maximum value of shear strength attainable for concrete with lightweight aggregates was lower than that of normalweight aggregates. Although one specific value of ρf_y was evaluated in this study, a similar relation should hold for moderate values of clamping stress.

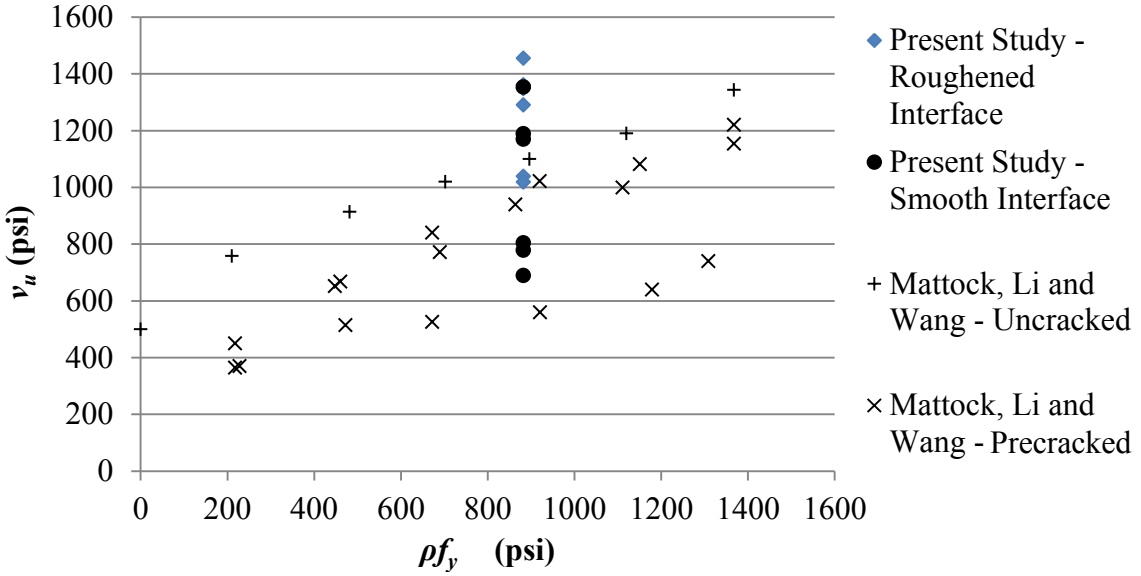

Figure 4.39. Comparison of shear strength v_u for specimens with different interface conditions for sand-lightweight concrete

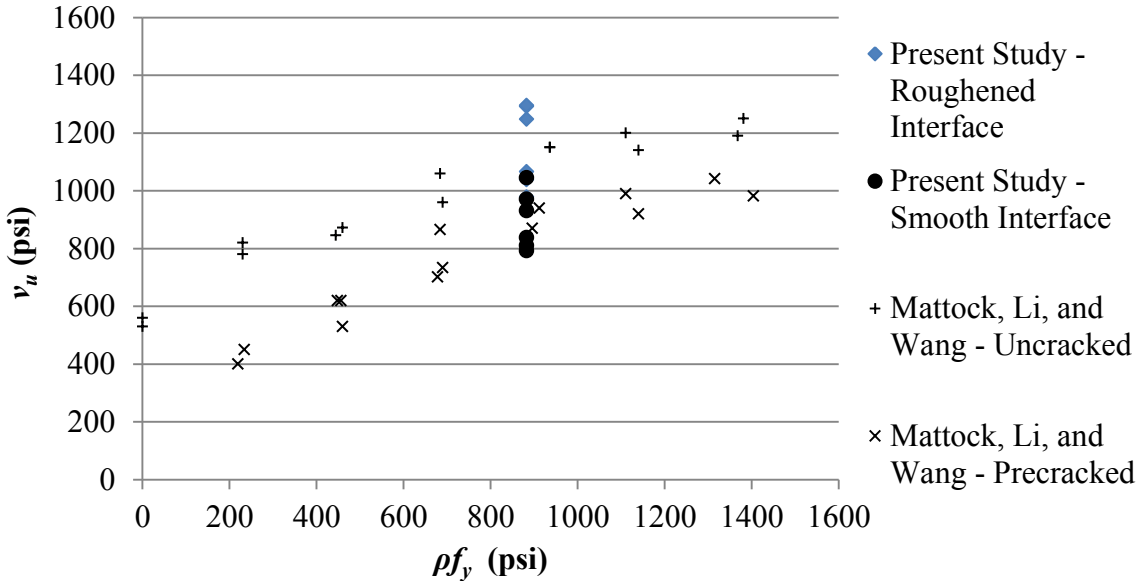

Figure 4.40. Comparison of shear strength v_u for specimens with different interface conditions for all-lightweight concrete

5. SUMMARY, CONCLUSIONS, AND RECOMMENDATIONS

5.1. SUMMARY

This study examined the influence of concrete unit weight on the direct shear transfer across a non-monolithic interface (cold-joint). This type of interface is common with structural precast concrete connections, such as corbels, for which shear friction design provisions are commonly used. Shear friction provisions in the PCI Design Handbook and ACI 318 code are largely empirical and are predominantly based on data from specimens constructed of normalweight concrete. Increasing use of lightweight concrete prompted this investigation to determine the appropriateness of the current provisions with respect to all-lightweight and sand-lightweight concrete.

The results of thirty-six push-off specimens were described in this report. Each specimen was constructed with a cold-joint along the shear plane. Test variables included unit weight of concrete (108, 120, and 145 pcf), target compressive strength (5,000 and 8,000 psi), and surface preparation of the shear plane (smooth and roughened). The specimens were reinforced with three No. 3 closed tie stirrups equally spaced throughout the shear plane area (49.5 in.^{2}) providing a reinforcement cross-sectional area of 0.66 in.^{2} (ρ=1.33%). Expanded shale aggregates were used in the production of the lightweight aggregate concretes in this study. Data presented for each series of specimens included shear force-slip, shear force-dilation, stress-strain, slip-dilation, and shear force-dilation relations. Results were compared to current design provisions in both the PCI Design Handbook and the ACI 318 code and to previous studies reported in the literature.

5.2. CONCLUSIONS

Based on the results of this study, the following conclusions can be made:

1. Specimens with the same interface condition and concrete compressive strength had nearly the same shear strength, v_u, irrespective of concrete unit weight (concrete type). These results suggest that concrete unit weight did not play a significant role in the interface shear strength for the cold-joint specimens in this study.
2. The shear strength of specimens with a smooth interface was found to be dependent upon concrete compressive strength. The shear strength of specimens with a roughened interface appeared to be independent of concrete compressive strength.
3. The shear transfer strength increased with increasing concrete compressive strength.
4. The residual shear strength was found to be insensitive to concrete type, concrete compressive strength, and interface condition.
5. Shear strengths computed by the PCI Design Handbook (2011) and the ACI 318 code (2011) using the coefficient of friction μ approach were conservative for the sand-lightweight and all-lightweight specimens cold-joint specimens in this study.
6. The value of the effective coefficient of friction μ_e computed using the PCI Design Handbook approach (6th Edition, 2004) was found to be conservative for the sand-lightweight and all-lightweight cold-joint specimens in this study. However, the approach

was not conservative for normalweight concrete specimens with a compressive strength of 5000 psi and a smooth interface condition.

7. The use of the lightweight concrete modification factor λ in the calculation for the effective coefficient of friction μ_e was found to be conservative for the lightweight aggregate concretes investigated in this study.

5.3. RECOMMENDATIONS FOR DESIGN EQUATIONS

As discussed in Section 5.2, the value of the effective coefficient of friction μ_e computed using the PCI Design Handbook approach was found to be conservative for both roughened and smooth non-monolithic interfaces for the specimens with lightweight aggregate concretes in this study. While the μ_e approach is applicable to non-monolithic interface conditions with either a roughened or smooth interface condition (Case 2 and 3 respectively) in the 6th Edition (2004), it is not applicable to non-monolithic interface conditions with a smooth interface condition (Case 3) in the 7th Edition of the PCI Design Handbook (2011). Results reported here support the previous version of the PCI Design Handbook (6th Edition) that allowed the application of the effective coefficient of friction for non-monolithic smooth interface conditions (Case 3) for lightweight aggregate concretes. Further study is needed for normalweight concrete.

5.4. RECOMMENDATIONS FOR FUTURE WORK

Many parameters have been shown to influence the shear transfer capacity of concrete sections designed using the shear friction mechanism. As this research focused on the unit weight of concrete, concrete compressive strength, and non-monolithic (cold-joint) interface conditions, many other aspects were isolated and removed from consideration. Following are recommendations for future work:

1. For the specimens tested in this study, a constant reinforcement ratio was considered. Further investigation is needed for all-lightweight concrete and sand-lightweight concrete cold-joint specimens with different reinforcement ratios for the specific type of aggregate used in this study (expanded shale).
2. Currently, lightweight aggregates used in the production of lightweight aggregate concretes are produced locally and supplied on a regional basis. As a result, lightweight aggregates can be produced from many different base materials (i.e. shale, clay, and slate) which can have different mechanical properties. Furthermore, due to different manufacturing processes, the void structures and material properties of expanded lightweight aggregates can vary widely. Therefore, additional study is also recommended to determine whether the type of lightweight aggregate and the manufacturing process play a role in the shear transfer strength for different interface conditions.
3. Investigations should be performed to evaluate the cold-joint interface condition. In this study, the cold-joint condition was formed with an eight hour delay between casting the two surfaces of the shear interface. While initial set of the first surface of the interface was achieved, it was not completely hardened when the second surface was cast. The delay period used in this program helped facilitate construction of the test specimens and minimize differences in concrete strength gain with time. However, in practice, the first

casting may occur many weeks or months before the secondary casting is complete. Therefore, it would be of interest to investigate whether and how the delay time between casting the different surfaces of the interface influences the shear transfer strength.

4. Additional investigation is needed to evaluate the effects of variable surface roughness, increased shear area, and variable concrete strengths with respect to each half of the pushoff specimen.

REFERENCES

AASHTO (2007) "AASHTO LRFD Bridge Design Specifications," Fourth edition, American Association of State Highway and Transportation Officials (AASHTO), Washington, DC.

ACI Committee 318 (1999). "Building Code Requirements for Structural Concrete (ACI 318-99) and Commentary (ACI 318R-99)," Farmington Hills, MI: American Concrete Institute.

ACI Committee 318 (2011). "Building Code Requirements for Structural Concrete (ACI 318-11) and Commentary (ACI 318R-11)," Farmington Hills, MI: American Concrete Institute.

ACI Committee 211 (1998). "Standard Practice for Selecting Proportions for Structural Lightweight Concrete. (ACI 211.2-98)" Farmington Hills, MI: American Concrete Institute.

Anderson, A. R. (1960). "Composite Designs in Precast and Cast-in-Place Concrete," *Progressive Architecture, Vol.* 41, No. 9, pp. 172-179.

ASTM A370 (2012a)." Standard Test Methods and Definitions for Mechanical Testing of Steel Products" Annual book of ASTM standards, ASTM, West Conshohocken, Pennsylvania.

ASTM A615 (2012)." Standard Specification for Deformed and Plain Carbon-Steel Bars for Concrete Reinforcement" Annual book of ASTM standards, ASTM, West Conshohocken, Pennsylvania.

ASTM C29 (2009). "Standard Test Method for Bulk Density (Unit Weight) and Voids in Aggregate" Annual book of ASTM standards, ASTM, West Conshohocken, Pennsylvania.

ASTM C127 (2012). "Standard Test Method for Density, Relative Density (Specific Gravity), and Absorption of Coarse Aggregate." Annual book of ASTM standards, ASTM, West Conshohocken, Pennsylvania.

ASTM C128 (2012). "Standard Test Method for Density, Relative Density (Specific Gravity), and Absorption of Fine Aggregate." Annual book of ASTM standards, ASTM, West Conshohocken, Pennsylvania.

ASTM C136 (2006). "Standard Test Method for Sieve Analysis of Fine and Coarse Aggregates."Annual book of ASTM standards, ASTM, West Conshohocken, Pennsylvania.

ASTM C138 (2012). "Standard Test Method for Density (Unit Weight), Yield, and Air Content (Gravimetric) of Concrete." Annual book of ASTM standards, ASTM, West Conshohocken, Pennsylvania.

ASTM Cl43 (2012). "Standard Test Method for Slump of Hydraulic-Cement Concrete." Annual book of ASTM standards, ASTM, West Conshohocken, Pennsylvania.

ASTM Cl73 (2012). "Standard Test Method for Air Content of Freshly Mixed Concrete by the Volumetric Method." Annual book of ASTM standards, ASTM, West Conshohocken, Pennsylvania.

ASTM C192 (2012). "Standard Practice for Making and Curing Concrete Test Specimens in the Laboratory." Annual book of ASTM standards, ASTM, West Conshohocken, Pennsylvania.

ASTM C231 (2010). "Standard Test Method for Air Content of Freshly Mixed Concrete by the Pressure Method." Annual book of ASTM standards, ASTM, West Conshohocken, Pennsylvania.

ASTM C330 (ASTM C330 (2009). "Standard Specification for Lightweight Aggregates for Structural Concrete." Annual book of ASTM standards, ASTM, West Conshohocken, Pennsylvania.

ASTM C469 (2010). "Standard Test Method for Static Modulus of Elasticity and Poisson's Ratio of Concrete in Compression." Annual book of ASTM standards, ASTM, West Conshohocken, Pennsylvania.

ASTM C494 (2012). "Standard Specification for Chemical Admixtures for Concrete." Annual book of ASTM standards, ASTM, West Conshohocken, Pennsylvania.

ASTM C496 (2011). "Standard Test Method for Splitting Tensile Strength of Cylindrical Concrete Specimens." Annual book of ASTM standards, ASTM, West Conshohocken, Pennsylvania.

ASTM C1231 (2012). "Standard Practice for Use of Unbonded Caps in Determination of Compressive Strength of Concrete Cylinders." Annual book of ASTM standards, ASTM, West Conshohocken, Pennsylvania.

Bass, R.A., Carrasquillo, R.L. , and J.O. Jirsa. (1989). "Shear Transfer Across New and Existing Concrete Interfaces," *ACI Structural Journal,* Vol. 84, No. 4, pp. 383-393.

Birkeland, H. W. (1968) "Class Notes for Course on "Precast and Prestressed Concrete," University of British Columbia, Spring 1968.

Birkeland, P.W. and Birkeland, H.W. (1966). "Connections in Precast Concrete Construction," ACI Journal*, Proceedings*, Vol. 63, No. 3, pp. 345-368.

Hanson, N.W. (1960). *"*Precast-Prestressed Concrete Bridges 2: Horizontal Shear Connections*,"* *PCA – Journal of the Research and Development Division*, Vol. 2, No. 2, pp. 38-58.

Harries, K.A., Zeno, G., and Shahrooz, B. (2012). "Toward an Improved Understanding of Shear-Friction Behavior," *ACI Structural Journal*, Vol. 109, No. 6, pp. 835-844

Hofbeck, J. A.; Ibrahim, I. O.; and Mattock, A. H. (1969). "Shear Transfer in Reinforced Concrete," ACI Journal*, Proceedings,* V. 66, No. 2, pp. 119-128.

Hoff, G.C. (1992). "High Strength Lightweight Aggregate Concrete for Arctic Applications--Part 3: Structural Parameters", *American Concrete Institute*, SP-136, pp. 175-246.

Hsu, Thomas T.C., Mau, S.T., and Chen, B. (1987). "Theory of Shear Transfer Strength of Reinforced Concrete," *ACI Structural Journal*, Vol. 84, No. 2, pp. 149-160.

Ivey and Buth. (1967) "Shear Capacity of Lightweight Concrete Beams." ACI Journal*, Proceedings*, Vol. 64, No. 10. pp. 634-43.

Kahn, L.F. and Mitchell, A.D. (2002). "Shear Friction Tests with High-Strength Concrete," *ACI Structural Journal*, Vol. 99, No. 1, pp. 98-103.

Loov, R.E. and Patnaik, A.K. (1994). "Horizontal Shear Strength of Composite Beams with a Rough Interface," *PCI Journal*, Vol. 39, No. 1, pp. 48-58.

Mansur, M.T., Vinayagam, T., and Tan, K-H. (2008). "Shear Transfer Across a Crack in Reinforced High-Strength Concrete," *ASCE Journal of Materials in Civil Engineering*, Vol. 20, No. 4, pp. 294-302.

Mast, R.F. (1968). "Auxiliary Reinforcement in Concrete Connections", *ASCE Journal of the Structural Division Proceedings*, Vol. 94, No. ST6, pp. 1485-1504

Mattock, A. H., W. K. Li, and T. C. Wang. (1976). "Shear Transfer in Lightweight Reinforced Concrete." *PCI Journal*, Vol. 21, No. 1, pp. 20-39.

Mattock, A.H. (1976). "Shear Transfer Under Monotonic Loading Across and Interface Between Concretes Cast at Different Times", *University of Washington Department of Civil Engineering Report SM 76-3*.

Mattock, A.H. (2001). "Shear Friction and High-Strength Concrete", *ACI Structural Journal*, Vol. 98, No. 1, pp. 50-59.

Mattock, A. H., Johal, L, and Chow, C. H. (1975). "Shear Transfer in Reinforced Concrete with Moment or Tension Acting Across the Shear Plane." *PCI Journal*, Vol. 20, No. 4, pp. 76-93.

Mattock, A.H. and Hawkins, N.M. (1972). "Shear Transfer in Reinforced Concrete – Recent Research," *PCI Journal*, Vol. 17, No. 2, pp. 55-75.

Nagle, T.J. and Kuchma, D.A. (2007). "Nontraditional Limitations on the Shear Capacity of Prestressed Concrete Girders" *University of Illinois at Urbana-Champaign NSEL Report-003*.

Paulay, T., Park, R., and Phillips, M.H. (1974). “Horizontal Construction Joints In Cast-In-Place Reinforced Concrete,” *American Concrete Institute*, SP-42, pp. 599-616.

Precast/Prestressed Concrete Institute (1992). *PCI Design Handbook: Precast and Prestressed Concrete Institute*. 4th ed. Chicago: Precast/Prestressed Concrete Institute.

Precast/Prestressed Concrete Institute (1999). *PCI Design Handbook: Precast and Prestressed Concrete Institute*. 5th ed. Chicago: Precast/Prestressed Concrete Institute.

Precast/Prestressed Concrete Institute (2004). *PCI Design Handbook: Precast and Prestressed Concrete Institute*. 6th ed. Chicago: Precast/Prestressed Concrete Institute.

Precast/Prestressed Concrete Institute (2010). *PCI Design Handbook: Precast and Prestressed Concrete Institute*. 7th ed. Chicago: Precast/Prestressed Concrete Institute.

PCI Committee on Connection Details (1973). *PCI Manual on Design of Connections for Precast Prestressed Concrete*, Prestressed Concrete Institute, Chicago, pp. 22.

Rahal, Khaldoun N. (2010). “Shear Transfer Strength of Reinforced Concrete.” *ACI Structural Journal,* Vol. 107, No.4, pp. 419-426.

Raths, C. H. (1977). “Reader Comments: Design Proposals for Reinforced Concrete Corbels.” *PCI Journal*, Vol. 21, No. 3, pp. 93–98.

Saemann, J. and Washa, G.W. (1964). “Horizontal Shear Connections Between Precast Beams and Cast-In Place Slabs,” ACI Journal*, Proceedings*, Vol 61, No. 11, pp. 1383-1408.

Scott, J. (2010) “Interface Shear Strength in Lightweight Concrete Bridge Girders.” MS Thesis. Virginia Polytechnic Institute.

Shaikh, F.A. (1978). "Proposed Revisions to Shear Friction Provisions." *PCI Journal,* Vol. 23, No. 2, pp. 12-21.

Tanner, J.A. (2008). "Calculating Shear Friction Using Effective Coefficient of Friction." *PCI Journal*, Vol. 53, No. 3, pp. 114-20.

Walraven, J. C.; Frenay, J.; and Pruijssers, A. (1987). "Influence of Concrete Strength and Load History on the Shear Friction Capacity of Concrete Members," *PCI Journal,* Vol. 32, No. 1, pp. 66-84.

Walraven, J. and Stroband, J. (1994). “Shear Friction in High-Strength Concrete”, *American Concrete Institute*, SP-42, pp. 311-330.

ACKNOWLEDGMENTS

This research was conducted with the sponsorship of the Precast/Prestressed Concrete Institute (PCI) and the National University Transportation Center (NUTC) at the Missouri University of Science and Technology. Lightweight aggregates were donated by Buildex, Inc. Longitudinal reinforcing steel bars used in this work were provided by Ambassador Steel Corporation. The authors wish to thank Neil Anderson of CRSI, Roger Becker of PCI, Harry Gleich of Metromont Precast, Dr. Neil Hawkins, Dr. Donald Meinheit of Wiss, Janney, Elstner, and Dr. Larbi Sennour of Consulting Engineering Group, Inc. who served as advisors to this project; their assistance and input are greatly appreciated. Additionally, the authors gratefully acknowledge the assistance provided by Metromont Precast and Coreslab Structures.

APPENDIX

SHEAR FRICTION SPECIMEN DATABASE

Specimen ID		Concrete Properties		Shear Plane Geometry and Condition			Shear Plane Reinforcement			Testing Data	
		f'_c at Test (psi)	Density (pcf)	Interface Condition	Casting Procedure	A_{cr} (sq. in.)	A_{vf} (sq. in)	f_y (ksi)	$\rho_{vf}f_y$ (psi)	V_u (kips)	v_u (psi)
Shaw, 2013	N-5-R-4	4860	147	Cold Joint - Rough	Composite	49.5	0.66	66.2	883	59.1	1193
	N-5-R-5	4860	147	Cold Joint - Rough	Composite	49.5	0.66	66.2	883	53.4	1079
	N-5-R-6	4860	147	Cold Joint - Rough	Composite	49.5	0.66	66.2	883	53.4	1080
	N-5-S-4	4860	147	Cold Joint - Smooth	Composite	49.5	0.66	66.2	883	30.9	623
	N-5-S-5	4860	147	Cold Joint - Smooth	Composite	49.5	0.66	66.2	883	34.7	701
	N-5-S-6	4860	147	Cold Joint - Smooth	Composite	49.5	0.66	66.2	883	39.2	791
	S-5-R-1	4580	118	Cold Joint - Rough	Composite	49.5	0.66	66.2	883	51.4	1039
	S-5-R-2	4580	118	Cold Joint - Rough	Composite	49.5	0.66	66.2	883	50.4	1018
	S-5-R-3	4580	118	Cold Joint - Rough	Composite	49.5	0.66	66.2	883	63.9	1291
	S-5-S-1	4580	118	Cold Joint - Smooth	Composite	49.5	0.66	66.2	883	38.5	778
	S-5-S-2	4580	118	Cold Joint - Smooth	Composite	49.5	0.66	66.2	883	34.1	689
	S-5-S-3	4580	118	Cold Joint - Smooth	Composite	49.5	0.66	66.2	883	39.8	804
	A-5-R-1	6080	108	Cold Joint - Rough	Composite	49.5	0.66	66.2	883	48.4	979
	A-5-R-2	6080	108	Cold Joint - Rough	Composite	49.5	0.66	66.2	883	52.8	1067
	A-5-R-3	6080	108	Cold Joint - Rough	Composite	49.5	0.66	66.2	883	51.4	1039
	A-5-S-1	6080	108	Cold Joint - Smooth	Composite	49.5	0.66	66.2	883	41.5	838
	A-5-S-2	6080	108	Cold Joint - Smooth	Composite	49.5	0.66	66.2	883	40.1	810

Specimen ID		Concrete Properties		Shear Plane Geometry and Condition			Shear Plane Reinforcement			Testing Data	
		f'_c at Test (psi)	Density (pcf)	Interface Condition	Casting Procedure	A_{cr} (sq. in.)	A_{vf} (sq. in)	f_y (ksi)	$\rho_{vf}f_y$ (psi)	V_u (kips)	v_u (psi)
Shaw, 2013	A-5-S-3	6080	108	Cold Joint - Smooth	Composite	49.5	0.66	66.2	883	39.2	793
	N-8-R-1	7550	144	Cold Joint - Rough	Composite	49.5	0.66	66.2	883	74.0	1496
	N-8-R-2	7550	144	Cold Joint - Rough	Composite	49.5	0.66	66.2	883	56.1	1133
	N-8-R-3	7550	144	Cold Joint - Rough	Composite	49.5	0.66	66.2	883	64.1	1296
	N-8-S-1	7550	144	Cold Joint - Smooth	Composite	49.5	0.66	66.2	883	65.6	1324
	N-8-S-2	7550	144	Cold Joint - Smooth	Composite	49.5	0.66	66.2	883	53.3	1077
	N-8-S-3	7550	144	Cold Joint - Smooth	Composite	49.5	0.66	66.2	883	55.3	1118
	S-8-R-1	7200	118	Cold Joint - Rough	Composite	49.5	0.66	66.2	883	72.0	1455
	S-8-R-2	7200	118	Cold Joint - Rough	Composite	49.5	0.66	66.2	883	67.4	1361
	S-8-R-3	7200	118	Cold Joint - Rough	Composite	49.5	0.66	66.2	883	66.7	1348
	S-8-S-1	7200	118	Cold Joint - Smooth	Composite	49.5	0.66	66.2	883	67.0	1354
	S-8-S-2	7200	118	Cold Joint - Smooth	Composite	49.5	0.66	66.2	883	57.9	1169
	S-8-S-3	7200	118	Cold Joint - Smooth	Composite	49.5	0.66	66.2	883	58.9	1189
	A-8-R-1	7843	109	Cold Joint - Rough	Composite	49.5	0.66	66.2	883	61.8	1248
	A-8-R-2	7843	109	Cold Joint - Rough	Composite	49.5	0.66	66.2	883	63.9	1292
	A-8-R-3	7843	109	Cold Joint - Rough	Composite	49.5	0.66	66.2	883	64.1	1295
	A-8-S-1	7843	109	Cold Joint - Smooth	Composite	49.5	0.66	66.2	883	46.1	931
	A-8-S-2	7843	109	Cold Joint - Smooth	Composite	49.5	0.66	66.2	883	48.0	970
	A-8-S-3	7843	109	Cold Joint - Smooth	Composite	49.5	0.66	66.2	883	51.7	1045

Specimen ID		Concrete Properties		Shear Plane Geometry and Condition			Shear Plane Reinforcement			Testing Data	
		f'_c at Test (psi)	Density (pcf)	Interface Condition	Casting Procedure	A_{cr} (sq. in.)	A_{vf} (sq. in)	f_y (ksi)	$\rho_{vf}f_y$ (psi)	V_u (kips)	v_u (psi)
Mattock and Hawkins, 1972	7.1	4850	NWC	Uncracked	Monolithic	57.0	0.44	49.5	1528	48.5	851
	7.2	5120	NWC	Uncracked	Monolithic	57.0	0.66	49.5	3439	51.8	908
	7.3	5050	NWC	Uncracked	Monolithic	57.0	0.88	49.5	6114	55.5	974
	7.4	5410	NWC	Uncracked	Monolithic	57.0		56.0	193	32.3	567
	7.5	5070	NWC	Uncracked	Monolithic	57.0		56.0	289	34.7	609
	7.6	5100	NWC	Uncracked	Monolithic	57.0		56.0	481	48.2	846
	8.1	4850	NWC	Uncracked	Monolithic	57.0	0.44	49.5	1528	39.7	697
	8.2	5120	NWC	Uncracked	Monolithic	57.0	0.66	49.5	3439	50.6	888
	8.3	5050	NWC	Uncracked	Monolithic	57.0	0.88	49.5	6114	52.7	925
	8.4	5410	NWC	Uncracked	Monolithic	57.0		56.0	384	29.7	521
	8.5	5070	NWC	Uncracked	Monolithic	57.0		56.0	576	32.6	572
	8.6	5100	NWC	Uncracked	Monolithic	57.0		56.0	768	42.5	746
	9.1	5500	NWC	Uncracked	Monolithic	72.0	1.1	52.4	8006	177.1	2460
	9.2	5500	NWC	Uncracked	Monolithic	72.0	1.32	52.2	11484	184.3	2560
	9.3	3940	NWC	Uncracked	Monolithic	72.0	1.32	52.3	11506	109.1	1515
	9.4	3940	NWC	Uncracked	Monolithic	72.0	1.32	53.7	11814	100.0	1389
	9.5	6440	NWC	Uncracked	Monolithic	72.0	0.88	51.0	4987	206.6	2870
	9.6	6440	NWC	Uncracked	Monolithic	72.0	0.44	51.0	1247	199.4	2770
	10.1	3450	NWC	Cracked	Monolithic	72.0	0.66	51.8	2849	62.1	862

Specimen ID		Concrete Properties		Shear Plane Geometry and Condition			Shear Plane Reinforcement			Testing Data	
		f'_c at Test (psi)	Density (pcf)	Interface Condition	Casting Procedure	A_{cr} (sq. in.)	A_{vf} (sq. in)	f_y (ksi)	$\rho_{vf}f_y$ (psi)	V_u (kips)	v_u (psi)
Mattock and Hawkins, 1972	10.2	4390	NWC	Cracked	Monolithic	72.0	0.66	52.0	2860	75.5	1049
	10.3	3450	NWC	Cracked	Monolithic	72.0	0.88	51.8	5065	115.9	1610
	10.4	4390	NWC	Cracked	Monolithic	72.0	0.88	53.0	5182	127.4	1770
	10.5	4630	NWC	Cracked	Monolithic	72.0	1.1	52.7	8051	163.1	2265
	10.6	4630	NWC	Cracked	Monolithic	72.0	1.32	52.0	11440	155.9	2165
	10.7	4020	NWC	Cracked	Monolithic	72.0	1.32	52.4	11528	104.0	1445
	10.8	4020	NWC	Cracked	Monolithic	72.0	1.32	53.7	11814	80.3	1115
	10.9	5800	NWC	Cracked	Monolithic	72.0	0.88	51.0	4987	186.5	2590
	10.10	5800	NWC	Cracked	Monolithic	72.0	0.44	51.0	1247	101.5	1410
Kahn and Mitchell, 2002	SF-7-1-CJ	11734	NWC	Cold Joint	Composite	60.0	0.22	83.0	220	54.0	900
	SF-7-2-CJ	11734	NWC	Cold Joint	Composite	60.0	0.44	83.0	440	82.1	1368
	SF-7-3-CJ	12471	NWC	Cold Joint	Composite	60.0	0.66	83.0	660	110.3	1838
	SF-7-4-CJ	12471	NWC	Cold Joint	Composite	60.0	0.88	83.0	880	132.7	2211
	SF-10-1-CJ	14326	NWC	Cold Joint	Composite	60.0	0.22	83.0	220	31.7	529
	SF-10-2-CJ	12053	NWC	Cold Joint	Composite	60.0	0.44	83.0	440	49.3	822
	SF-10-3-CJ	12953	NWC	Cold Joint	Composite	60.0	0.66	83.0	660	113.9	1899
	SF-10-4-CJ	12953	NWC	Cold Joint	Composite	60.0	0.88	83.0	880	126.0	2101
	SF-14-1-CJ	14756	NWC	Cold Joint	Composite	60.0	0.22	83.0	220	90.9	1515
	SF-14-2-CJ	14756	NWC	Cold Joint	Composite	60.0	0.44	83.0	440	99.2	1653

Specimen ID		Concrete Properties		Shear Plane Geometry and Condition			Shear Plane Reinforcement			Testing Data	
		f'_c at Test (psi)	Density (pcf)	Interface Condition	Casting Procedure	A_{cr} (sq. in.)	A_{vf} (sq. in)	f_y (ksi)	$\rho_{vf}f_y$ (psi)	V_u (kips)	v_u (psi)
Kahn and Mitchell, 2002	SF-14-3-CJ	15218	NWC	Cold Joint	Composite	60.0	0.66	83.0	660	134.7	2245
	SF-14-4-CJ	15218	NWC	Cold Joint	Composite	60.0	0.88	69.5	880	153.1	2552
	SF-4-1-C	6805	NWC	Cracked	Monolithic	60.0	0.22	69.5	220	35.0	583
	SF-4-2-C	6805	NWC	Cracked	Monolithic	60.0	0.44	69.5	440	55.7	928
	SF-4-3-C	6805	NWC	Cracked	Monolithic	60.0	0.66	69.5	660	71.1	1186
	SF-7-1-C	11734	NWC	Cracked	Monolithic	60.0	0.22	83.0	220	41.7	695
	SF-7-2-C	12410	NWC	Cracked	Monolithic	60.0	0.44	83.0	440	51.7	862
	SF-7-3-C	13103	NWC	Cracked	Monolithic	60.0	0.66	83.0	660	71.5	1192
	SF-7-4-C	12471	NWC	Cracked	Monolithic	60.0	0.88	83.0	880	62.7	1046
	SF-10-1-C-a	12053	NWC	Cracked	Monolithic	60.0	0.22	83.0	220	25.8	430
	SF-10-1-C-b	14326	NWC	Cracked	Monolithic	60.0	0.22	83.0	220	30.0	500
	SF-10-2-C-a	14676	NWC	Cracked	Monolithic	60.0	0.44	83.0	440	50.8	846
	SF-10-2-C-b	14804	NWC	Cracked	Monolithic	60.0	0.44	83.0	440	48.1	802
	SF-10-3-C-a	16170	NWC	Cracked	Monolithic	60.0	0.66	83.0	660	64.7	1078
	SF-10-3-C-b	13924	NWC	Cracked	Monolithic	60.0	0.66	83.0	660	63.4	1056
	SF-10-4-C-a	15468	NWC	Cracked	Monolithic	60.0	0.88	83.0	880	74.2	1236
	SF-10-4-C-b	16476	NWC	Cracked	Monolithic	60.0	0.88	83.0	880	76.3	1271
	SF-14-1-C	16015	NWC	Cracked	Monolithic	60.0	0.22	83.0	220	24.9	415
	SF-14-2-C	15496	NWC	Cracked	Monolithic	60.0	0.44	83.0	440	40.2	670

Specimen ID		Concrete Properties		Shear Plane Geometry and Condition			Shear Plane Reinforcement			Testing Data	
		f'_c at Test (psi)	Density (pcf)	Interface Condition	Casting Procedure	A_{cr} (sq. in.)	A_{vf} (sq. in)	f_y (ksi)	$\rho_{vf}f_y$ (psi)	V_u (kips)	v_u (psi)
Kahn and Mitchell, 2002	SF-14-3-C	15392	NWC	Cracked	Monolithic	60.0	0.66	83.0	660	55.5	925
	SF-14-4-C	15982	NWC	Cracked	Monolithic	60.0	0.88	83.0	880	73.3	1221
	SF-4-1-U	6805	NWC	Uncracked	Monolithic	60.0	0.22	69.5	220	57.9	965
	SF4-2-U	6805	NWC	Uncracked	Monolithic	60.0	0.44	69.5	440	80.1	1335
	SF-4-3-U	6805	NWC	Uncracked	Monolithic	60.0	0.66	69.5	660	85.8	1431
	SF-7-1-U	11734	NWC	Uncracked	Monolithic	60.0	0.22	83.0	220	87.6	1459
	SF-7-2-U	12410	NWC	Uncracked	Monolithic	60.0	0.44	83.0	440	118.1	1969
	SF-7-3-U	13103	NWC	Uncracked	Monolithic	60.0	0.66	83.0	660	138.4	2307
	SF-7-4-U	12471	NWC	Uncracked	Monolithic	60.0	0.88	83.0	880	149.1	2485
	SF-10-1-U-a	12053	NWC	Uncracked	Monolithic	60.0	0.22	83.0	220	100.1	1668
	SF-10-1-U-b	14326	NWC	Uncracked	Monolithic	60.0	0.22	83.0	220	91.9	1531
	SF-10-2-U-a	14767	NWC	Uncracked	Monolithic	60.0	0.44	83.0	440	130.7	2178
	SF-10-2-U-b	14804	NWC	Uncracked	Monolithic	60.0	0.44	83.0	440	124.1	2068
	SF-10-3-U-a	16170	NWC	Uncracked	Monolithic	60.0	0.66	83.0	660	144.8	2414
	SF-10-3-U-b	13934	NWC	Uncracked	Monolithic	60.0	0.66	83.0	660	147.9	2465
	SF-10-4-U-a	15468	NWC	Uncracked	Monolithic	60.0	0.88	83.0	880	156.0	2601
	SF-10-4-U-b	16476	NWC	Uncracked	Monolithic	60.0	0.88	83.0	880	160.0	2667
	SF-14-1-U	17957	NWC	Uncracked	Monolithic	60.0	0.22	83.0	220	95.0	1583
	SF-14-2-U	17362	NWC	Uncracked	Monolithic	60.0	0.44	83.0	440	108.5	1808

Specimen ID		Concrete Properties		Shear Plane Geometry and Condition			Shear Plane Reinforcement			Testing Data	
		f'_c at Test (psi)	Density (pcf)	Interface Condition	Casting Procedure	A_{cr} (sq. in.)	A_{vf} (sq. in)	f_y (ksi)	$\rho_{vf}f_y$ (psi)	V_u (kips)	v_u (psi)
	SF-14-3-U	16255	NWC	Uncracked	Monolithic	60.0	0.66	83.0	660	146.2	2437
	SF-14-4-U	16059	NWC	Uncracked	Monolithic	60.0	0.88	83.0	880	156.0	2600
Mattock, 1976	A1	6020	NWC	Cracked	Monolithic	50.0	0.22	51.64	227	38.0	760
	A2	6020	NWC	Cracked	Monolithic	50.0	0.44	51.64	454	40.0	800
	A3	5820	NWC	Cracked	Monolithic	50.0	0.66	55.45	732	57.5	1150
	A4	5880	NWC	Cracked	Monolithic	50.0	0.88	55.45	976	71.0	1420
	A5	6125	NWC	Cracked	Monolithic	50.0	1.1	51.27	1128	75.0	1500
	A6	5900	NWC	Cracked	Monolithic	50.0	1.6	48	1536	88.0	1760
	A6A	5970	NWC	Cracked	Monolithic	50.0	1.6	48	1536	93.0	1860
	A7	5970	NWC	Cracked	Monolithic	50.0	2	48.2	1928	97.0	1940
	B1	6085	NWC	Cracked - Rough	Composite	50.0	0.22	51.27	226	24.4	487
	B2	6085	NWC	Cracked - Rough	Composite	50.0	0.44	50.55	445	35.0	700
	B3	6140	NWC	Cracked - Rough	Composite	50.0	0.66	51.27	677	52.7	1054
	B4	6362.5	NWC	Cracked - Rough	Composite	50.0	0.88	53.82	947	63.8	1276
	B5	5967.5	NWC	Cracked - Rough	Composite	50.0	1.24		0	78.5	1570
	B6	5967.5	NWC	Cracked - Rough	Composite	50.0	1.6	49.25	1576	85.0	1700
	C1	6030	NWC	Cracked - Smooth	Composite	50.0	0.22	50.91	224	10.5	210
	C2	6030	NWC	Cracked - Smooth	Composite	50.0	0.44	50.91	448	18.0	360
	C3	5980	NWC	Cracked - Smooth	Composite	50.0	0.66	50.55	667	21.4	428

Specimen ID		Concrete Properties		Shear Plane Geometry and Condition			Shear Plane Reinforcement			Testing Data	
		f'_c at Test (psi)	Density (pcf)	Interface Condition	Casting Procedure	A_{cr} (sq. in.)	A_{vf} (sq. in)	f_y (ksi)	$\rho_{vf}f_y$ (psi)	V_u (kips)	v_u (psi)
Mattock, 1976	C4	5980	NWC	Cracked - Smooth	Composite	50.0	0.88	51.64	909	30.0	600
	C5	6175	NWC	Cracked - Smooth	Composite	50.0	1.1	52.73	1160	39.0	780
	C6	6175	NWC	Cracked - Smooth	Composite	50.0	1.6	45.25	1448	44.1	882
	D1	5007.5	NWC	Cracked - Rough	Composite	50.0	0.22	51.27	226	29.5	590
	D2	5007.5	NWC	Cracked - Rough	Composite	50.0	0.44	51.27	451	46.0	920
	D3	4425	NWC	Cracked - Rough	Composite	50.0	0.66	56	739	50.5	1010
	D4	4425	NWC	Cracked - Rough	Composite	50.0	0.88	56	986	50.1	1002
	D4A	4290	NWC	Cracked - Rough	Composite	50.0	0.88	54	950	49.7	994
	D5	4577.5	NWC	Cracked - Rough	Composite	50.0				60.5	1210
	D5A	4540	NWC	Cracked - Rough	Composite	50.0				62.5	1250
	D6	4577.5	NWC	Cracked - Rough	Composite	50.0	1.6	48.5	1552	73.5	1470
	G1	6030	NWC	Cracked - Smooth	Composite	50.0	0.22	50.91	224	8.0	160
	G2	6030	NWC	Cracked - Smooth	Composite	50.0	0.44	50.91	448	13.2	264
	G3	5980	NWC	Cracked - Smooth	Composite	50.0	0.66	50.55	667	19.2	384
	G4	5980	NWC	Cracked - Smooth	Composite	50.0	0.88	51.64	909	25.0	500
	G5	6175	NWC	Cracked - Smooth	Composite	50.0	1.1	52.73	1160	29.3	586
	G6	6175	NWC	Cracked - Smooth	Composite	50.0	1.6	45.25	1448	38.9	778
	H1	6077.5	NWC	Cracked - Smooth	Composite	50.0	0.22	55.45	244	9.4	188
	H2	6125	NWC	Cracked - Smooth	Composite	50.0	0.44	55.45	488	16.1	322

Specimen ID		Concrete Properties		Shear Plane Geometry and Condition			Shear Plane Reinforcement			Testing Data	
		f'_c at Test (psi)	Density (pcf)	Interface Condition	Casting Procedure	A_{cr} (sq. in.)	A_{vf} (sq. in)	f_y (ksi)	$\rho_{vf}f_y$ (psi)	V_u (kips)	v_u (psi)
Mattock, 1976	H3	6125	NWC	Cracked - Smooth	Composite	50.0	0.66	55.45	732	23.0	460
	H4	6397.5	NWC	Cracked - Smooth	Composite	50.0	0.88	53.64	944	25.5	510
	H5	6415	NWC	Cracked - Smooth	Composite	50.0			0	32.7	654
	H6	6217.5	NWC	Cracked - Smooth	Composite	50.0	1.6	46.8	1498	38.0	760
Hofbeck, Ibrahim, and Mattock, 1969	1	4040	145	Uncracked	Monolithic	50.0	0	0	0	24.0	480
	1.1A	3920	145	Uncracked	Monolithic	50.0	0.22	50.7	223	37.5	750
	1.1B	4340	145	Uncracked	Monolithic	50.0	0.22	48	211	42.2	844
	1.2A	3840	145	Uncracked	Monolithic	50.0	0.44	50.7	446	50.0	1000
	1.2B	4180	145	Uncracked	Monolithic	50.0	0.44	48	422	49.0	980
	1.3A	3840	145	Uncracked	Monolithic	50.0	0.66	50.7	669	55.0	1100
	1.3B	3920	145	Uncracked	Monolithic	50.0	0.66	48	634	53.5	1070
	1.4A	4510	145	Uncracked	Monolithic	50.0	0.88	50.7	892	68.0	1360
	1.4B	3855	145	Uncracked	Monolithic	50.0	0.88	48	845	64.0	1280
	1.5A	4510	145	Uncracked	Monolithic	50.0	1.1	50.7	1115	70.0	1400
	1.5B	4065	145	Uncracked	Monolithic	50.0	1.1	48	1056	69.2	1384
	1.6A	4310	145	Uncracked	Monolithic	50.0	1.32	50.7	1338	71.6	1432
	1.6B	4050	145	Uncracked	Monolithic	50.0	1.32	48	1267	71.0	1420
	2.1	3100	145	Cracked	Monolithic	50.0	0.22	50.7	223	29.5	590
	2.2	3100	145	Cracked	Monolithic	50.0	0.44	50.7	446	34.0	680

Specimen ID		Concrete Properties		Shear Plane Geometry and Condition			Shear Plane Reinforcement			Testing Data	
		f'_c at Test (psi)	Density (pcf)	Interface Condition	Casting Procedure	A_{cr} (sq. in.)	A_{vf} (sq. in)	f_y (ksi)	$\rho_{vf}f_y$ (psi)	V_u (kips)	v_u (psi)
Hofbeck, Ibrahim, and Mattock, 1969	2.3	3900	145	Cracked	Monolithic	50.0	0.66	50.7	669	42.0	840
	2.4	3900	145	Cracked	Monolithic	50.0	0.88	50.7	892	50.0	1000
	2.5	4180	145	Cracked	Monolithic	50.0	1.1	50.7	1115	65.0	1300
	2.6	4180	145	Cracked	Monolithic	50.0	1.32	50.7	1338	69.3	1385
	3.1	4040	145	Cracked	Monolithic	50.0	N/A	50.1	49	12.0	240
	3.2	4010	145	Cracked	Monolithic	50.0	N/A	56.8	223	26.0	520
	3.3	3100	145	Cracked	Monolithic	50.0	0.22	50.7	446	34.0	680
	3.4	4040	145	Cracked	Monolithic	50.0	0.4	47.2	740	51.4	1028
	3.5	4040	145	Cracked	Monolithic	50.0	0.62	42.4	1040	57.6	1152
	4.1	4070	145	Cracked	Monolithic	50.0	0.22	66.1	291	35.2	704
	4.2	4070	145	Cracked	Monolithic	50.0	0.44	66.1	582	49.0	980
	4.3	4340	145	Cracked	Monolithic	50.0	0.66	66.1	873	59.0	1180
	4.4	4340	145	Cracked	Monolithic	50.0	0.88	66.1	1163	70.0	1400
	4.5	4390	145	Cracked	Monolithic	50.0	1.1	66.1	1454	66.0	1320
	5.1	2450	145	Cracked	Monolithic	50.0	0.22	50.7	223	25.5	510
	5.2	2620	145	Cracked	Monolithic	50.0	0.44	50.7	446	35.0	700
	5.3	2385	145	Cracked	Monolithic	50.0	0.66	50.7	669	40.5	810
	5.4	2580	145	Cracked	Monolithic	50.0	0.88	50.7	892	39.8	795
	5.5	2620	145	Cracked	Monolithic	50.0	1.1	50.7	1115	50.5	1010

Specimen ID		Concrete Properties		Shear Plane Geometry and Condition			Shear Plane Reinforcement			Testing Data	
		f'_c at Test (psi)	Density (pcf)	Interface Condition	Casting Procedure	A_{cr} (sq. in.)	A_{vf} (sq. in)	f_y (ksi)	$\rho_{vf}f_y$ (psi)	V_u (kips)	v_u (psi)
Mattock, Li, and Wang, 1976	B1	3740	111	Cracked	Monolithic	50.0	0.22	49.6	218	22.5	450
	B2	3360	107	Cracked	Monolithic	50.0	0.44	50.9	448	32.6	652
	B3	3910	110	Cracked	Monolithic	50.0	0.66	50.9	672	42.0	840
	B4	4100	108	Cracked	Monolithic	50.0	0.88	49.1	864	47.0	940
	B5	3960	108	Cracked	Monolithic	50.0	1.10	50.5	1111	50.0	1000
	B6	4250	110	Cracked	Monolithic	50.0	1.32	51.8	1368	57.7	1154
	C1	2330	102	Cracked	Monolithic	50.0	0.22	49.6	218	18.2	364
	C2	2330	102	Cracked	Monolithic	50.0	0.44	53.6	472	25.7	514
	C3	2000	103	Cracked	Monolithic	50.0	0.66	50.9	672	26.3	526
	C4	2050	105	Cracked	Monolithic	50.0	0.88	52.3	921	28.0	560
	C5	2330	106	Cracked	Monolithic	50.0	1.10	53.6	1179	32.0	640
	C6	2330	106	Cracked	Monolithic	50.0	1.32	49.6	1309	37.0	740
	D1	5995	108	Cracked	Monolithic	50.0	0.22	51.8	228	18.5	370
	D2	5995	108	Cracked	Monolithic	50.0	0.44	52.3	460	33.4	668
	D3	5710	107	Cracked	Monolithic	50.0	0.66	52.3	690	38.6	772
	D4	5710	107	Cracked	Monolithic	50.0	0.88	52.3	920	51.1	1022
	D5	5600	109	Cracked	Monolithic	50.0	1.10	52.3	1151	54.1	1082
	D6	5600	109	Cracked	Monolithic	50.0	1.32	51.8	1368	61.0	1220
	F1	4150	97	Cracked	Monolithic	50.0	0.22	53.2	234	22.5	450

Specimen ID		Concrete Properties		Shear Plane Geometry and Condition			Shear Plane Reinforcement			Testing Data	
		f'_c at Test (psi)	Density (pcf)	Interface Condition	Casting Procedure	A_{cr} (sq. in.)	A_{vf} (sq. in)	f_y (ksi)	$\rho_{vf}f_y$ (psi)	V_u (kips)	v_u (psi)
Mattock, Li, and Wang, 1976	F2	4030	94	Cracked	Monolithic	50.0	0.44	52.3	460	26.5	530
	F2A	3970	94	Cracked	Monolithic	50.0	0.44	50.9	448	31.0	620
	F3	4065	96	Cracked	Monolithic	50.0	0.66	52.3	690	36.7	734
	F3A	3970	94	Cracked	Monolithic	50.0	0.66	51.4	678	35.1	702
	F4	4040	96	Cracked	Monolithic	50.0	0.88	50.9	896	43.5	870
	F5	4115	98	Cracked	Monolithic	50.0	1.10	51.8	1140	46.0	920
	F6	4050	94	Cracked	Monolithic	50.0	1.32	53.2	1404	49.1	982
	H1	4145	98	Cracked	Monolithic	50.0	0.22	49.8	219	20.0	400
	H2	3880	96	Cracked	Monolithic	50.0	0.44	51.8	456	31.0	620
	H3	4100	96	Cracked	Monolithic	50.0	0.66	51.8	684	43.3	866
	H4	4420	97	Cracked	Monolithic	50.0	0.88	51.8	912	47.0	940
	H5	3950	99	Cracked	Monolithic	50.0	1.10	50.5	1111	49.5	990
	H6	4080	98	Cracked	Monolithic	50.0	1.32	49.8	1315	52.1	1042
	N1	4180	145	Cracked	Monolithic	50.0	0.22	50.9	224	23.0	460
	N2	3900	145	Cracked	Monolithic	50.0	0.44	52.7	464	39.0	780
	N3	3995	145	Cracked	Monolithic	50.0	0.66	52.3	690	48.0	960
	N4	4150	145	Cracked	Monolithic	50.0	0.88	50.9	896	57.5	1150
	N5	3935	145	Cracked	Monolithic	50.0	1.10	50.9	1120	58.8	1175
	N6	4120	145	Cracked	Monolithic	50.0	1.32	50.9	1120	59.5	1190

Specimen ID		Concrete Properties		Shear Plane Geometry and Condition			Shear Plane Reinforcement			Testing Data	
		f'_c at Test (psi)	Density (pcf)	Interface Condition	Casting Procedure	A_{cr} (sq. in.)	A_{vf} (sq. in)	f_y (ksi)	$\rho_{vf}f_y$ (psi)	V_u (kips)	v_u (psi)
Mattock, Li, and Wang, 1976	A0	4320	111	Uncracked	Monolithic	50.0	0.00	0	0	25.0	500
	A1	3740	111	Uncracked	Monolithic	50.0	0.22	47.7	210	37.9	758
	A2	4095	105	Uncracked	Monolithic	50.0	0.44	53.6	482	45.7	914
	A3	3910	110	Uncracked	Monolithic	50.0	0.66	53.2	702	51.0	1020
	A4	4100	108	Uncracked	Monolithic	50.0	0.88	50.9	896	55.0	1100
	A5	3960	108	Uncracked	Monolithic	50.0	1.10	50.9	1120	59.5	1190
	A6	4250	110	Uncracked	Monolithic	50.0	1.32	51.8	1368	67.2	1344
	E0	3960	92	Uncracked	Monolithic	50.0	0.00	0	0	28.0	560
	E1	4150	97	Uncracked	Monolithic	50.0	0.22	52.3	230	39.0	780
	E2	4030	94	Uncracked	Monolithic	50.0	0.44	52.3	460	43.6	872
	E3	4065	96	Uncracked	Monolithic	50.0	0.66	52.3	690	48.0	960
	E4	4040	96	Uncracked	Monolithic	50.0	0.88	53.2	936	57.5	1150
	E5	4115	98	Uncracked	Monolithic	50.0	1.10	50.5	1111	60.0	1200
	E6	4050	94	Uncracked	Monolithic	50.0	1.32	52.3	1381	62.5	1250
	G0	4030	98	Uncracked	Monolithic	50.0	0.00	0	0	26.5	530
	G1	4145	98	Uncracked	Monolithic	50.0	0.22	52.3	230	41.0	820
	G2	3880	96	Uncracked	Monolithic	50.0	0.44	50.5	444	42.3	846
	G3	4100	96	Uncracked	Monolithic	50.0	0.66	51.8	684	53.0	1060
	G4	4420	97	Uncracked	Monolithic	50.0	0.88	53.2	936	57.5	1150

Specimen ID		Concrete Properties		Shear Plane Geometry and Condition			Shear Plane Reinforcement			Testing Data	
		f'_c at Test (psi)	Density (pcf)	Interface Condition	Casting Procedure	A_{cr} (sq. in.)	A_{vf} (sq. in)	f_y (ksi)	$\rho_{vf}f_y$ (psi)	V_u (kips)	v_u (psi)
Mattock, Li, and Wang, 1976	G5	4005	99	Uncracked	Monolithic	50.0	1.10	51.8	1140	57.0	1140
	G6	4005	99	Uncracked	Monolithic	50.0	1.32	51.8	1368	59.5	1190
	M0	3935	145	Uncracked	Monolithic	50.0	0.00	0	0	29.5	590
	M1	4180	145	Uncracked	Monolithic	50.0	0.22	50.9	224	38.0	760
	M2	3900	145	Uncracked	Monolithic	50.0	0.44	52.7	464	49.0	980
	M3	3995	145	Uncracked	Monolithic	50.0	0.66	52.3	690	55.5	1110
	M4	4150	145	Uncracked	Monolithic	50.0	0.88	50.9	896	57.0	1140
	M5	3935	145	Uncracked	Monolithic	50.0	1.10	52.7	1160	64.0	1280
	M6	4120	145	Uncracked	Monolithic	50.0	1.32	52.7	1392	66.0	1320
Walraven, Frenay, and Pruijssers	110208t	4426	NWC	Cracked	Monolithic	55.5			352	40.9	737
	110208	3785	NWC	Cracked	Monolithic	55.5			352	44.3	798
	110208g	3624	NWC	Cracked	Monolithic	55.5			352	40.9	737
	110408	3785	NWC	Cracked	Monolithic	55.5			705	51.8	934
	110608	3785	NWC	Cracked	Monolithic	55.5			1057	59.5	1072
	110808h	3624	NWC	Cracked	Monolithic	55.5			1410	67.5	1217
	110808h	3624	NWC	Cracked	Monolithic	55.5			1410	69.0	1245
	110706	3908	NWC	Cracked	Monolithic	55.5			809	57.8	1043
	210204	4512	NWC	Cracked	Monolithic	55.5			154	25.9	467
	210608	4512	NWC	Cracked	Monolithic	55.5			1057	78.2	1410

Specimen ID		Concrete Properties		Shear Plane Geometry and Condition			Shear Plane Reinforcement			Testing Data	
		f'_c at Test (psi)	Density (pcf)	Interface Condition	Casting Procedure	A_{cr} (sq. in.)	A_{vf} (sq. in)	f_y (ksi)	$\rho_{vf}f_y$ (psi)	V_u (kips)	v_u (psi)
Walraven, Frenay, and Pruijssers, 1987	210216	4512	NWC	Cracked	Monolithic	55.5			1468	74.4	1342
	210316	4512	NWC	Cracked	Monolithic	55.5			2200	81.3	1467
	210808h	3107	NWC	Cracked	Monolithic	55.5			1410	64.1	1156
	120208	3637	NWC	Cracked	Monolithic	55.5			352	43.1	778
	120408	3637	NWC	Cracked	Monolithic	55.5			705	52.5	947
	120608	3637	NWC	Cracked	Monolithic	55.5			1057	54.5	984
	120808	3637	NWC	Cracked	Monolithic	55.5			1410	58.8	1060
	120706	3637	NWC	Cracked	Monolithic	55.5			809	55.7	1004
	120216	3637	NWC	Cracked	Monolithic	55.5			1468	52.5	947
	230208	6916	NWC	Cracked	Monolithic	55.5			352	54.1	975
	230408	6916	NWC	Cracked	Monolithic	55.5			706	87.1	1571
	230608	6916	NWC	Cracked	Monolithic	55.5			1057	101.1	1822
	230808	6916	NWC	Cracked	Monolithic	55.5			1410	114.2	2059
	240208	2453	NWC	Cracked	Monolithic	55.5			352	37.4	675
	240408	2453	NWC	Cracked	Monolithic	55.5			705	48.6	876
	240608	2453	NWC	Cracked	Monolithic	55.5			1057	52.7	950
	240808	2453	NWC	Cracked	Monolithic	55.5			1410	50.6	912
	250208	4709	NWC	Cracked	Monolithic	55.5			352	55.0	991
	250408	4709	NWC	Cracked	Monolithic	55.5			705	69.9	1261

Specimen ID		Concrete Properties		Shear Plane Geometry and Condition			Shear Plane Reinforcement			Testing Data	
		f'_c at Test (psi)	Density (pcf)	Interface Condition	Casting Procedure	A_{cr} (sq. in.)	A_{vf} (sq. in)	f_y (ksi)	$\rho_{vf}f_y$ (psi)	V_u (kips)	v_u (psi)
	250608	4709	NWC	Cracked	Monolithic	55.5			1057	77.6	1400
	250808	4709	NWC	Cracked	Monolithic	55.5			1410	80.0	1442
Mattock, Johal, and Chow, 1975	E1C	3855	NWC	Cracked	Monolithic	84.0	0.88	51.8	543	74.0	881
	E2C	4220	NWC	Cracked	Monolithic	84.0	0.88	52.1	546	78.0	929
	E3C	3960	NWC	Cracked	Monolithic	84.0	0.88	52.7	552	60.0	714
	E4C	3820	NWC	Cracked	Monolithic	84.0	0.88	50.5	529	56.5	673
	E5C	4020	NWC	Cracked	Monolithic	84.0	0.88	52.3	548	44.3	527
	E6C	3985	NWC	Cracked	Monolithic	84.0	0.88	50.9	533	31.0	369
	F1C	4220	NWC	Cracked	Monolithic	84.0	0.88	50.1	525	83.0	988
	F4C	3890	NWC	Cracked	Monolithic	84.0	0.88	51.3	537	70.5	839
	F6C	4150	NWC	Cracked	Monolithic	84.0	0.88	51.7	542	67.5	804
	F1U	4035	NWC	Uncracked	Monolithic	84.0	0.88	52.2	547	115.0	1369
	F4U	4175	NWC	Uncracked	Monolithic	84.0	0.88	53.2	557	96.0	1143
	F6U	4245	NWC	Uncracked	Monolithic	84.0	0.88	51.0	534	89.5	1066
	E1U	4060	NWC	Uncracked	Monolithic	84.0	0.88	52.7	552	91.5	1089
	E4U	3860	NWC	Uncracked	Monolithic	84.0	0.88	49.1	514	79.5	946
	E6U	4120	NWC	Uncracked	Monolithic	84.0	0.88	50.8	532	51.0	607